POLITECNICO DI MILANO

School of Industrial and Information Engineering

Master of Science in Electrical Engineering

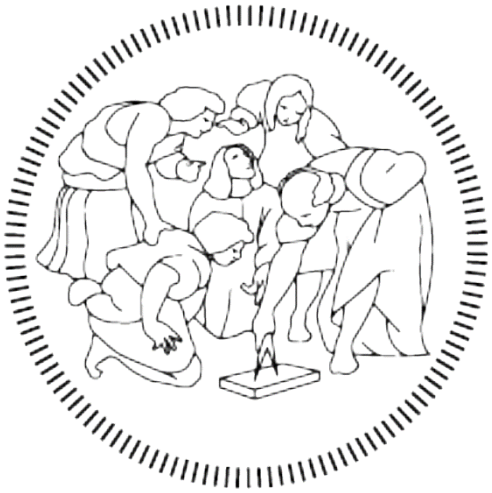

Modelling and Validation in OpenModelica of a Large-scale Three-phase Grid-connected Photovoltaic Model

Supervisor:

Prof. Alberto Berizzi

Company co-supervisor:

Ing. Ferdinando Parma

Master Thesis of:

Silvia Boncompagni

ID n. 898479

Academic year 2018/2019

Abstract

The current energy sector is oriented towards a sustainable transition, outlined by the use of renewable sources in generation systems. In particular, solar photovoltaic generation has grown significantly in the recent decades and now plays an important role in electrical energy distribution and transmission systems. However, despite the positive environmental impact, there are several critical issues introduced, due to the variability and uncertainty of these sources, which make the management of the transmission network complex. In this scenario, simulation tools are essential to assess power plant performances and predict network responses to ensure continuity and quality of service. In recent years, initiatives of data exchange among different European countries have emerged in order to improve coordination of the various Transmission System Operators (TSOs) and provide a more accurate control of the European network security. In this framework, the CGMES (Common Grid Model Exchange Standard) project has been introduced in the ENTSO-E area, aimed at exchanging information through the direct sharing, among the different European operators, of standardized generation models, implemented in Modelica® language. In this context, CESI S.p.A, as consultant of the Italian grid operator Terna S.p.A, has extended in the last two years the 'BasicPowerSystem' library in OpenModelica®, composed of passive and dynamic elements, to be inserted in its own dynamic simulator Dyana, module of the network analysis application TESEO. This thesis, carried out during an internship in CESI S.p.A, focuses on the development and validation of a dynamic model of a large-scale photovoltaic system, aimed at enriching the 'BasicPowerSystem' library for the execution of transients stability studies. This model, equipped with frequency, voltage, active/reactive power and power factor controls, is able to withstand voltage drops due to faults and ensure grid stability; it is based on international standards (NERC, WECC) and will be proposed to ENTSO-E as a basis for the realization of CGMES standard models. The first phase of the activity, which concerns the modelling stage, involved the use of the OpenModelica® tool, provided with the flexibility and accuracy necessary for the development of this project. The model validation was then fine-tuned through simulations in TESEO/ Dyana environment using a sample test network.

Estratto

Il panorama energetico attuale è rivolto ad uno sviluppo sostenibile, delineato dall' impiego di fonti rinnovabili nei sistemi di produzione e di trasporto. In particolare, la generazione solare fotovoltaica ha avuto negli ultimi decenni una crescita importante, e oggigiorno svolge un ruolo rilevante nei sistemi elettrici di distribuzione e trasmissione dell'energia. Nonostante il positivo impatto ambientale, tuttavia, la variabilità e l'incertezza delle risorse alternative hanno introdotto criticità nella gestione della rete, rendendone complessa la pianificazione da parte dell'operatore. In un tale scenario, gli strumenti di simulazione sono fondamentali per giudicare le prestazioni degli impianti di potenza e prevedere le risposte della rete, in modo da garantire continuità e qualità del servizio. Negli ultimi anni sono emerse iniziative di scambio dati tra i diversi paesi europei per migliorare il coordinamento dei vari gestori del sistema di trasmissione e fornire un controllo più accurato della sicurezza della rete europea. A tal proposito, è stato introdotto in ambito ENTSO-E il progetto CGMES (Common Grid Model Exchange Standard), finalizzato allo scambio di informazioni tramite la diretta condivisione, tra i diversi operatori europei, di modelli di generazione standardizzati, implementati in linguaggio Modelica®. In questo contesto, CESI S.p.A, in qualità di consulente del gestore di rete italiano Terna S.p.A, ha esteso negli ultimi due anni la libreria 'BasicPowerSystem' in OpenModelica®, composta da elementi passivi e dinamici, da inserire nel proprio simulatore dinamico Dyana, modulo dell'applicazione di analisi di rete TESEO. Questa tesi, svolta durante un internship in CESI S.p.A, è incentrata sullo sviluppo e la validazione di un modello dinamico di un sistema fotovoltaico in larga scala, volto ad arricchire la libreria 'BasicPowerSystem' per l'esecuzione di studi sulla stabilità dei transitori. Questo modello, dotato di controlli di frequenza, tensione, potenza attiva/reattiva e fattore di potenza, è in grado di resistere alle cadute di tensione dovute a guasti e garantire la stabilità della rete; è basato su standard internazionali (NERC, WECC) e verrà proposto a ENTSO-E come base per la realizzazione di modelli standard CGMES. L'attività prevede l'utilizzo dello strumento OpenModelica®, che dispone della flessibilità e della precisione necessarie per lo sviluppo di questo progetto, per lo stage di modellazione e per una prima fase di test. La validazione del modello è stata poi messa a punto attraverso simulazioni in ambiente TESEO/ Dyana tramite l'impiego di una semplice rete di prova.

Summary

The first chapter [1] has an introductory role related to the use of solar photovoltaic in power generation systems. Starting with an explanation of the current situation in Italy and Europe [1.1], it continues by listing the various grid connection configurations [1.2.1], detailing the individual network elements. Sections dedicated to the panel operation [1.2.2], the DC-DC and DC-AC converters functioning [1.3] and their relative controls [1.4] can be found in this chapter.

Chapter two [2] is dedicated to the state of the art of standard models for large-scale photovoltaic systems. It contains a description of the reference module used in the implementation of the PV generator [2.2], with an illustration of the system control diagrams and a general overview of their operation [2.2.3]. This chapter also includes a preamble [2.1] to introduce the North American regulatory authorities, which are the promoters of the guidelines used in the thesis activity.

The third chapter [3] presents the main network connection requirements of a large-scale photovoltaic system, with reference to attachment A.68 of the Italian Grid Code [3.3]. An introductory preface about ENTSO-E [3.1] and Terna S.p.A [3.2] is also included in this part of the thesis.

The fourth chapter [4] deals with the description of the simulation environments adopted in the development of the thesis project. The first part is aimed at motivating the choice of Modelica® language for the dynamic model development [4.1, 4.2], while the following paragraphs explain the OpenModelica® software [4.3] and the Dyana simulation tool [4.4].

In the fifth chapter [5] the implemented photovoltaic model is analyzed. Each section is dedicated to the detailed presentation of the structure and operation of the sub-modules constituting the PV generator. The chapter also provides illustrative diagrams of the system configurations implemented in the OMEdit graphical user interface.

Finally, in the sixth chapter [6], the model validation is carried out by two distinct testing procedures. The first section [6.1] concerns the simulation analysis of the single sub-system blocks in the OpenModelica® environment, aimed at verifying their correct

operations. The second part [6.2] is related to the tests conducted in Dyana/TESEO simulator tool, which involves the use of a sample test network provided by CESI.

Contents

List of figures

List of Tables

List of Acronyms

AC	Alternating Current
BSFM	Band of Frequency Sensitive Mode
BPS	Bulk Power System
CC	Current Controlled
CCM	Continuous Conduction Mode
CCVSI	Current-Controlled Voltage Source Inverter
CGMES	Common Grid Model Exchange Standard
CIM	Common Information Model
CSI	Current Source Inverter
DAE	Differential Algebraic Equations
DC	Direct Current
DYANA	Dynamic Analyser
DSO	Distribution System Operator
ENTSO-E	European Network of Transmission System Operators
ERO	Electric Reliability Organization
FERC	Federal Energy Regulatory Commission
FMI	Functional Muck-up Interfaces
FMU	Functional Mock-up Units
FRT	Fault ride through
FSM	Frequency Sensitive Mode
GSE	Gestore dei Servizi Energetici
GTO	Gate Turn Off
HV	High Voltage
HVDC	High Voltage Direct Current
HVRCM	High Voltage Reactive Current Management
IEC	International Electrotechnical Commission
IEEE	Institute of Electronic and Electrical Engineers
IGBT	Insulated-Gate Bipolar Transistor
I/O	Input/Output
LFSM-O	Limited Frequency Sensitive Mode Over Frequency
LFSM-U	Limited Frequency Sensitive Mode Under Frequency
LV	Low Voltage
LVACM	Low Voltage Active Current Management
LVPL	Low Voltage Power Logic
MOD	Modeling Data
MOSFET	Metal Oxide Semiconductor Field Effect Transistor
MPP	Maximum Power Point
MPPT	Maximum Power Point Tracking
MV	Medium Voltage
NERC	North American Electric Reliability Corporation
NREAP	National Renewable Energy Action Plan
NREL	National Renewable Energy Laboratory
OC	Open Circuit
OMEdit	OpenModelica Connection Editor
OVRT	Over Voltage Ride Through

PI	Proportional Integral
PLL	Phase Locked Loop
POI	Point of Interconnection
PV	Photovoltaic
PWM	Pulse Width Modulation
RE	Regional Entity
REEC	Renewable Energy Electrical Control
REGC	Renewable Energy Generator Control
REMTF	Renewable Energy Modeling Task Force
REPC	Renewable Energy Plant Control
SC	Short Circuit
SPWM	Sinusoidal Pulse Width Modulation
TESEO	Terna Sistemi Elettrici Ottimizzati
THD	Total Harmonic Distortion
TSO	Transmission System Operator
VC	Voltage Controlled
VCVSI	Voltage-Controlled Voltage Source Inverter
VRE	Variable Renewable Energy
VSI	Voltage Source Inverter
UHV	Ultra High Voltage
UVRT	Under Voltage Ride Through
WECC	Western Electricity Coordinating Council

1. The Photovoltaic System

A central theme in today's world is climate change and, in particular, global warming. This issue, which has been developing since the end of the 19th century, is still ongoing and is mainly attributed to the high atmospheric concentration of greenhouse gases. CO_2 emissions are one of the main causes of global warming and their increase is mainly due to the use of fossil fuels in industrial plants, energy production plants and in transportation. The urgent need to solve the global environmental concern, together with the foreseen deficiency of fossil fuel-based energy sources, have been the main driving forces to seek and develop clean and renewable alternatives. In order to promote a sustainable policy, the use of renewable sources in energy production plays an important role and the solar Photovoltaic (PV) option is nowadays one of the most commercially implemented and widely adopted solution. However, despite the benefits of eco-sustainability and inexhaustible availability, solar energy is a source of intermittence, since highly dependent on environmental conditions such as temperature and solar irradiation. In addition, unlike conventional generators, the connection of solar systems to the grid requires the use of converters, which feature a lack of inertia, as they are static machines. Wide penetration level of PV systems is therefore critical and imposes challenging issues for the network safety and reliability since it may not guarantee the continuity and quality of the electricity service. The focus is to innovate and improve control strategies through the advancement of electronic power systems and storage technologies in a way to create more sustainable, grid friendly and reliable photovoltaic energy conversion systems that comply with grid standards and are able to participate in reducing energy costs.

1.1 The Current Penetration of Solar Energy

Solar photovoltaic is one of the most favourable renewable energy type capable of enabling a future sustainable society for the next generation of people. Its worldwide capacity is growing at a fast pace, and is expected to grow much more in the future due to the continuous decline in prices. By the end of 2018, global cumulative installed PV capacity reached about $512\,GW$, representing a growth of 27% from 2017, which is sufficient to supply about 3% of worldwide electricity demand. The cumulative capacity of

grid-connected PV system in Europe is depicted in the graph of Figure 1.1, where it is shown that already in 2014, the National Renewable Energy Action Plan (NREAP) target for 2020 of 83.7 GW was exceeded, reaching about 88.4 GW [33]. The diagram also highlights the great Italian involvement in the use of solar energy, occupying the second position in Europe after Germany, which maintains its supremacy.

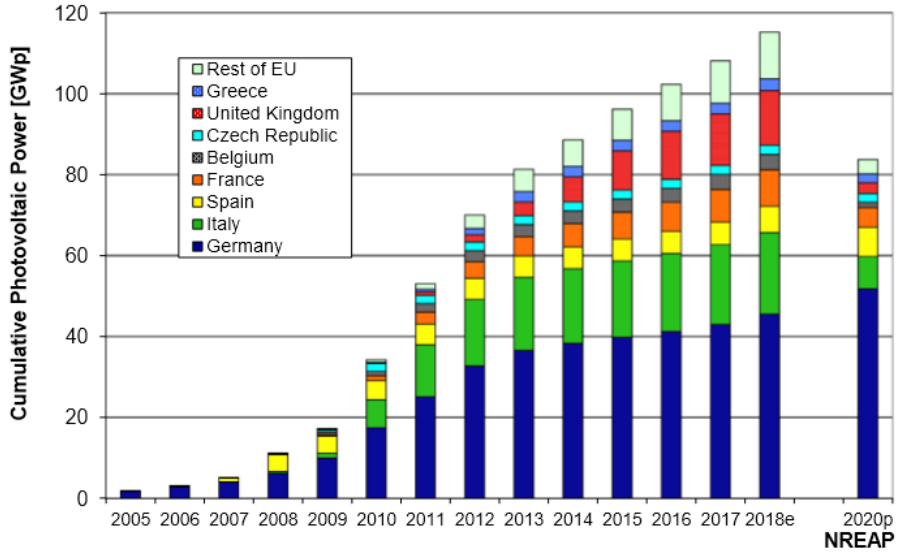

Figure 1.1- Connected PV capacity in EU (2005-2018) compared with the NREAP target for 2020.

In particular, in 2018, solar PV contributed between 7% and 8% to the annual domestic consumption in Italy, whose gradual increase from 2008 to 2018 in installed photovoltaic power and number of installations is illustrated in Figure 1.2 [34].

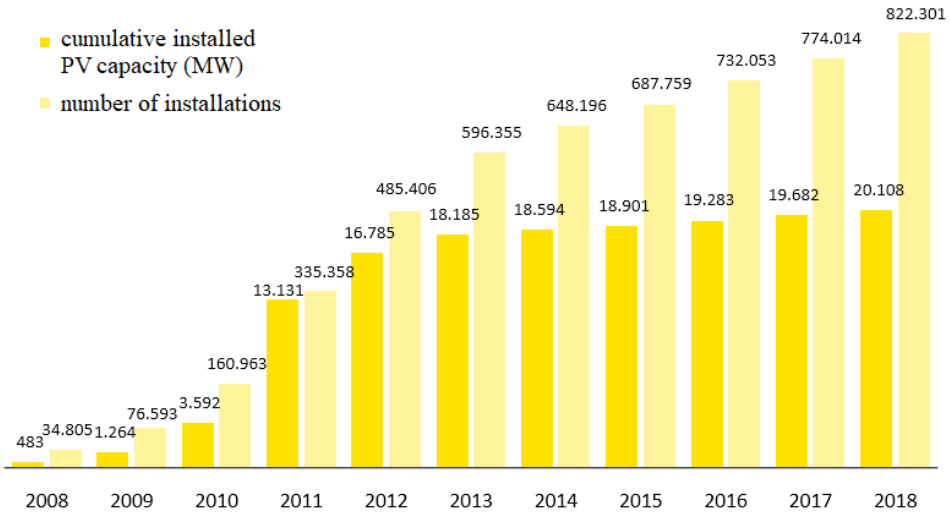

Figure 1.2- Evolution of the power and number of photovoltaic systems in Italy.

Data provided by Gestore dei Servizi Energetici (GSE) in 2018 record that almost all the plants installed in Italy (97.5%) are connected to the low-voltage grid, about 20,000 systems are associated to the medium-voltage network, concentrating 56.9% of the overall installed power, and only a small number of installations are connected to the high voltage lines, for around 1,286 MW (6.4% of the total), as shown in Figure 1.3 [34].

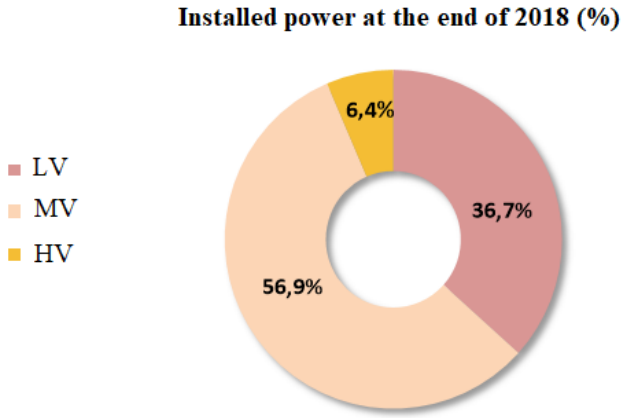

Figure 1.3- Installed power at the end of 2018 (%).

Today there are increasingly worldwide expectations for energy production through solar energy systems, which have led many countries to set ambitious targets for the next few decades. For example, on 11 *December* 2018, the EU adopted Directive 2018/2001/*EU* on the promotion of the use of energy from renewable sources with the objective of achieving a 32% trade in renewables by 2030. In Italy in particular, an installed capacity solar target of 50 *GW* was defined in the new National Integrated Plan for Climate and Energy 2030. On 11 *December* 2019, the European Commission also presented the European Green Deal, the most ambitious package of measures that should enable European citizens and businesses to benefit from a sustainable green transition to become the world's first climate neutral continent by 2050 [35]. The measures to achieve the greatest challenge of our time are accompanied by a first roadmap of key policies aimed at reducing emissions, investing in cutting-edge research and innovation, and preserving Europe's natural environment. Designed so that no individual or region is left behind, the European Green Deal establishes a path for a fair and socially just transition.

1.2 The Photovoltaic Power Generation

Solar energy is widely adopted in today's energy paradigms across the globe and will assume an increasingly important share in the near future. In fact, due to the cost reduction of photovoltaic modules and the development of PV cell technology, the PV power generation is becoming dominant in the renewable energy supplies of some countries. In particular, grid-connected PV systems have become very popular, and the use continues to increase around the world: about 99% of all European solar power systems are today connected to the electrical network. An effective integration of these technologies is therefore necessary in order to efficiently and reliably transfer and convert the solar energy, which is highly dependent on the environmental conditions (i.e. irradiance level and ambient temperature). There are various possibilities to achieve the conversion of solar PV energy. Figure 1.4 shows the general PV power system for grid-connected applications [12].

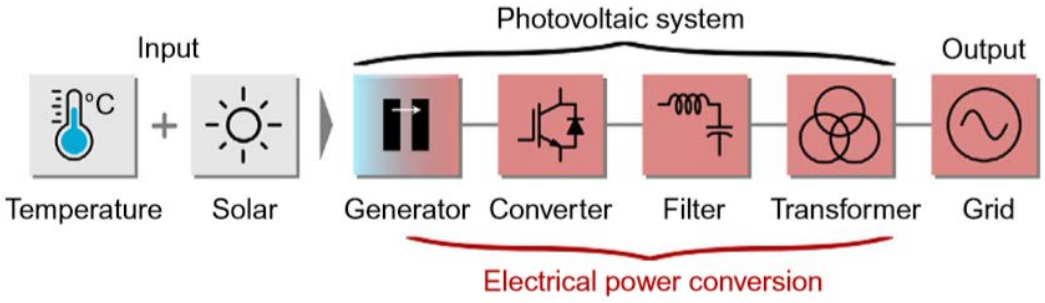

Figure 1.4- General structure of a grid-connected PV power conversion system.

The core of a PV plant is the photovoltaic cell, as it allows the conversion of solar energy into electricity, based on the photovoltaic effect. However, in order to achieve an effective transferring of the generated PV energy in compliance with the network standards, the PV panels must interface the grid through a power electronic system. Within the PV conversion structure, there is typically a DC-DC converter stage, which controls the PV panel's operation to maximize its power, and a DC-AC inverter stage, aimed at synchronizing and safely transferring power to the AC grid.

1.2.1 PV Grid-connected System Configurations

According to the state of the art, different configurations can be adopted to interconnect the system to the grid. Indeed, the connection scheme can vary depending on the plant size, the converters used and the grid topology. Photovoltaic modules are typically interfaced to the network through the DC-AC converter; however, depending on the voltage level, a first DC–DC stage may be required to boost up the DC-link voltage to an acceptable level of the PV inverter. There are mainly four concepts to organize and deliver the PV power to the public grid (Figure 1.5) [12]:

1. *Central Inverter*

   PV panels are arranged in paralleled strings and are connected to one common central inverter. It is typically used in large-scale or utility-scale PV power plants with high power ratings and usually consists of two-level voltage source inverters. The major disadvantage is the use of a common maximum power point tracking (MPPT) for many modules, which may increase the energy losses in case of mismatch among panels. However, the high voltage level achieved by the employment of several modules, allows to avoid the DC-DC boost stage and consequently reduce conversion losses and costs.

2. *String Inverter*

   PV strings are made up of series-connected PV panels, and are connected to separate string inverters (single- or three-phase). Then, the string inverters are paralleled and connected to the grid. They are therefore promising for a low power application as they result in a better yield due to an individual MPPT for each string.

3. *Multi-string Inverter*

   The multi-string concept is a flexible solution that involves series of multiple strings interconnected with individual DC-DC converters and then paralleled to a single grid-connected inverter through a common DC-link. They are an intermediate solution between string inverters and central inverters as they combine the advantages of both high energy production due to individual MPPT and low cost thanks to the common central DC-AC.

4. *Module Inverter*

This configuration consists in a single panel connected through the grid with its own converter. Every single module has its own MPPT control, thus maximizing the power production, and the modular structure allows a simplified modification and maintenance of the whole system. However, the main disadvantage is the low overall efficiency due to the large need of voltage amplification units for grid connection.

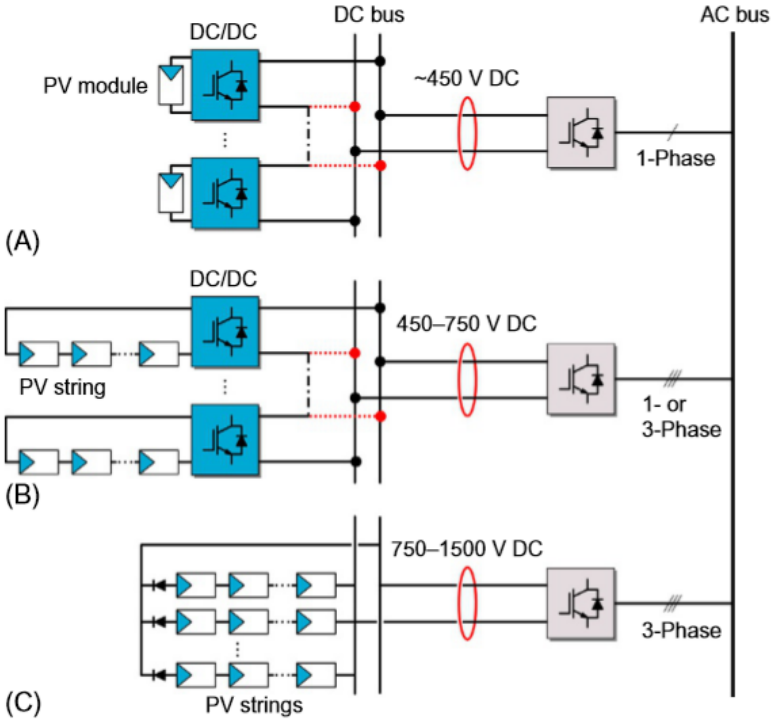

Figure 1.5- (A) module PV converter for low power applications, (B) string/ multi-string inverter for medium power applications, and (C) central inverters for commercial or utility scale systems. (DC/DC converters for the string inverter are optional).

For high power PV applications, with a high DC voltage up to $1500\,V$, transformers are typically required. Those large PV power plants, rated over tens and even hundreds of MW, adopt many central inverters with the power rating of up to 900 kW. A typical large-scale PV power plant is shown in Figure 1.6, where DC–DC converters are also used upstream of central inverters [14].

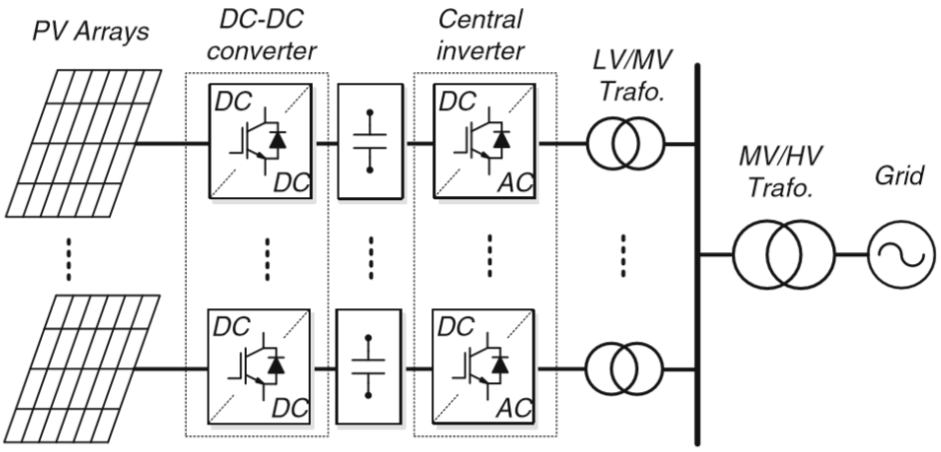

Figure 1.6- Typical large-scale PV power plant based on central inverters for utility application.

1.2.2 The Photovoltaic Cell Technology

The photovoltaic solar cell is the key element for the conversion of sunlight into electricity. They are semi-conductor devices which generate DC voltage when exposed to light, based on the photovoltaic effect. In order to obtain the appropriate voltages and outputs for different applications, single solar cells are interconnected in series (for larger voltage) and in parallel (for larger current) to form the photovoltaic module, which can then be combined to create strings and consequently solar power systems, ranging from a few watts of electricity output to multi-megawatt power stations (Figure 1.7) [42].

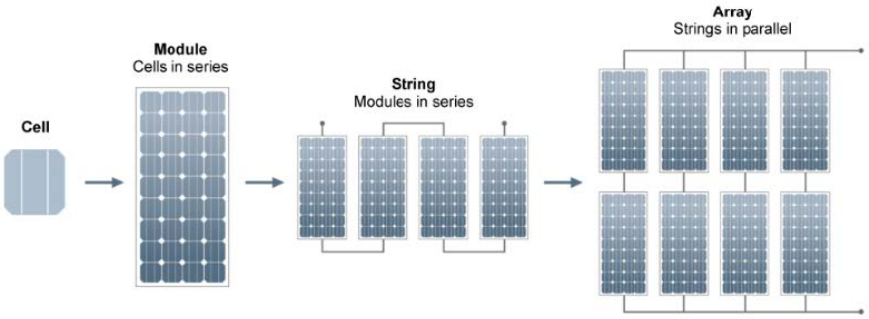

Figure 1.7- Solar PV configurations, from solar cell to solar array.

Solar cells are composed of various semiconductor materials which become electrically conductive when supplied by heat or light. Different materials with varying efficiencies and costs can be employed to make PV cells. The majority of solar cells produced today are composed of Silicon, in particular mono-crystalline silicon, that dominates about 90% of the market and can achieve high performances exceeding efficiency of even 20%. The

voltage across a solar cell is primarily dependent on the design and materials of the cell and in the case of silicon is around $0.5\,V$. Conversely, the electrical current depends mainly on the incident solar radiation and the cell area.

The Photovoltaic Effect

The photovoltaic effect is a process that generates voltage in a photovoltaic cell when it is exposed to sunlight. Its operating principle is based on the transfer of the energy contained in the photons to the semiconductor material of the cell to generate free electrons that contribute to the electricity flow. A typical solar cell is composed of the overlapping of an n-type and a p-type semiconductor, characterized by a difference in electron and holes concentration. From the contact of the two doped silicon layers, a diffusion of electrons towards the p-region starts, resulting in the generation of positive and negative ions in the n-side and p-side respectively. A consequent electrostatic field of around $0.8\,\text{eV}$ extends beyond the boundary surface corresponding to a potential difference V_D, called diffusion voltage. A schematic representation of this process is given in Figure 1.8 [44].

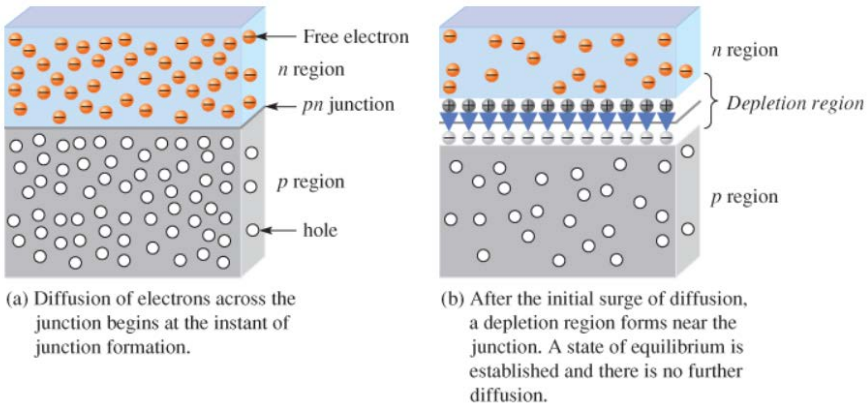

Figure 1.8- a) Juxtaposition of the n- and p-type layer at the first instant. b) Formation of the depletion layer and the resulting electric field.

When a photon with sufficient energy is absorbed by the cell, electron-hole pairs are generated and consequently separated by the electric field in the vicinity of the p-n junction. Once the electrons have passed the depletion region, they can no longer go back, because the field prevents them from reversing the direction. Connecting the two sides of the junction with an external conductor will result in a closed circuit in which the current flows from the higher to the lower potential as long as the cell remains lit. The contribution to the current is provided by the area surrounding the p-n junction since in remote areas the

electrical charges recombine due to the absence of the electric field. Figure 1.9 shows the behaviour of an illuminated photovoltaic cell [43].

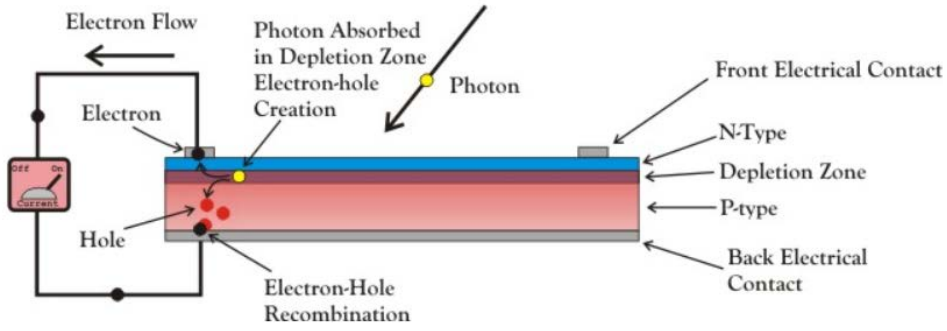

Figure 1.9- Behaviour of an irradiated photovoltaic cell.

The Equivalent Circuit of the Cell

The evaluations in the previous paragraph show a cell behaviour comparable to a diode. The mathematical process at the p-n junction can therefore be expressed as:

$$i_d = I_0 \left[e^{\frac{qV}{NkT}} - 1 \right] \tag{1.1}$$

where:

$i_d \rightarrow$ diode current $[A]$

$I_0 = AT^3 e^{\frac{-E_g}{kT}} \rightarrow$ dark or saturation current of the diode

$q \rightarrow$ magnitude of electron charge $[1.6 * 10^{-19} C]$

$V \rightarrow$ applied voltage $[V]$ (>0 forward bias <0 reverse bias)

$k \rightarrow$ Boltzmann's constant $[8.65 * 10^{-5}\ eV/K]$

$T \rightarrow$ absolute temperature $[K]$

$N \rightarrow$ coefficient dependent on generation and recombination phenomena (for an ideal diode N=1)

$A \rightarrow$ constant depending on the semiconductor

$E_g \rightarrow$ energy gap $[eV]$

For a detailed description of the mathematical process characteristic of the cell please refer to [2] and [3]. When the cell is illuminated, the junction becomes a source of electron-hole pairs. The open circuit voltage at the terminal of the cell reaches a value such that it allows the passage through the junction of a current proportional to the photo-generated one. If n-

emitter and p-base are electrically connected through an external load, this is parallel to the cell junction and the photocurrent is therefore divided between the load and the junction itself. A solar cell can be represented by the simplified equivalent circuit illustrated in Figure 1.10 [12]. The current source i_{ph} represents the cell photocurrent. R_p and R_s are the intrinsic shunt and series resistances of the cell, respectively. The first one considers the leakage current to earth, while R_s represents the resistance internal to the generated current flow and depends on the thickness of the p-n junction, on the impurities and on the contact resistances.

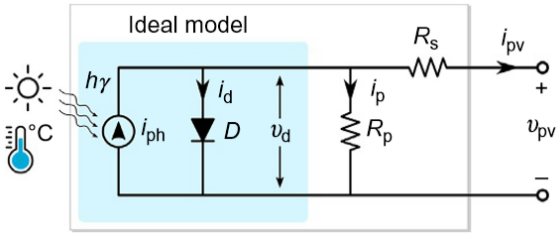

Figure 1.10- The equivalent circuit of photovoltaic cell.

Considering a load connected to the terminals of the equivalent circuit, the current supplied to the load assumes the following expression:

$$i_{pv} = i_{ph} - i_d - i_p = i_{ph} - I_0\left[e^{\frac{q(v_{pv}+i_{pv}R_s)}{NkT}} - 1\right] - \frac{v_{pv} + i_{pv}R_s}{R_p} \tag{1.2}$$

Since the value of R_p is usually very large and that of R_s is very small, i_p can be neglected to simplify the analysis.

I-V and P-V Characteristics of a Cell

The electrical circuit of Figure 1.10 can be used to model the characteristics of a PV module or cell. A solar cell produces its maximum current I_{sc} when there is a short circuit between its positive and negative terminals. Under this condition no current i_d flows through the diode and therefore the entire photocurrent i_{ph} generated from the radiation flows to the output:

$$I_{sc} = i_{ph} \tag{1.3}$$

Conversely, the maximum voltage V_{oc} occurs under no-load condition. In this case the current is null since the resistance is infinitely high. The expression of the open circuit voltage, considering an infinite R_P, is:

$$V_{oc} = \frac{kT}{q} ln\left(\frac{i_{ph}}{I_0} + 1\right) \tag{1.4}$$

These two extremes in the load resistance, and the entire range of conditions between them, are represented on the *I-V* curve of Figure 1.11 [12].

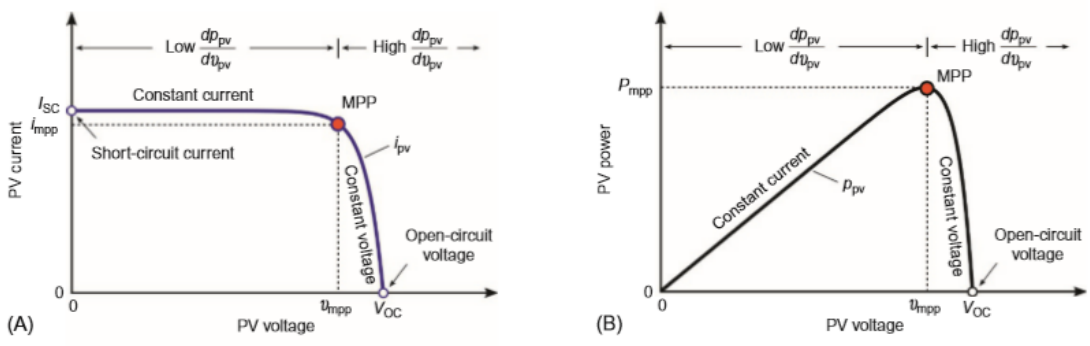

Figure 1.11- Current-voltage (I-V) and power-voltage (P-V) characteristics for a PV panel showing the MPP.

The amplitude of the I-V characteristic curve of the solar cell varies from the short circuit current at zero output volts, to zero current at the full open circuit voltage. Of course, neither of these two conditions generates any electrical power. However, there is a particular combination of current and voltage for which the power reaches its maximum value. This point is called 'Maximum Power Point' (MPP) and represents the ideal working point of a cell or module. The values of current and voltage at MPP are indicated with i_{mpp} and v_{mpp} respectively and estimated as follows:

$$v_{mpp} = (0.75 - 0.9)V_{oc} \tag{1.5}$$

$$i_{mpp} = (0.85 - 0.95)\, I_{sc} \tag{1.6}$$

The generated power of a PV panel is dramatically affected by the solar irradiance level and the ambient temperature. In particular, the voltage decreases significantly as the temperature rises while the current is directly influenced by the intensity of the radiation, as illustrated in Figure 1.12 [14].

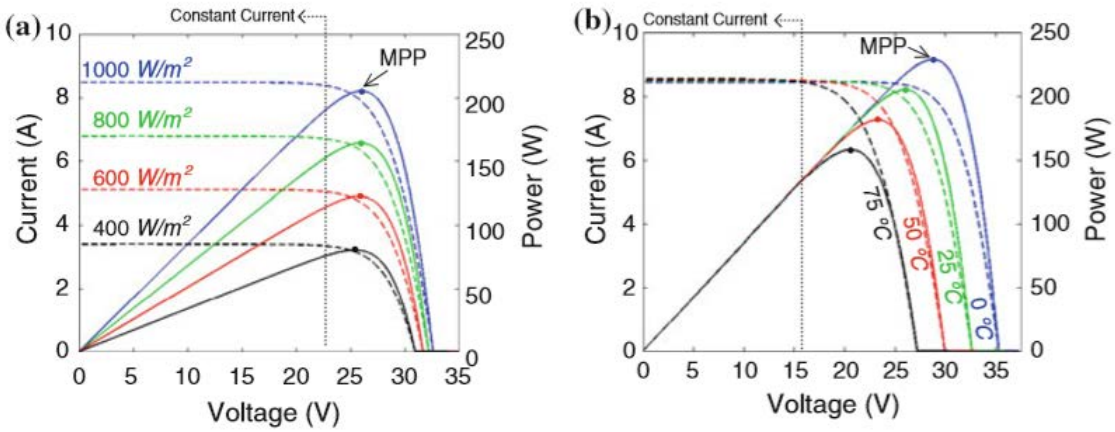

Figure 1.12- - I-V and P-V characteristics of a PV panel: a) different solar irradiance levels at 25 °C, b) different ambient temperatures at 1000 W/m2.

Due to the properties of non-linearity and environmental dependency of the PV panel, a Maximum Power Point Tracking (MPPT) algorithm is necessary to maximize the generated power. The output of the MPPT control system is the reference to be controlled by a DC–DC converter or directly a DC-AC inverter, depending on the configuration of the PV system. In addition, with series and parallel connection, the risk of mismatch created by shading or local degradation increases, requiring a robust control system capable of meeting network requirements.

1.3 The Photovoltaic Power Conversion

In order to convert the photo-generated direct current power to an alternative one, panels must interface with the network through conversion structures. At the same time, fluctuation and unpredictability characteristics of solar energy are un-preferred for the operation of the power grid. Thereby, technologies that can guarantee more reliable and controllable electricity production/conversion are crucial needs. Power electronic converters play an important role in this renewable sector, which, thanks to their advanced control methods, are able to make the current generated compatible in terms of amplitude and frequency with the grid requirements. Depending on the voltage levels and the power ratings the interface can be implemented by a DC-DC converter and/or a DC-AC inverter. The typical configuration for large-scale PV units connected to a 3-phase grid coincides with the one shown in Figure 1.13 [18].

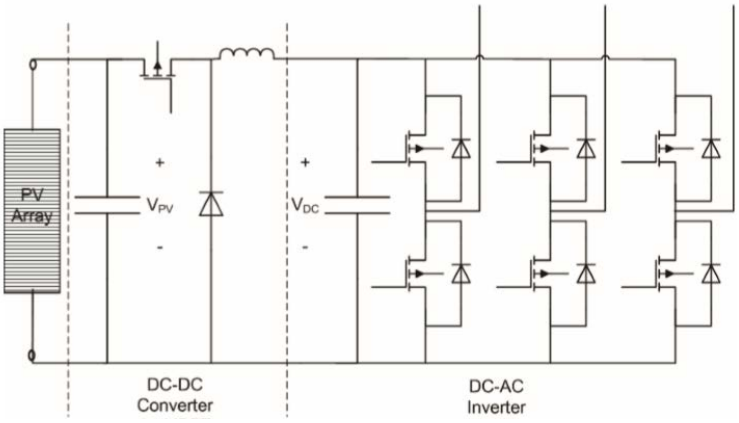

Figure 1.13- Typical double-stage configuration for 3-phase grid-connected PV system.

1.3.1 The DC-DC Step-up (Boost) Converter

The switch-mode DC-DC converter is responsible for maximizing the energy that can be transferred from the PV array to an electrical system. It allows energy at one potential to be drawn, stored as magnetic energy in an inductor, and then released at a different potential. Depending on the converter type, the switch-mode can be either high-to-low (Buck converter) or low-to-high (Boost converter). Since in large-scale grid-connected configuration the DC-DC stage is typically used to step up the voltage level to the desired amplitude, the structure of a boost converter is considered below. The basic topology consists of a DC input voltage source V_S, a boost inductor L, a controlled switch S, a diode D, a filter capacitor C, and a load resistance R, as shown in Figure 1.14 [39].

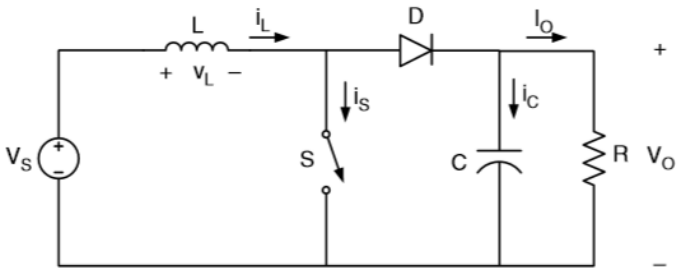

Figure 1.14- Circuit diagram of a Boost converter.

The active switch is usually controlled using a Pulse Width Modulation (PWM) signal and it is being operated with a duty cycle *D* defined as a ratio of the switch *on* time to the sum of the *on* and the *off* times.

For a constant frequency operation:

$$D = \frac{t_{on}}{t_{on} + t_{off}} = \frac{t_{on}}{T} \tag{1.7}$$

where $T = 1/f$ is the period of the switching frequency f.

During the *on* state of the switch the diode is reverse biased, thus the output stage is isolated and the input supplies energy to the boost inductor, whose current increases linearly. When the switch S is turned off, the energy stored in the inductor is released through the diode to the input RC circuit. The converter waveforms in the Continuous Conduction Mode (CCM) are presented in Figure 1.15 [39].

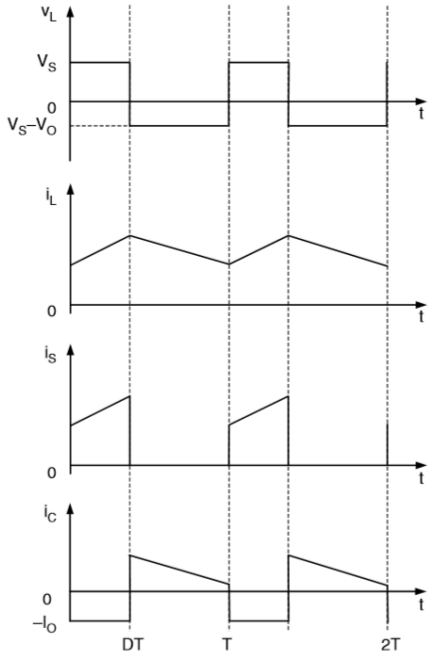

Figure 1.15- Voltage and current waveforms of a Boost converter.

The relationship among the input and output voltage can be derived from the inductor voltage waveform according to Faraday's law:

$$V_S t_{on} + (V_S - V_0) t_{off} = 0 \tag{1.8}$$

from which the DC voltage transfer function turns out to be:

$$M_V \equiv \frac{V_0}{V_S} = \frac{1}{1 - D} \tag{1.9}$$

As the name of the converter suggests, the output voltage is always greater than the input voltage.

1.3.2 The DC-AC Three-Phase Voltage Source Inverter

The main objective of static power converters is to produce an AC output waveform from a DC power supply. It is the key to obtain a successful performance and as such must ensure a wide range of operating voltages and currents, output voltage and frequency regulation and good power quality. The inverters used for the grid interfacing are broadly classified as:

- Voltage source inverters (VSI)
- Current source inverters (CSI)

Whereas the inverters based on the control schemes can be divided in:

- Current controlled (CC)
- Voltage controlled (VC)

Even though solar arrays are fairly good approximated to a current source, for several reasons, including reduced losses, easiness of control, reduction of filtering requirement, quality of the produced voltages and currents, most PV inverters nowadays are voltage source. Regarding the control scheme, there are advantages and limitations associated with each mechanism. For example, voltage-controlled voltage source inverter (VCVSI) provides voltage support to the load (here the VSI operates as a voltage source) and accomplishes active power transfer from the PV panels by controlling the phase angle δ between the converter voltage and the grid voltage. On the other hand, current-controlled voltage source inverter (CCVSI) provides current support (here the VSI operates as a current source) to control separately active and reactive components of the current fed into the grid. There are several strategies to perform these controls based on modulating techniques. Switch mode voltage source inverters using Sinusoidal Pulse Width Modulation (SPWM) switching control, are the most popular for the grid connection of PV systems.

Voltage source converters cover medium- to high-power applications with the main purpose of providing a three-phase voltage with controllable amplitude, phase, and frequency. They are based on the active switches technologies (IGBTs, MOSFETs, GTOs etc...) and require a capacitor on the DC link, in order to guarantee a stable DC voltage. The standard topology is shown in Figure 1.16 [39].

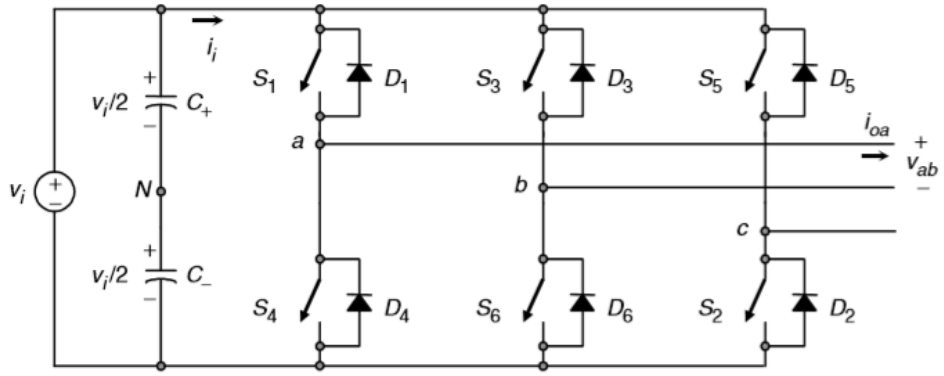

Figure 1.16- Three-phase VSI topology.

Since the switches of any leg of the inverter (S1 and S4, S3 and S6, or S5 and S2) cannot be switched on simultaneously, to avoid short circuit across the DC-link voltage supply, there are eight valid switch states, given in Figure 1.17 [39].

State	State #	v_{ab}	v_{bc}	v_{ca}
S_1, S_2, and S_6 are on and S_4, S_5, and S_3 are off	1	v_i	0	$-v_i$
S_2, S_3, and S_1 are on and S_5, S_6, and S_4 are off	2	0	v_i	$-v_i$
S_3, S_4, and S_2 are on and S_6, S_1, and S_5 are off	3	$-v_i$	v_i	0
S_4, S_5, and S_3 are on and S_1, S_2, and S_6 are off	4	$-v_i$	0	v_i
S_5, S_6, and S_4 are on and S_2, S_3, and S_1 are off	5	0	$-v_i$	v_i
S_6, S_1, and S_5 are on and S_3, S_4, and S_2 are off	6	v_i	$-v_i$	0
S_1, S_3, and S_5 are on and S_4, S_6, and S_2 are off	7	0	0	0
S_4, S_6, and S_2 are on and S_1, S_3, and S_5 are off	8	0	0	0

Figure 1.17- Valid switch states for a three-phase VSI.

In order to generate a given voltage waveform, the inverter moves from one state to another resulting in an AC output line voltages with discrete values that are v_i, 0 and $-v_i$. The selection of the states to generate the desired waveform is done by modulating technique such as sinusoidal PWM. In this case, the relationship between the amplitude of the fundamental AC output line voltage and the DC-link voltage v_i becomes:

$$\hat{v}_{ab1} = m_a\sqrt{3}\frac{v_i}{2} \tag{1.10}$$

where m_a represents the modulation index, also known as the amplitude-modulation ratio.

Figure 1.18 shows the ideal waveforms of three-phase VSI SPWM [39].

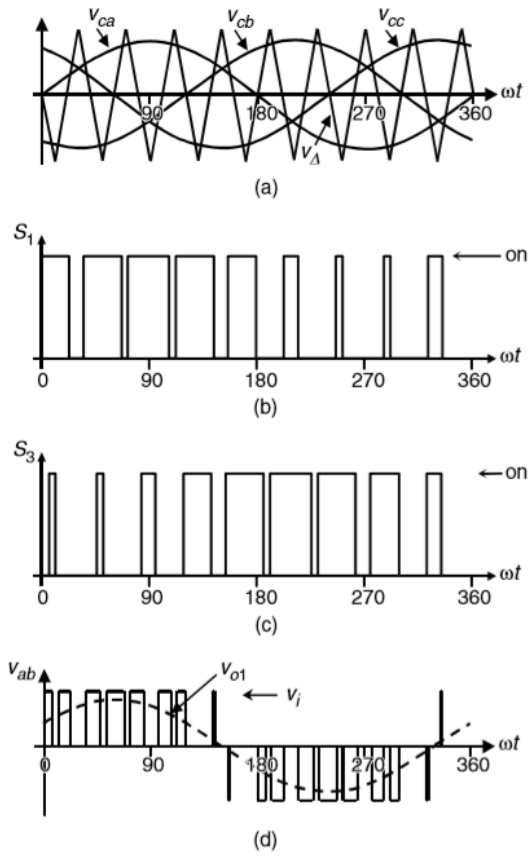

Figure 1.18- a) carrier and modulating signals, b) switch S1 state, c) switch S3 state, d) ac output voltage.

1.4 The Photovoltaic Control

According to network requirements, grid-connected PV systems must be controlled to perform their functions reliably and efficiently. Electronic power converters associated by intelligent control techniques play a key role in this process, providing a responsible management on both the panel and network sides. The control system changes depending on the configuration of the plant. A general control includes Maximum Power Point Tracking (MPPT), DC-link control, grid synchronization, voltage/current control, anti-islanding protection, system condition monitoring (grid and PV panels), and ancillary services. All these functions are performed through the use of communications following the set-point commands given by Distribution/Transmission System Operators (DSO/TSO). Moreover, energy storage systems can help the management of the power flowing. High power PV systems, in addition, are equipped with delta power production control, frequency control through active power, voltage control through reactive power, ride-through operation of the grid faults in order to provide grid support in both normal and abnormal conditions. In large-scale three-phase grid-connected PV system, two conversion stages are generally used: DC-DC and DC-AC, whose general control structure is shown in Figure 1.19 [14].

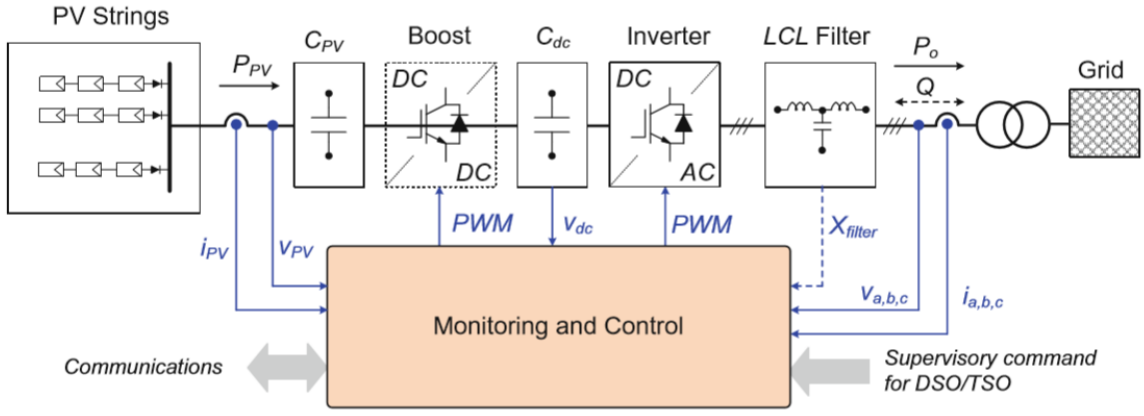

Figure 1.19- Schematic and general control structure of a three-phase grid-connected PV system with an LCL-filter.

The first stage of the conversion system is typically performed by a DC-DC converter that manages the control so that PV panels operate at MPP. The converted power is then delivered to the inverter stage and finally released to the load, which is represented by the AC grid.

1.4.1 DC-DC Converter Stage

As mentioned before, photovoltaic solar cells produce their maximum power with a unique combination of voltage and current, called the maximum power point (MPP), which changes with the radiation and temperature. The main purpose of this stage is to control, through a MPPT algorithm, the PV panel connected to the input side so that it operates at the MPP of the PV string regardless of environmental conditions. If the input voltage is high enough for the PV inverter, the DC-DC stage might be eliminated. The scheme of a DC-DC boost converter controlling a PV string is depicted in Figure 1.20 [12].

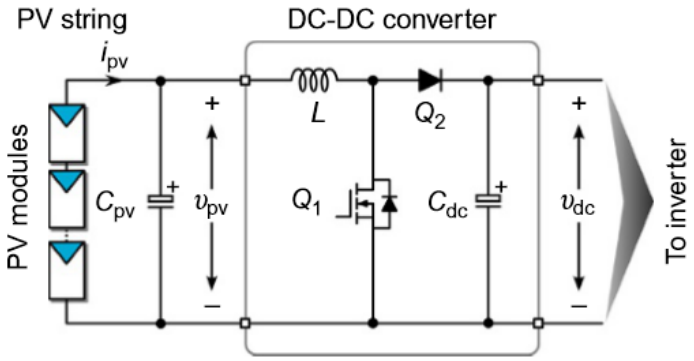

Figure 1.20- Schematic of a DC-DC boost converter controlling a PV string.

The diagram shows the input and output voltages of the converter, v_{pv} and v_{dc} respectively. The first one coincides with the output potential of the photovoltaic field, the second with the DC-link voltage, which is also the input voltage at the inverter stage. Assuming the ideal case, v_{pv} can be expressed as:

$$v_{pv} = v_{dc}(1 - D) \tag{1.11}$$

Since the DC-link voltage is considered constant during a switching cycle of the boost converter, the duty cycle D is inversely proportional to the PV voltage. In other words, using this relationship, the duty ratio D on the active switch Q_1 can be adjusted to control the input voltage v_{pv} in order to achieve v_{mpp}.

1.4.2 DC-AC Inverter Stage

The purpose of this stage is to synchronize with the frequency of the AC grid and transfer the available PV power to the grid while meeting the basic requirements of safety and efficiency. A scheme of a three-phase inverter for grid-connected applications is shown in Figure 1.21 [12].

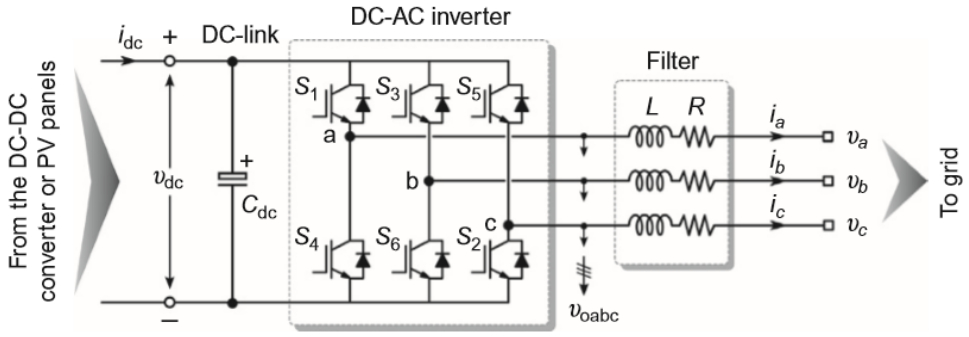

Figure 1.21- Schematic of a three-phase two-level inverter for grid-connected applications.

The applied control strategy typically provides two cascading configurations:

- the outer voltage/power control loop → It offers active and reactive power regulation strategies for safety and network support in case of abnormal conditions, such as frequency and voltage adjustment and ride-through operation of the grid faults. Based on the comparison between input reference and measured quantity, it generates in output the current reference for the second stage. It also includes detection methods to extract the phase angle for the network synchronization.
- the inner current control loop → It has the responsibilities of the power quality issues and current protection of the inverter. It therefore receives the input reference quantities from the external loop and shapes the final injected grid current trough harmonic compensators and current amplitude limiters.

The basic control structure of a three-phase grid-connected PV system is shown in Figure 1.22 [14]. The implementation of the control system can be done in different reference frames, such as synchronous rotating (dq), stationary ($\alpha\beta$), and natural (abc). The first solution is ideal in the case of a three-phase inverter. In fact, the Park transformation applied to the network voltage and current waveforms convert them into a reference frame

which rotates synchronously with the grid voltage. Consequently, the variables involved become DC quantities leading to an easy solution of control by means of Proportional-Integral (PI) based controllers. Finally, the output signals from the controller are usually anti-transformed into abc values again and used as modulation waveforms for the creation of the PWM signals, which will be used to activate the converter power switches.

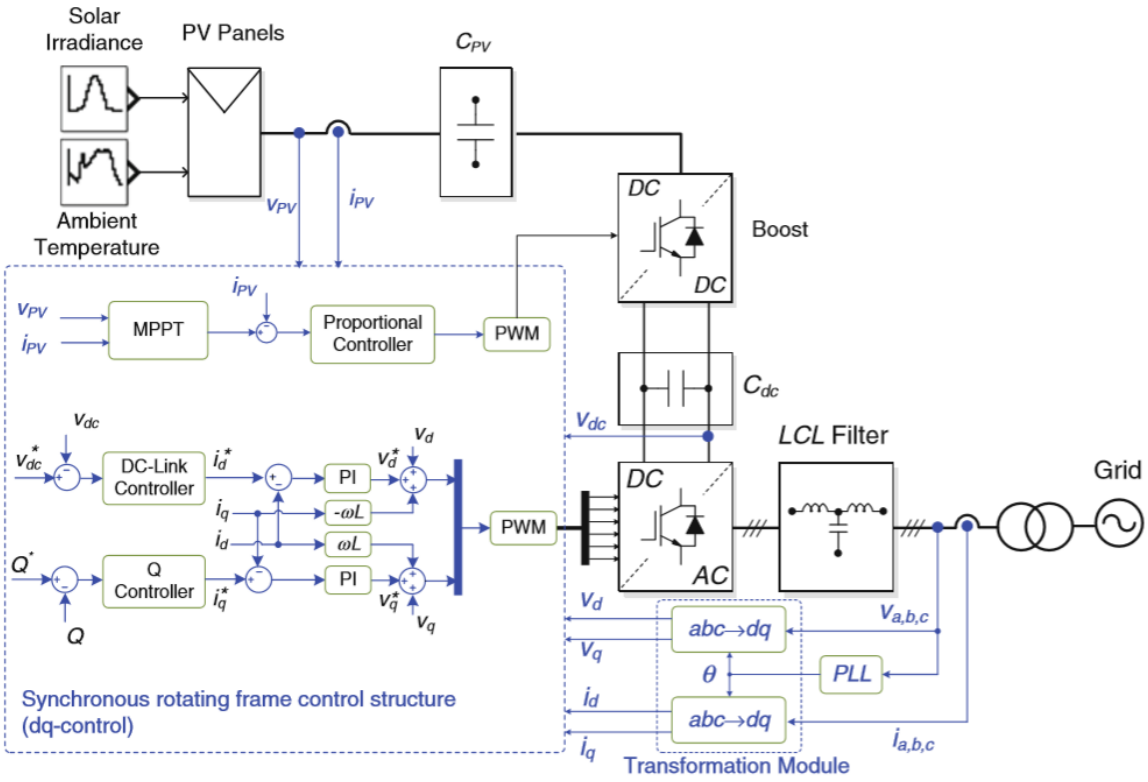

Figure 1.22- Basic control structure of a three-phase grid-connected PV system.

2. The Standard Model for PV Generation

Planning and managing large interconnected power systems is a complex task that requires daily analysis and computer simulations. Simulation studies are essential to estimate the potential impact of credible, and sometimes extreme, emergency scenarios and to assess the ability of the power system to withstand such events while remaining stable and safe. In addition, through the simulation of disturbance events it is possible to observe the performance and consequently develop appropriate operational strategies to mitigate the problem. To help ensure correct and reliable assessments and to minimise capital investment, models that reasonably represent the actual performance of the equipment in the simulations are required. With the increasing penetration of renewable energy plants into the grid, it is necessary to consider also their models in stability analyses. In particular, there are two attributes of variable generation that can impact the reliability of the bulk power system if not properly addressed:

- Variability: the power generated depends on the availability of the primary source causing fluctuations in plant production.
- Uncertainty: the variable power output is less predictable than conventional generation.

From a modelling standpoint for power system studies, the development of generic and standard PV models is presently a topic for further research. In fact, no agreed and generic standard models exist for photovoltaic systems, except for some user-written manufacturer specific models designed by various PV producers. Unfortunately, this latter category requires significant input data/parameters not free available to general public and can lead to model incompatibilities among different PV manufacturers. However, the Renewable Energy Modeling Task Force (REMTF) of the Western Electricity Coordinating Council (WECC) developed an excellent document titled ‘WECC Solar Plant Dynamic Modeling Guidelines’ [17], suitable for transient stability studies on the impact of PV plants in the network. This paperwork has been realized in accordance with North American Electric Reliability Corporation (NERC) standards [19] in order to fulfil the urgent need of defined PV model structure publicly available and not specific to any particular design.

2.1 Preamble

The North American Electric Reliability Corporation (NERC) is a not-for-profit international regulatory authority whose mission is to assure the reliability of the bulk power system (BPS) in North America. It is responsible for:

- developing and enforcing reliability standards
- annually evaluating seasonal and long-term reliability
- monitoring the BPS
- educating and certifying staff in the sector.

NERC has been certified by the Federal Energy Regulatory Commission (FERC) as the Electric Reliability Organization (ERO) for North America and assesses adequacy on the national BPS. The latter is divided into eight Regional Entity (RE), including WECC, which ensures the system security of their portions of the BES in compliance with the standards. In order to distribute key practices and information on the system reliability, guidelines, representing the collective experience, expertise, and judgment of the industry, have also been developed by NERC. These papers are a collection of recommendations and considerations but do not provide binding rules. They are strictly voluntary and designed to help develop practices to support system security.

2.1.1 Generic Renewable Energy System Models

With the increasing of renewable energy penetration, the NERC Modeling, Data, and Analysis (MOD) Reliability Standards required Regional Entities to create appropriate procedures for model development aimed at analyzing the steady-state and dynamic performance of the power system. Specifically, standard, valid, generic and non-confidential models were required to perform power-flow, short circuit, and stability studies necessary to ensure bulk power system reliability. With this purpose, the Renewable Energy Modeling Task Force (REMTF) of the WECC provided tested and validated models according to WECC guidelines, available as standard-library and listed in the ‘WECC Approved Dynamic Model Library’ [41]. As a continuation of the WECC effort, the Institute of Electronic and Electrical Engineers (IEEE) and the International Electrotechnical Commission (IEC) Working Groups collaborated for the validation and

consequently dissemination of some variable generation models. For example, today the four different types of wind turbine models are documented in IEC Standards. However, although generic models for PV plants have been approved under the WECC Modeling and Validation Working Group, there is no currently IEC standard on PV modelling.

2.2 WECC Generic Model for PV plant

The document is presented as a specification for generic large-scale ($> 10\,MW$) solar photovoltaic (PV) system positive-sequence dynamic models for use in bulk system transient stability simulations in accordance with NERC MOD standards. In order to capture the most important dynamic characteristics of the system, the model is defined as a single equivalent unit represented a Central Station PV System with a central Point of Interconnection (POI) at the transmission level.

2.2.1 General Requirements

The requirements and limitations of the model are summarized below:

- It shall be non-proprietary and accessible to transmission planners and grid operators.
- It shall provide a reasonably representation and dynamic electrical performance of PV power plants at the point of interconnection with the network.
- It shall be suitable for studying external electrical disturbances such as balanced transmission grid faults, loss of generation and variable load.
- The model is not intended for the study of solar radiation transients: the available solar power is assumed constant through the duration of the simulation.
- Differences among specific inverter and/or plant controller shall be represented by appropriate selection of model parameters and feature flags.
- A solved power flow shall be used to initialize the model.
- The model shall be valid for analyzing electrical phenomena in the frequency range of zero to approximately 10 Hz. Therefore, electromagnetic phenomena due to the high inverter switching frequency are not considered.
- The model shall incorporate protections by means of external modules to accomplish the PV generator tripping.

- The simulations performed typically cover a 20-30 second time frame, with integration time steps in the range of 1 to 10 milliseconds.
- External reactive compensation and control equipment, beyond the capabilities of the PV inverters, shall be modelled separately.
- Performance shall be valid within a range of 25% to 100% of rated power.

2.2.2 Modeling Assumptions

The main assumption resulting from the investigations and discussions carried out by WECC REMTF is to ignore the dynamics on the DC side of the inverter, which includes the dynamics of the PV array, the inverter DC link and the voltage regulator. In fact, consultations with various manufacturers have shown that the time constants associated with these dynamics may, in some cases, be too short to ensure stability and reliability in the simulation phase. Moreover, it has been established that aggregated PV generation can be represented at a suitable transmission node by an equivalent generator. A block diagram illustrating an overview of PV power plant control is shown in Figure 2.1.

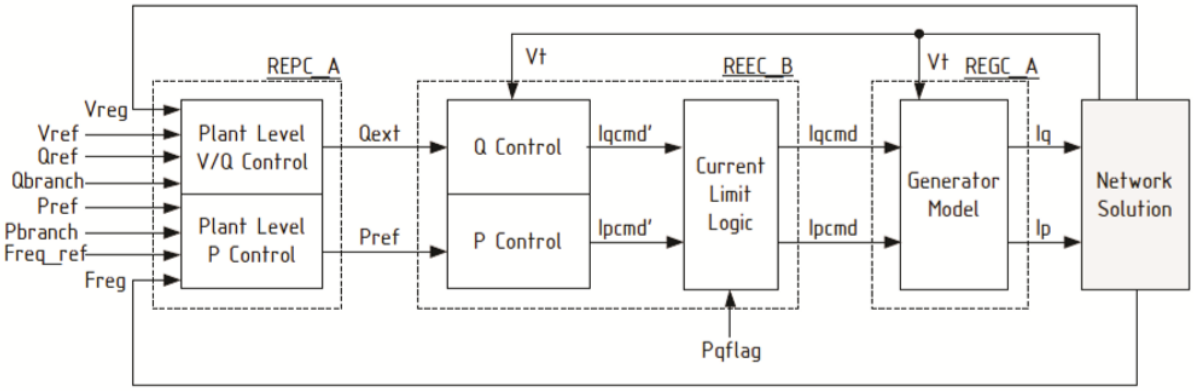

Figure 2.1- Block diagram representing a central station PV power system.

The overall model structure consists of the assembly of three major blocks defined separately in the 'WECC Approved Dynamic Model Library':

1. (REGC_A): generator model.
2. (REEC_B): electrical control model.
3. (REPC_A): plant-level active and reactive power control (optional).

These modules do not include inverter or plant protection. Moreover, the model parameters are expressed in per unit of the generator MVA base, which must be adjusted to scale the dynamic model to the size of the plant.

2.2.3 Subsystem Models

For large-scale PV plants intended for general bulk system planning studies, WECC approved the use of a generic dynamic model consisting of plant controller, electrical controls and grid interface modules. The detailed structures are represented below.

REGC_A Generator Interface

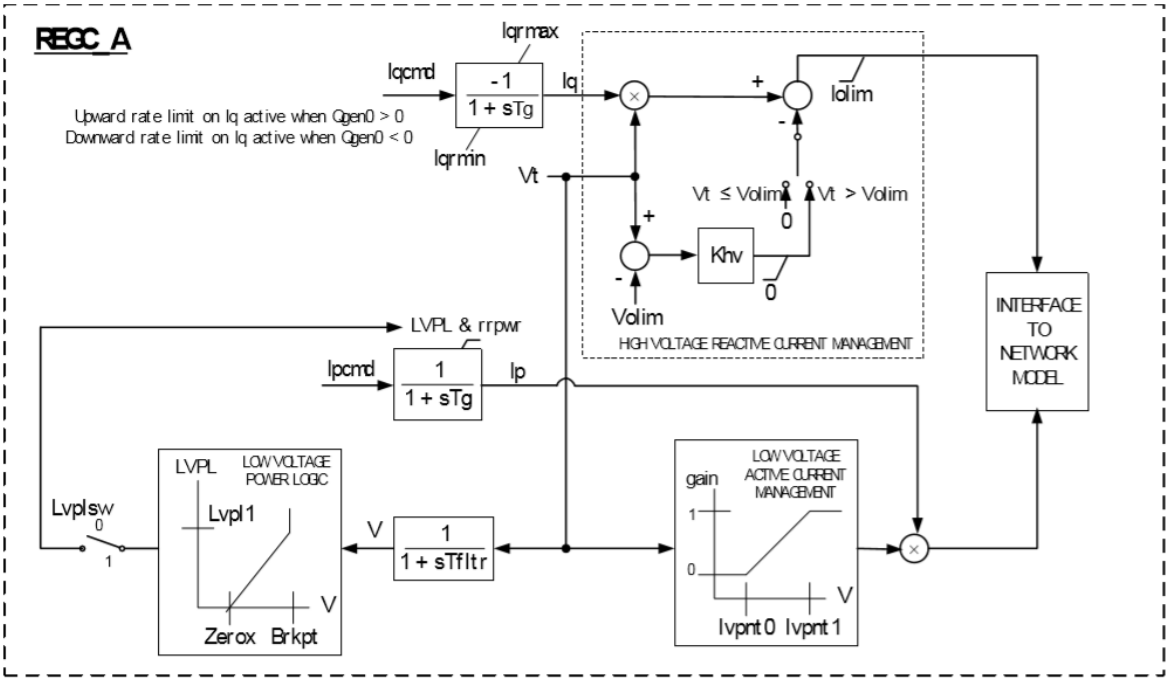

Figure 2.2- REGC_A model block diagram.

This module represents the Generator/Inverter interface with the grid. It therefore injects real and reactive current components into the network based on the set points output (I_{qcmd}, I_{pcmd}) from the control block. Real and Reactive current management are also provided in this stage in case of low or high voltage events, aimed at increasing the reactive power injection and absorption respectively. A more detailed description of these processes is given in section 5.4.

REEC_B Electric Control

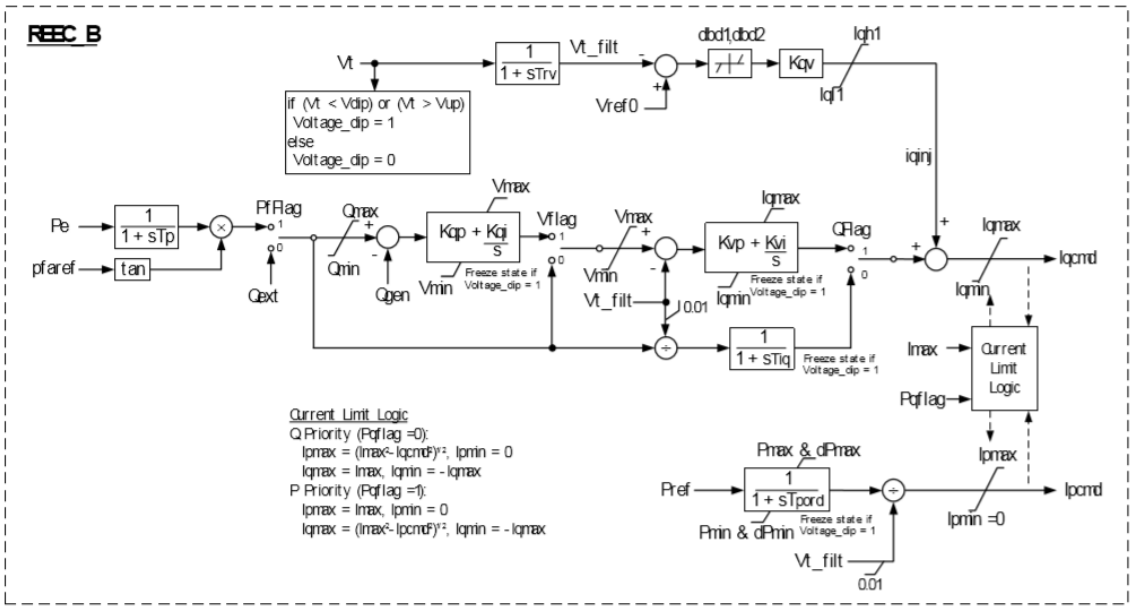

Figure 2.3- REEC_B model block diagram.

This block is used to represent the electrical controls of the inverters. It acts on the active and reactive power reference (Q_{ext}, P_{ref}) given by the REPC_A module and consequently provides the real and reactive current commands (I_{pcmd}, I_{qcmd}) to the REGC_A block by means of proportional integrators (PIs) and closed loops. By setting the appropriate switches, various control combinations are possible:

- Reactive power control through constant power factor.
- Reactive power regulation by a linear control.
- Reactive power control via a cascaded set of PI regulators.
- Voltage control through a PI regulator.

The model also incorporates a current limit logic block in order to enforce over-current protection, which allows a user-selectable priority between active and reactive component. REEC_B provides also the implementation of the freeze control logic aimed at limiting the impact of short disturbances, during the transient, through freezing the states that control the output power. Moreover, this stage offers the detection of grid faults through voltage monitoring on the inverter side, involving additional reactive injection (I_{qinj}) to counteract

under- and over-voltage conditions. The mechanisms developed in the REEC block are widely described in paragraph 5.3.

REPC_A Plant Level Control

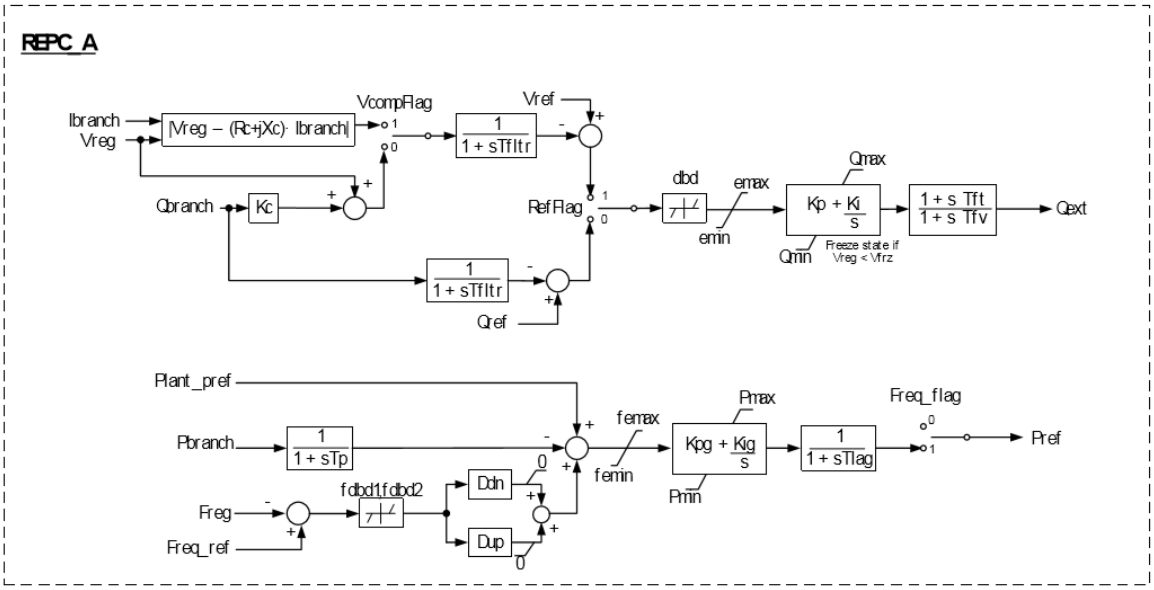

Figure 2.4- REPC_A model block diagram.

REPC_A is an optional model that constitutes the plant controller module, used when plant-level control of active and/or reactive power is desired. It coincides with the configuration proposed for the Type 3 and Type 4 generic wind turbine models and shall include:

- Closed loop voltage regulation at a user-designated bus.
- Closed loop reactive power regulation on a user-designated branch.
- A signal response to frequency deviation at a user-designated bus using a droop control, valid both for over- and under-frequency events. The droop response shall be applied to active power flow on a user-designated branch.

This block provides the input reference of active (P_{ref}) and reactive power (Q_{ext}) for the REEC_B module, based on the reference voltage (V_{ref}), the real ($Plant_{\_pref}$) and the reactive power (Q_{ref}) set by the user. A full description of the functionalities available in the REPC_A block is given in section 5.2.

3. The Grid Code Requirements

The power sector is globally accelerating its transition towards a sustainable energy regime. A set of grid codes including connection, operating, planning and market codes are therefore essential for a successful integration of Variable Renewable Energy (VRE) into electricity network. They provide the rules for the power system and energy market management ensuring operational stability, security of supply and well-functioning wholesale markets. Although renewable sources pose challenges that contrast with conventional generation, technological innovations in parallel with the development of appropriate grid codes have allowed VRE generators to comply with grid requirements for helping network stability. For example, they can now provide:

- reactive power for voltage control
- active power for frequency regulation
- network support during faults.

Grid requirements for integration of renewable energy into electric system are usually supported by international standards developed by the International Electrotechnical Commission (IEC) and the Institute of Electrical and Electronics Engineers (IEEE). Although each country follows its own grid codes specific to its needs, many requirements can be harmonised between different TSOs thanks coherent frameworks provided by regional network codes. In Italy the national grid code is issued by Terna S.p.A, the Italian TSO, which adopted and extended the European code produced by the European Network of Transmission System Operators (ENTSO-E).

3.1 ENTSO-E

ENTSO-E stands for "European Network of Transmission System Operators for Electricity" and is an association of 43 TSOs from 36 European countries. It aims at developing an efficient electricity system and energy market capable of combining sustainability and innovation, while ensuring a safe and reliable power supply to users. ENTSO-E pursues these objectives by supporting collaboration among TSOs, implementing European network development plans and providing guiding principles for the coordination of TSOs' R&D activities. ENTSO-E is in charge of developing and

revising the European Network Codes, based on a list of annual priorities defined by the European Commission. European Network Codes can be defined as a set of rules applied to several areas of the energy sector for "cross border" issues in relation to:

- connection to the network (Connection Network Codes),
- market integration and congestion management among networks (Market Network Codes),
- security and interoperability of transmission networks (System Operation Network Codes).

3.2 Terna S.p.A.

Terna - Rete Elettrica Nazionale S.p.A. is the Italian TSO, responsible in Italy for the transmission and dispatching of electricity on the High Voltage (HV) and Ultra High Voltage (UHV) grid throughout the country. Among its functions, Terna provides the Grid Transmission, Dispatching, Development and Security Code (the so-called Grid Code), which regulates the procedures for connection, management, planning, development and maintenance of the national transmission grid, as well as those for dispatching and measuring electricity. The code is also integrated with continuously updated attachments that include the connection criteria, the technical, functional and control specifications of the generation units connected to the network.

3.3 Italian Grid Code for Photovoltaic Plants

The requirements that a Photovoltaic Power Plant connected to the National Transmission Grid must comply with are listed in attachment A.68 of the Italian Grid Code, updated in December 2019 by Terna S.p.A [31]. This document applies to Photovoltaic Installations connected directly to the National Transmission Grid or indirectly to the National Transmission Grid through a portion of the network with a nominal voltage equal to or greater than 110 kV. It provides a description of the mandatory requirements for the Photovoltaic connection in terms of general performance, regulation and functionality, the main features of which are summarized in the following sections.

3.3.1 Operating Limits

The photovoltaic power plant must remain in parallel even in emergency and network recovery operations. In particular, in any load condition, the plant has to maintain the connection to the HV grid for voltage values at the delivery point included in the following range:

$$85\%\ V_n \leq V \leq 115\%\ V_n \tag{3.1}$$

with V_n the nominal voltage at the point of interconnection (POI).

In terms of frequency, the operating range is:

$$47{,}5\ Hz \leq f \leq 51{,}5\ Hz \tag{3.2}$$

and the operation without disconnection must be guaranteed for frequency rate of change up to 2,5 Hz/s evaluated at least over 5 cycles (100 ms).

3.3.2 Insensitivity to Voltage Variations (FRT)

Fault ride through (FRT) mode requires inverters to maintain connection to the grid during external fault events by complying with the under-voltage and over-voltage profiles shown in Figure 3.1.

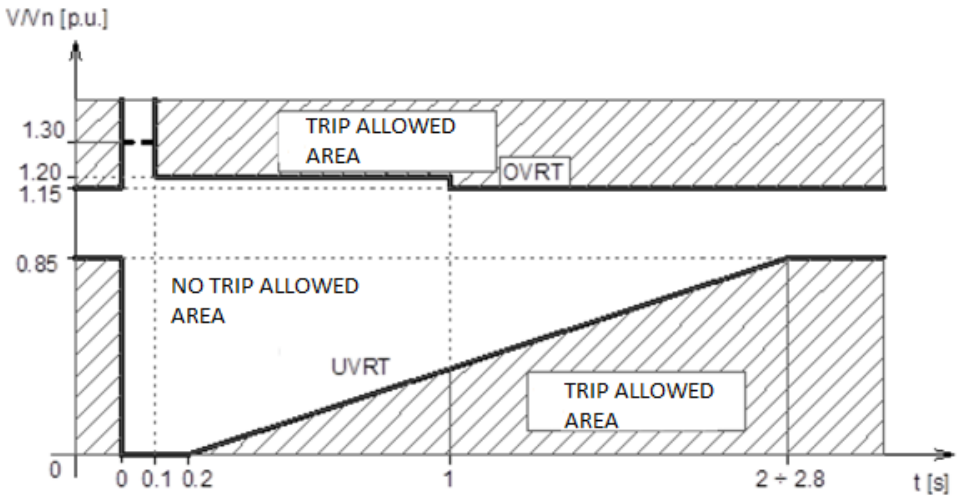

Figure 3.1- FRT characteristic at the interconnection point for Photovoltaic Power Plants.

The disconnection logic is applied both for symmetrical and dissymmetrical faults and it is activated when at least one of the three concatenated measured potentials at the POI exceeds in depth (or height) and in duration the hole (or peak) of permitted voltage. The following requirements are indicated:

- In the first $100\,ms$ the upper limit (not less than 130 % V_n) is defined by the manufacturer.
- The end point of the inclined segment in the UVRT characteristic corresponds to $2\,s$ for $132/150\,kV$ and $2.8\,s$ for $220\,kV$ at the POI.
- The complete cancellation of the voltage must be sustained for $200\,ms$.
- Within the not allowed disconnection area, for voltage values lower than $0.85\,V_n$ or higher than $1.15\,V_n$ no strict requirements are imposed on the active and reactive power supply. However, when the voltage returns within this range, the pre-transient power values must be restored within $500\,ms$.

3.3.3 Voltage and Current Disturbances

Due to the high switching frequency of the inverters, interference and disturbances can be generated, causing a drop of network performances. Therefore, current and voltage harmonic distortion limits are defined.

Harmonic Voltage Distortion

The maximum total harmonic distortion of the voltage (THD_V) at the connection point, calculated up to the $50th$ harmonic, must respect the following limits:

$$THD_V \leq 2{,}5\% \text{ for } V_n < 220\,kV \tag{3.3}$$

$$THD_V \leq 1{,}5\% \text{ for } V_n \geq 220\,kV \tag{3.4}$$

Harmonic Current Distortion

The following tables, for $V_n \leq 110\,kV$ and $V_n > 110\,kV$, are based on the IEEE 519 standard and show the values of the individual harmonic currents and the maximum total harmonic distortion level (THD_I) calculated up to the $50th$ harmonic. I_{sc} and I_n indicate the maximum short-circuit current and the nominal current at the POI respectively.

I_{sc}/I_n	$3 \leq h < 11$	$11 \leq h < 17$	$17 \leq h < 23$	$23 \leq h < 35$	$35 \leq h \leq 50$	THD_I
< 20	2	1	0,75	0,3	0,15	2,5
$< 20 < 50$	3,5	1,75	1,25	0,5	0,25	4
$50 < 100$	5	2,25	2	0,75	0,35	6
$100 < 1000$	6	2,75	2,5	1	0,5	7,5
≥ 1000	7,5	3,5	3	1,25	0,7	10

Table 3.1- Harmonic current limits for systems with Vn ≤ 110 kV.

I_{sc}/I_n	$3 \leq h < 11$	$11 \leq h < 17$	$17 \leq h < 23$	$23 \leq h < 35$	$35 \leq h \leq 50$	THD_I
< 25	1	0,5	0,38	0,15	0,1	1,5
$< 25 < 50$	2	1	0,75	0,3	0,15	2,5
≥ 50	3	1,5	1,15	0,45	0,22	3,75

Table 3.2- Harmonic current limits for systems with Vn > 110 kV.

3.3.4 Regulation and Control Systems

The increase in electric power produced by photovoltaic systems has made their contribution important to grid support functions, traditionally performed by conventional rotating machines. Historically, electricity system operators have seen photovoltaic systems as potential sources of problems due to intermittency and lack of controllability. However, the flexibility achieved by today's electronic power inverters enables grid-friendly features, including:

- Production control through active power injection
- Volt-var control
- Frequency regulation

Production Control

The power plant must guarantee controllable active power injection, providing temporary restrictions or complete cancellation of production within a maximum of 15 minutes after communication. The generation is reduced by steps with a maximum width of 5% of installed power and can be directly imposed by the operator via a remote signal. On the

other hand, when starting or reconnecting the power plant to the grid, the injection must respect a maximum positive gradient of 20% per minute of the photovoltaic rated power in order to avoid oscillatory phenomena on the power flows.

Reactive Power Regulation

The grid-connected photovoltaic plant must participate in the voltage control of the network through the reactive power regulation, based on the characteristic curve $Q = f(\Delta V)$, depicted in Figure 3.2.

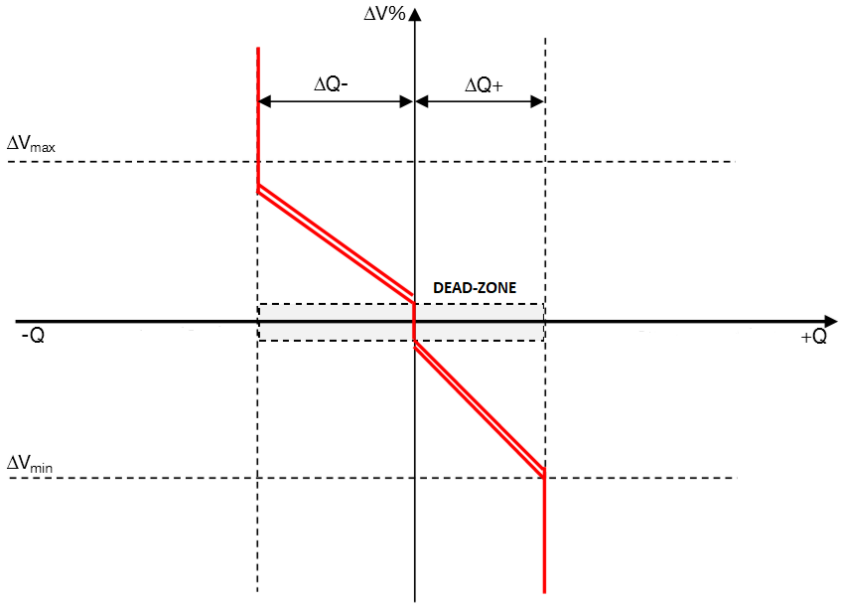

Figure 3.2- Characteristic curve Q = f(ΔV).

The control system uses a grid side reference voltage value (V_{ref}), set by Terna, variable within the range:

$$95\%V_n \leq V_{ref} \leq 105\%V_n \qquad (3.5)$$

The difference between the set-point and the measured voltage value determines the amount of reactive power released or absorbed by the system. When voltage deviation occurs, the generation unit must provide 90% of the required reactive power variation within $2\,s$ and 100% within $5\,s$. In order to limit excessive mobility around the equilibrium point the regulator provides an insensitivity band called dead-zone. The implementation of control requires also a proportional/integral closed-loop configuration to avoid instability in the regulation cycle, represented in the block diagram of Figure 3.3.

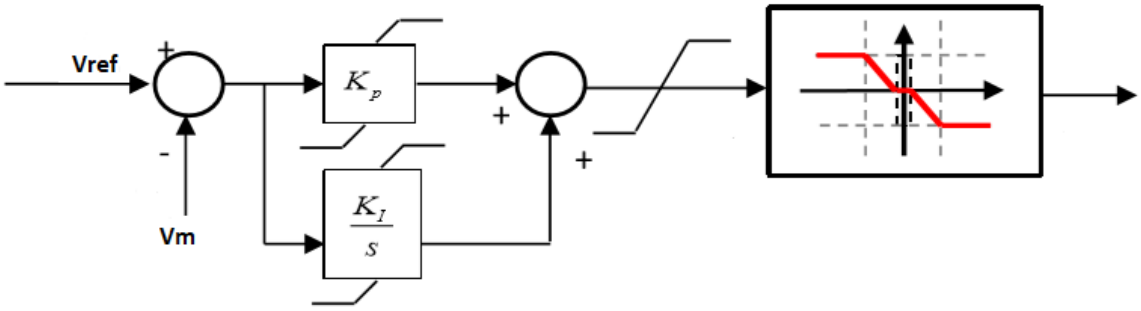

Figure 3.3- Block diagram for reactive power regulation.

Parameters will be optimized to obtain a sufficiently rapid response without overshoot or oscillatory trends.

Frequency Regulation

The grid frequency control is achieved by active power regulation according to the steady-state characteristic curve displayed in Figure 3.4.

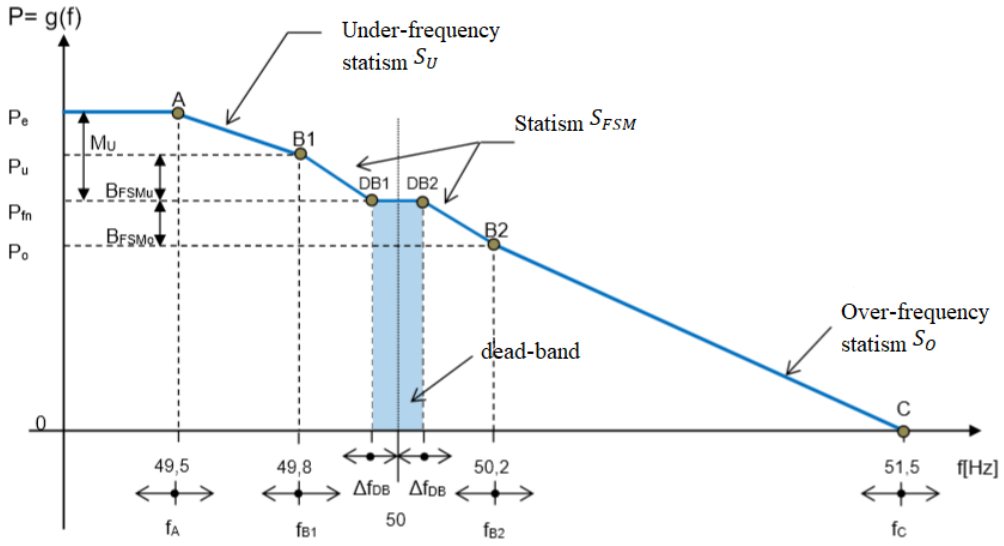

Figure 3.4- Characteristic curve P = g(f).

The diagram shows three different areas of regulation:

- around nominal frequency: Frequency Sensitive Mode (FSM)
- during under-frequency event: Limited Frequency Sensitive Mode Under Frequency (LFSM-U)
- during over-frequency event: Limited Frequency Sensitive Mode Over Frequency (LFSM-O)

Frequency Sensitive Mode (FSM)

Around the nominal frequency, in the adjustable range $[f_{B1} \div f_{B2}]$, photovoltaic systems are designed to provide primary frequency regulation. This mode presents two control bands BFSM_U and BFSM_O, respectively under- and over-frequency zones between 1.5% and 10% of the nominal available power, within which the system must remain connected. The regulation must be carried out within $2\,s$ according to an S_{FSM} droop line with a settable dead band Δf_{DB} in the range $[0 \div 500\,mHz]$.

Under-Frequency Regulation (LFSM-U)

In sub-frequency transients, which occur when f_{B1} threshold is exceeded, photovoltaic plants must support the grid by increasing the power fed into the network by following the S_U statism.

Over-Frequency Regulation (LFSM-O)

Photovoltaic systems must provide support in over-frequency transients by reducing the power fed into the grid according to the amount of frequency error and the droop S_O. This mode is activated for frequencies between f_{B2} and f_C (in Figure 3.4) and it cancels the input power for values reaching $51.5\,Hz$.

Table 3.3 shows the points of the $P(f)$ regulation curve with their range of calibration.

Points of the curve	Calibration range $[Hz]$	
A	f_A	$47{,}5 \div 50$
B_1	f_{B1}	$49{,}5 \div 50$
B_2	f_{B2}	$50 \div 50{,}5$
$DB_1 - DB_2$	Δf_{DB}	$0 \div \pm 0{,}5$
C	f_C	$50{,}2 \div 51{,}5$

Table 3.3- Points of P(f) characteristic.

The developed photovoltaic model may also be used in a simplified way to represent photovoltaic aggregates connected to the LV/MV lines. In this case, reference is made to attachment A.70 for distributed generation, also released in the grid code by Terna S.p.A.

4. Modelling and Simulation Environments

The current scenario of the electricity system implies an increasingly complex management of the network. Grid security issues are becoming more and more important due to the continuous penetration of renewable energy sources, diffusion of new controllable devices such as HVDCs and arduous construction operations for new overhead power lines. In recent years, initiatives of data exchange among different European countries have emerged in order to improve coordination of the various Transmission System Operators (TSOs) and provide a more accurate control of the European network security. In particular, the Common Information Model (CIM) is one of the most relevant data formats for the interchange of information among TSOs on their transmission system models. Although the information exchange is currently mainly focused on the static model of the network, a growing interest also for dynamic models' consideration is developing. In order to perform coordinated dynamic simulations among the various TSOs, Modelica® language has been introduced by ENTSO-E as a standard for the network models interchange. CESI S.p.A as consultant of the Italian TSO Terna S.p.A has adopted the Modelica® language for the description of the models inside its dynamic network simulator TESEO. In this context, the 'BasicPowerSystem' library, composed of passive elements and dynamic generators, has been extended in OpenModelica® in the last two years. The object of the activity proposed by CESI is the development of a dynamic model of Photovoltaic System aimed at enriching the 'BasicPowerSystem' library to be included in the CESI's network simulator for the execution of voltage and transient stability studies.

4.1 Adoption of Modelica® in dynamic CIM models

The CIM project was introduced by ENTSO-E with the aim of creating a common model able to represent electric transmission networks and capable of supporting coordinated grid management in both normal and emergency situations. In particular, Common Grid Model Exchange Standard (CGMES) was developed to facilitate the interchange of operational and grid planning data among TSOs, including information on:

- equipment (parameters of grid elements)
- topology (grid configurations)

- power system state variables (results of load flow simulations)
- steady state hypothesis (load and generation values)

In addition, some dynamic prototypes have been developed according to IEC standards. However, the designing features used for dynamic formats had the following limitations:

- dynamic models were not executable from different simulation platforms
- the sharing involved only parameters and predefined structures instead of the equations/logics that govern them.

It was therefore appropriate to introduce the description of CIM models in Modelica® language to ensure unambiguous modelling for dynamic simulation of electrical systems, as it guarantees standardized frameworks based on equations and clear separation between models and numerical solvers.

4.2 The Modelica® Language

Modelica® is an object-oriented language for modelling of large, complex, and heterogeneous physical systems, designed to support effective library development and model exchange. It is a non-proprietary language defined by the non-profit Modelica Association, which includes Tool Developers, Researchers and Users.

Figure 4.1- Modelica® language logo.

Thanks to its multi-domain capability it offers the possibility of combining different application areas (electrical, mechanical, hydraulic, thermodynamic, etc...) resulting in a suitable solution for model development in power systems environment. Modelica® mathematically defines models through differential, algebraic and discrete equations, allowing graphical and textual description of them. It thus supports both 'high level' modelling, by composition of basic elements from standard library, and 'low level'

development by writing equations directly in the code. Unlike many traditional programming languages (e.g. C, Pascal, etc...), Modelica® is not based on assignment instructions, as input and output variables are not decided a priori in the code. The physical and logical parts of the model are thus defined through equations and algorithm respectively and the input/output causality is not fixed but decided during the solution calculation. This approach is called 'a-causal modelling' and is one of the main advantages of the Modelica® language, as it increases the flexibility in computation. The most important features of the Modelica® language can be summarized as follows:

1) *a-causality*: equations are written in declarative notation without setting a priori input and output variables, which will be directly determined by the language compiler when calculating the solution.
2) *code transparency*: the equations are similar to those of mathematical-physical formalism and therefore easy to understand and modify.
3) *encapsulation:* different components can interact through compatible interfaces called ‘pins’.
4) *inheritance*: the models can be organized through a hierarchical structure in order to obtain more complex configurations, greatly simplifying their development and management.

In addition, the adoption of Modelica® introduces a clear separation between the modelling part and the numerical solver, thus promoting a "non-ambiguous" models exchange between the various TSOs in order to increase the reliability of network simulations. A peculiar characteristic of Modelica® language is its "tool independency", i.e. it can be supported by different tools, both commercial and open source. The OpenModelica® environment has been adopted as the tool for the Photovoltaic model description.

4.3 The OpenModelica® Environment

OpenModelica® is an open source tool used for modelling and simulation environment, based on Modelica® language. It consists of several interconnected subsystems aimed at processing Modelica® code allowing the generation of C/C++ code, which will be used for the simulation itself by connecting the system of equations to the numerical solver. The

simulations can take place directly in the Modelica® environment, using graphic editors such as OMEdit, or alternatively by interfacing the compiled C/C++ code with a different solver through Functional Muck-up Interfaces (FMI). Many versions of OpenModelica® exist and are continuously updated, even if the new generations do not always ensure the correct functioning of the models implemented in previous versions. Version 12 has been chosen for the photovoltaic model, as it is compatible with the Dyana dynamic simulation environment.

4.3.1 The OMEdit Interface

The Photovoltaic System has been modelled in OpenModelica Connection Editor (OMEdit), which is the graphical user interface for creating, editing, and simulating graphical models in OpenModelica.

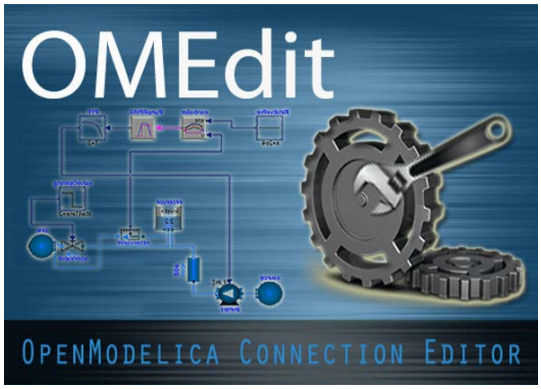

Figure 4.2- OMEdit splash screen.

The model has been developed starting from the basic components of both the Modelica Standard Library provided by OMEdit and the 'BasicPowerSystem' library extended by CESI. OMEdit provides a modelling window where users can easily build the model by dragging the library components into it and consequently connect them in order to obtain the desired scheme. Every single component belonging to the library is described by a more or less complex code that represents it. Therefore, the final scheme displayed in the OMEdit graphic window will also be represented by a text code, easily accessible and editable. An example, is shown in Figure 4.3.

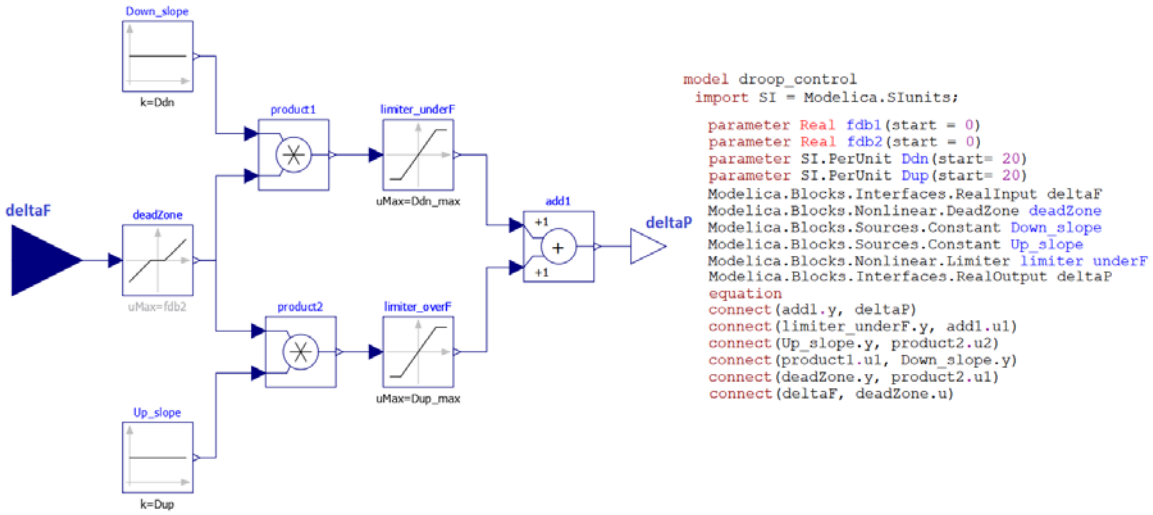

Figure 4.3- Graphical and textual representation of a model in OpenModelica.

Each model created can then be compacted within a single block and interact with other elements through input/output interfaces, as depicted in Figure 4.4.

Figure 4.4- Icon view of the model.

This type of operation shows an intuitive view of the final configuration resulting from the interconnection of the blocks previously implemented, simplifying considerably the development and management of even very complex models. The graphical interface also allows the user to easily set the parameters of each component by double clicking on the corresponding icon, thus promoting the use of common models adapted to their needs through the choice of appropriate values. The simulation options for each model are also stored inside the OMEdit data structure. Successful simulation of model produces the result file which contains the instance variables that are candidate for plotting. The list of such parameters is shown in the Variables Browser and can be plotted putting a check mark in the relative check box. The first step for the Photovoltaic model validation has been done via simulations in OMEdit, through the use of ‘source’ blocks as inputs for the implemented system. Subsequently, for the final network connection test, the simulation

tool TESEO/Dyana implemented by CESI has been adopted. In this case, the Functional Muck-Up Interface provided by OMEdit was necessary.

Functional Muck-up Interface

The Functional Mock-up Interface allows export of pre-compiled models, i.e., C-code or binary code, from a tool for import in another tool, and vice versa, providing the possible exchange of dynamic models between different types of simulation tools. In order to connect the model to the test network implemented in the TESEO/Dyana tool, the creation of a Functional Mock-up Units (FMU) file based on the IMF interface was necessary. FMU code can be automatically generated from Modelica® models, using the FMI-export functionality. The purpose of the FMU is to allow the simulation of the model by keeping only the list of model variables, its equations and additional data (icon associated with the model, documentation, maps and tables) but does not report the block structure and connections of the original model.

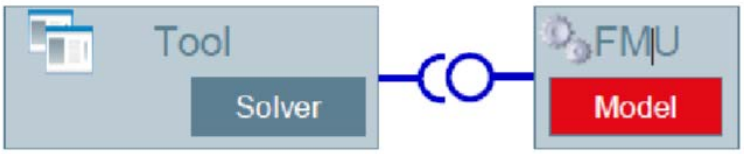

Figure 4.5- FMI for model exchange.

4.4 The TESEO Environment

The final tests for the model validation have been done in the 'Terna Sistemi Elettrici Ottimizzati' application (TESEO), which is a tool for network calculation developed by CESI for Terna. The general architecture contains a database, which acquires data from Dava/Dadir (Italian Electrical network description formats) and from the CIM source. The system is based on a computing logic for steady-state network calculations and supports several functions including:

- Editing of parameters and network structure.
- Determination of a new grid steady-state from an initial assigned state (e.g. load flow calculation).
- Verification of the grid status (e.g. n-1 security).
- Support for the analysis of the network situation (list of out-of-service items).

Moreover, through the graphical interface the system provides the visualization of the grid structure, in which generators, loads, lines, transformers and voltage regulators can be easily distinguished, together with a user-accessible mask of editable values. In order to achieve dynamic simulation, 'Dynamic Analyser' module (Dyana) has been integrated in TESEO by CESI. The two systems share the database, part of the graphical interface and applications with common functionality (such as reading Dadir/Dava/CIM formats). In addition, Dyana includes all the activity necessary to handle dynamic simulations (modules for acquisition and initialization of dynamic models, solver of equations in dynamic mode, panel for dynamic commands, etc...).

4.4.1 Dynamic Calculation in Dyana System

Each component of the simulated network provides its own characteristic equations. The calculation module assembles them into a single system of differential/algebraic equations (DAE) involving the exchange of variables between the various modules. The DAE system is consequently discretized and transformed into a system of algebraic equations to be solved by the Newton-Raphson method. The entire dynamic model is divided into two distinct components:

- Generators/Loads: they are called 'injectors' and provide nodal currents I_i, I_j as output variables (real and imaginary part).
- Power Grid: it receives as input the nodal currents and calculates as output the nodal voltages V_i, V_j (real and imaginary part), which are in turn passed to the injectors as input variables.

The subscripts 'i' and 'j' represent the respective nodes of the grid, as shown in Figure 4.6.

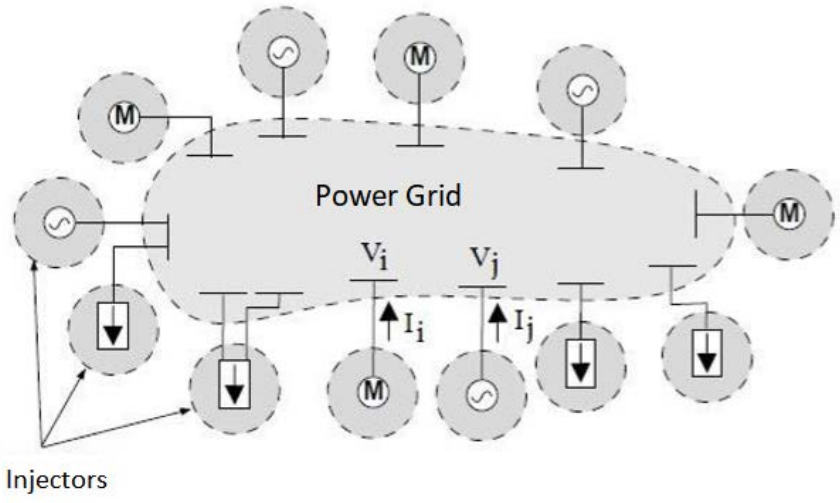

Figure 4.6- General structure of the dynamic model.

The network, directly implemented within the calculation module, includes power lines and transformers that connect the system nodes according to an assigned topology. In terms of calculation it can be considered a matrix of admittances Y that relates nodal currents and voltages through the known equation:

$$I = Y * V \tag{4.1}$$

Generator Modelling

As mentioned above, the mathematical model of the generator is developed as an FMU module. In the graphic construction of the FMU, it is important to uniquely identify the input and output variables of the model using the appropriate I/O interfaces of the Modelica® standard library. The Figure 4.7 shows the main interface of Photovoltaic System model developed in OMEdit.

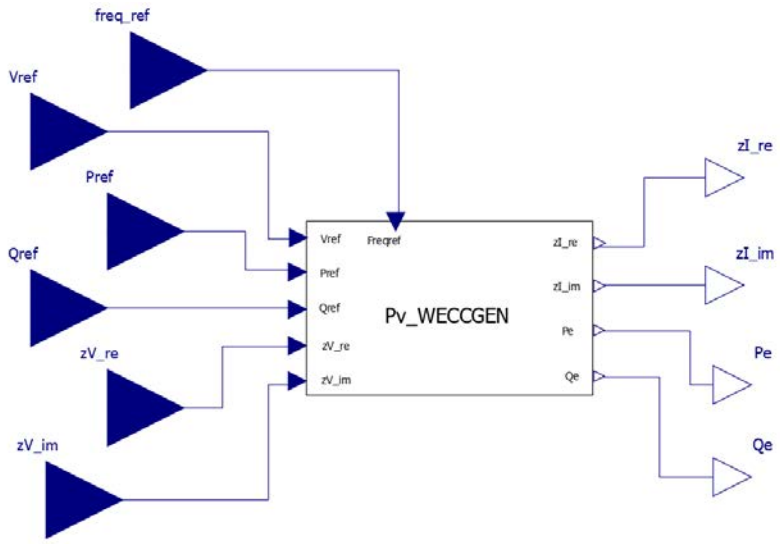

Figure 4.7- Photovoltaic System model.

To allow the automatic connection among generator and network input/output variables, the names assigned to I/O interfaces must be standardized. The implemented model is defined by the following input parameters:

- $freq\_ref$: reference grid frequency
- $Vref$: reference grid voltage
- $Pref$: reference active power
- $Qref$: reference reactive power
- zV_re: real part of the voltage grid at the Point Of Interconnection (POI)
- zV_im: imaginary part of the voltage grid at the POI

and output variables:

- zI_re: real part of the nodal current injected
- zI_im: imaginary part of the nodal current injected
- Pe: injected active power
- Qe: injected reactive power

Calculation Procedure

The procedure for a dynamic simulation can be summarized in the following steps:

A. Load flow

A first load flow analysis is carried out by a specific TESEO function in order to obtain reference parameters of injected power and nodal voltage at the point of interconnection with the grid ($P_{loadflow}$, $Q_{loadflow}$, $V_{mod\_loadflow}$, $V_{arg\ \_loadflow}$).

B. Initialization

The result data are set as initialization of the dynamic models:

$$P_e = P_{loadflow} \tag{4.2}$$

$$Q_e = Q_{loadflow} \tag{4.3}$$

$$V_{mod} = V_{mod\_loadflow} \tag{4.4}$$

The internal state-variables of the model are also estimated by zeroing the derivatives of the DAE system.

C. Calculation of the transient:

Finally, the dynamic simulation is launched using as initial states the values previously calculated. Appropriate commands allow to change the model input references and signals in order to simulate load variations and grid failures.

5. The Photovoltaic Model

The implemented dynamic model for large-scale PV systems follows the approach provided in the report released by the National Renewable Energy Laboratory (NREL) [18]. This document is based on the guideline written by WECC [17], in accordance with NERC standards [19].

5.1 Introduction

The model is based on a three-phase inverter, whose control architecture is characterized by three main blocks:

1. the generator model (REGC_A),
2. the electrical control model (REEC_B),
3. the plant-level active and reactive power control (REPC_A),

arranged in the following configuration.

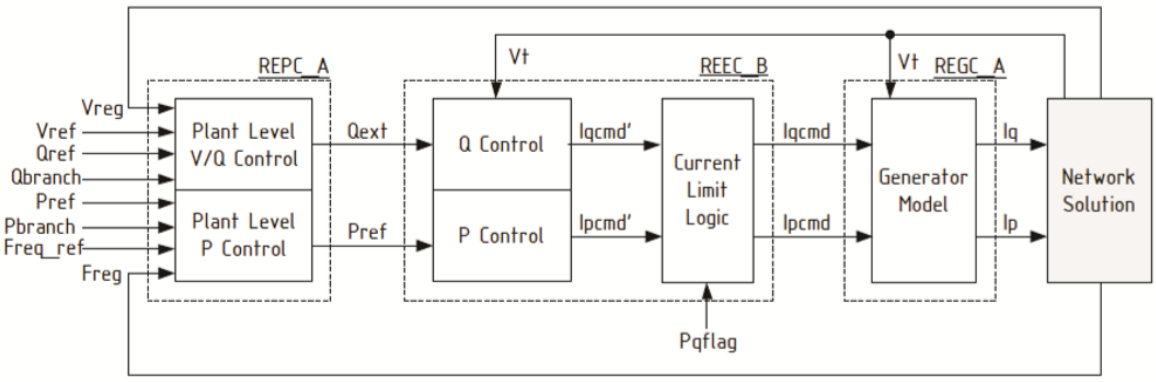

Figure 5.1- Block diagram representing a central station PV power system.

The system is defined as a single equivalent unit represented in a single-stage DC-AC topology, while the control is performed in a continuous form through the *dq* axes principle. The parameters of the model are set following the values reported in the WECC document and readjusted, also through CESI experience on PV models, to obtain reasonable dynamic responses in compliance with the Italian network code. In addition, in order to develop a generic model, the use of 'per unit' parameters in the control process was chosen, converted accordingly into physical quantities at the grid interface by means of an appropriate multiplication/division of characteristic plant base values (e.g. Generator

MVA base). Therefore, this mechanism results in the possibility of scaling the dynamic model to the size of the considered plant, leading to the use of same controllers for differently sized power converters. An overview of the complete PV dynamic generator model is given in Figure 5.2. Here, the input references of active/reactive powers (P_{ref}, Q_{ref}), voltage (V_{ref}) and frequency (*freq_ref*) are set by the steady-state calculation, actuated in TESEO environment [4.4.1], while the voltage quantity, provided in real and imaginary components (*zV_re, zV_im*), is instantaneously measured at the POI during the dynamic simulation. Through the control mechanisms offered by the series of the main modules (REPC, REEC, REGC), the generator feeds the grid by injecting current, in real and imaginary parts (*zI_re, zI_im*), into the interconnection node, with consequent active and reactive power supply (P_e, Q_e), illustrated as output signals in the scheme of Figure 5.2. The model is responsible for providing the appropriate output quantities to meet network demand, while maintaining grid stability in both normal and fault situations. The control procedure can be summarised as follows:

1. REPC → It manages active and reactive power input (P_{ref}, Q_{ref}) to generate new power references (P_{ext}, Q_{ext}) for keeping voltage and frequency within tolerable limits.
2. REEC → It provides set point values for active and reactive currents (I_{pcmd}, I_{qcmd}), corresponding to the reference power quantities (P_{ext}, Q_{ext}) given by the REPC block, and modifies them in case of fault event.
3. REGC → Being the block of interface with the grid, it is responsible for the injection into the node of the real and reactive currents (I_{pord}, I_{qord}), based on the reference commands (I_{pcmd}, I_{qcmd}), given by the REEC module, and readjusted during low voltage or high voltage situations.

Since the control is carried out through *dq* quantities, two blocks of conversions, depicted in green and yellow in Figure 5.2, are also implemented for the interfaced variables of voltage and current.

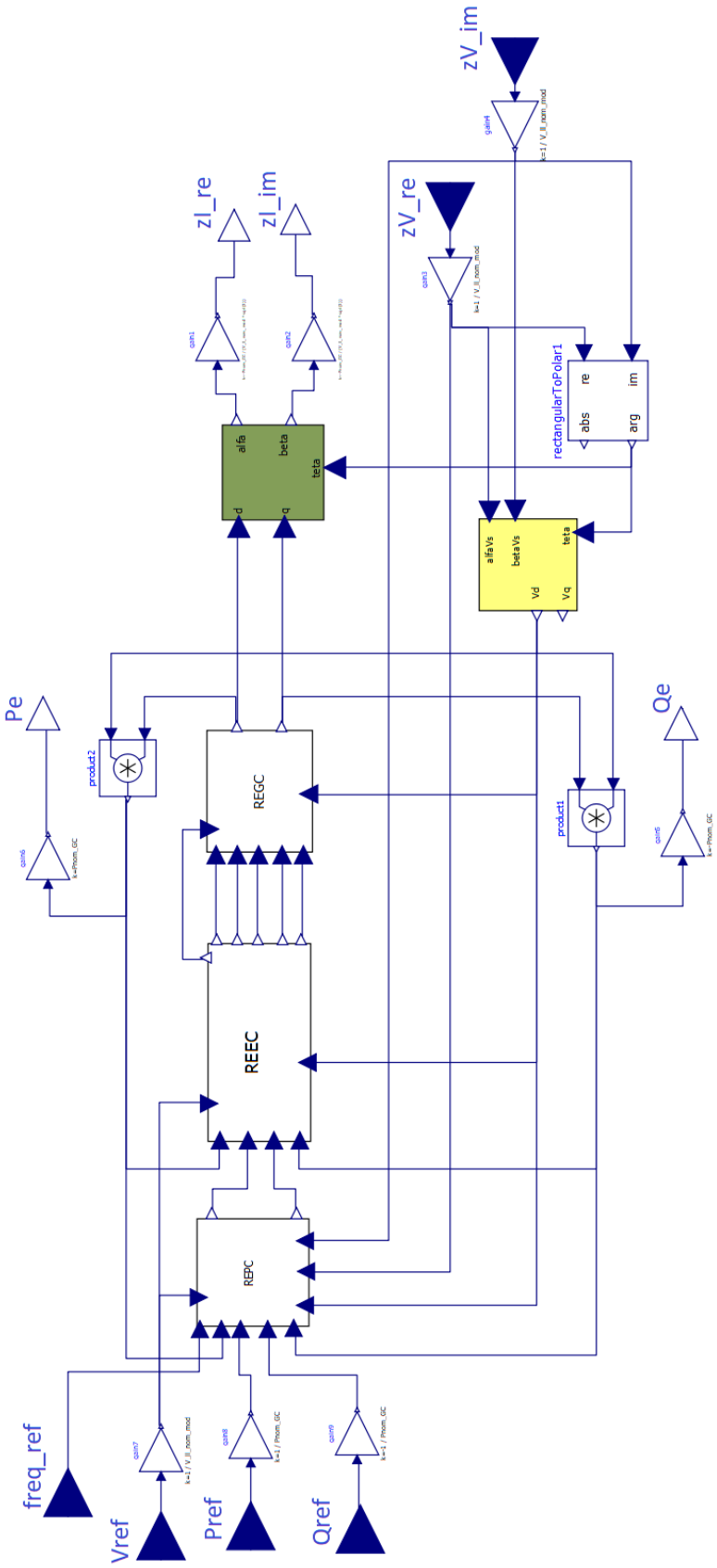

Figure 5.2- PV generator complete scheme.

5.1.1 *dq* axes and PLL for DC Control

The rotating *dq* transformation allows AC three-phase circuits to be operated as if they were DC circuits. This is based upon a mathematical operation (Park Transform), that is the transformation of a set of variables from the stationary *abc* frame to the rotational *dq0* frame, which rotates at a speed ω equal to the angular frequency of the AC quantities:

$$X^{dq0} = \sqrt{\frac{2}{3}} \begin{bmatrix} \cos(\omega t) & \cos(\omega t - 2\pi/3) & \cos(\omega t + 2\pi/3) \\ -\sin(\omega t) & -\sin(\omega t - 2\pi/3) & -\sin(\omega t + 2\pi/3) \\ 1/\sqrt{2} & 1/\sqrt{2} & 1/\sqrt{2} \end{bmatrix} X^{abc} \tag{5.1}$$

Figure 5.3 illustrates how DC control is achieved, resulting in constant direct (v_d) and quadrature (v_q) voltage projections, independent on the position of the rotating vector $\bar{V}$.

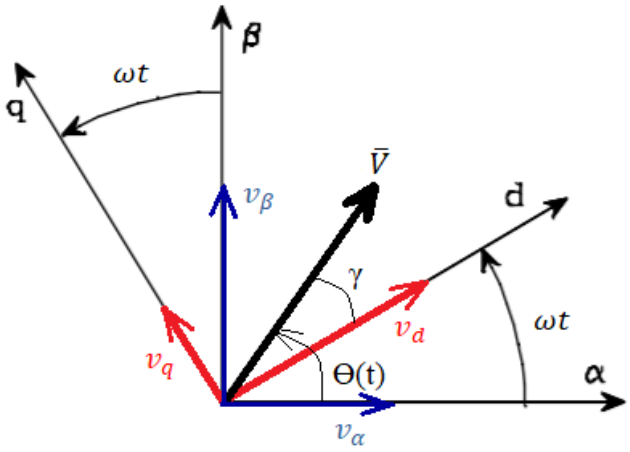

Figure 5.3- illustrated scheme of rotating dq and fixed αβ axes.

As an orthogonal transformation, the conversion into rotating axes does not alter the powers, which assume the following expressions:

$$P = v_d i_d + v_q i_q \tag{5.2}$$

$$Q = v_q i_q - v_d i_q \tag{5.3}$$

In addition, in order to achieve an independent control for active and reactive power, Phase Locked Loop (PLL) has been then introduced to synchronize the direct axis with the model input voltage phasor, as illustrated in Figure 5.4.

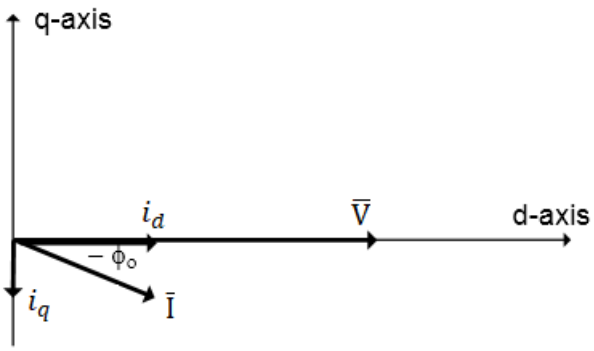

Figure 5.4- Voltage phasor synchronized with direct axis and current phasor decoupled in direct and quadrature components.

The result leads to the cancellation of the quadrature voltage value and the consequently real and reactive power control by directly adjusting the real i_d and reactive i_q current component respectively:

$$P = v_d i_d \tag{5.4}$$

$$Q = -v_d i_q \tag{5.5}$$

As mentioned in Chapter 4, the input voltage of the model is already provided in real and imaginary components; moreover, the omopolar element X^0 is neglected because the considered sinusoidal system is symmetric. Therefore, in order to obtain the direct and quadrature voltage terms, it is sufficient to apply the rotational matrix below, coincident with the rotational terms $e^{-j\omega t}$ in the complex plane:

$$V^{dq} = \begin{bmatrix} \cos(\omega t) & \sin(\omega t) \\ -\sin(\omega t) & \cos(\omega t) \end{bmatrix} V^{\alpha\beta} \tag{5.6}$$

Alternatively, in order to directly synchronize the voltage phasor with the d-axis, it is possible to multiply $\bar{\bar{V}} = V_\alpha + jV_\beta$ for the rotational term $e^{-j\Theta}$, as shown in Figure 5.6, where Θ is provided by the PLL and it represents the phase of the vector $\bar{\bar{V}}$ (Figure 5.3). Generally, the PLL implies the use of a PI regulator to reduce the shift between direct axis and voltage input phasor to zero. However, for simplicity, an ideal behaviour of the regulator has been assumed in the model, involving its replacement with a block, depicted in Figure 5.5, that directly provides the angle to achieve this matching.

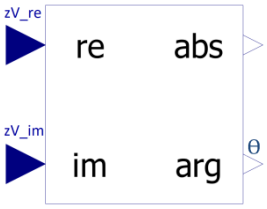

Figure 5.5- Ideal PLL.

Since both the voltage input and current output interfaced with the network are available in real and imaginary components, two blocks have been implemented within the model to obtain their conversion, illustrated in Figure 5.6 and Figure 5.7, respectively correspondent to the yellow and green blocks of Figure 5.2.

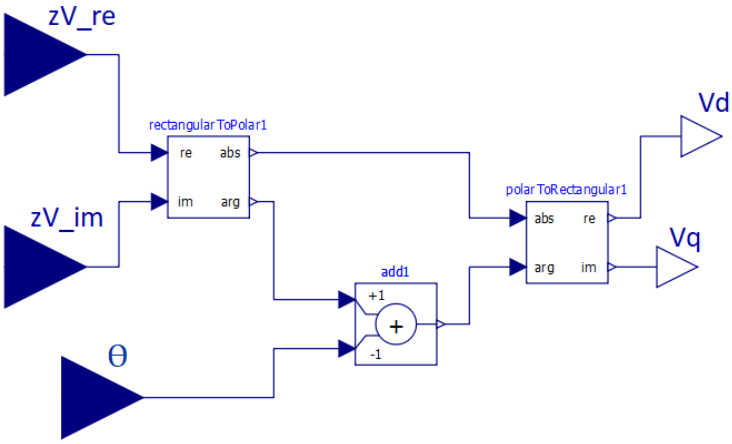

Figure 5.6- Conversion of voltage from real and imaginary parts to direct and quadrature components.

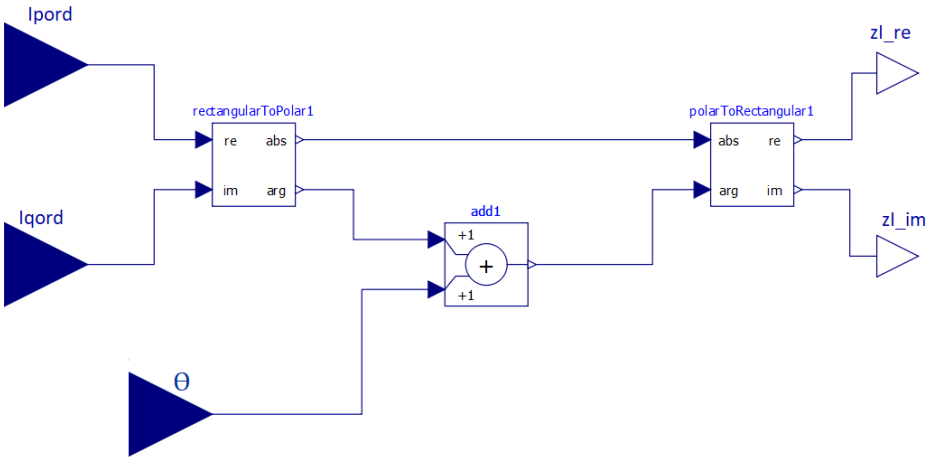

Figure 5.7- Conversion of current from direct and quadrature components to real and imaginary parts.

It is worth mentioning that, in the model, the active current component is specified through the subscript '*p*', instead of '*d*', for the only purpose of correspondence with the standard guideline. The following sections are dedicated to the description of the detailed configurations developed inside the three main control blocks of Figure 5.2.

5.2 The Plant Level Control: REPC

In order to achieve plant-level objectives, a supervisory control has been implemented within the power plant. It is represented by the REPC control block, whose purpose is to provide ancillary service capabilities to the renewable energy generator. Based on the reference quantities of active/reactive power (P_{ref}, Q_{ref}), voltage (V_{ref}) and frequency (*freq_ref*), received as input, it aims to provide adjusted power references (P_{ext}, Q_{ext}) for the next module (REEC), in order to guarantee voltage and frequency regulation. In particular, supervisory control to both the real and reactive power have been modelled separately through the implementation of the two following subsystems:

- Reactive power control: 'Q_{ext} control' block.
- Active power control: 'P_{ext} control' block.

5.2.1 The Reactive Power Control

The components of this block are shown in the diagram of Figure 5.8, where it is possible to recognize two available user-settable paths, thanks to the logical switch Ref_{flag}:

- $Ref_{flag} = 1 \rightarrow$ The controller is configured to regulate the voltage V_d at the POI based on the reference value V_{ref}.
- $Ref_{flag} = 0 \rightarrow$ The controller aims to regulate the reactive power injection q in order to match the reference Q_{ref}.

In both the two cases, the mechanism involves the use of a PI regulator, which considering the discrepancy between the reference variables and the measured quantities, results the reactive power Q_{ext}. This value will be used as input reference in the following block REEC, for the computation of the reactive current set point I_{qcmd}, whose injection into the grid will determine the matching between V_d and V_{ref} or alternatively between q and Q_{ref},

depending on the setting of the switch Ref_{flag}. While V_d is given by the conversion block of Figure 5.6, the measured reactive power quantity q is estimated according to the equation (5.5). Moreover, since in reality the measurements do not take place instantaneously, filters have been placed after the measured variables in order to emulate this delay. Table 5.1 shows the Q_{ext} control parameters adopted in the simulations.

Name	***Symbol***	***Value***	***Unit of measurement***
Voltage filter gain	K_{rv}	1	*[p.u.]*
Voltage filter time constant	T_{rv}	0.02	*[s]*
Max reactive power limit	Q_{max}	1	*[p.u.]*
Min reactive power limit	Q_{min}	-1	*[p.u.]*
Reactive power filter gain	$K_{\_qe}$	1	*[p.u.]*
Reactive power filter time constant	$T_{\_qe}$	0.02	*[s]*
Conversion coefficient	$K_{\_qv}$	1	*[p.u.]*
lower threshold dead-band	*Dbd2*	0	*[p.u.]*
upper threshold dead-band	*Dbd1*	0	*[p.u.]*
Upper limit on dead-band output	e_{max}	1	*[p.u.]*
Lower limit on dead-band output	e_{min}	-1	*[p.u.]*
PI control proportional gain	K_p	0.9	*[p.u.]*
PI control integral gain	K_i	5	*[p.u.]*
Lead time constant	T_{ft}	0	*[s]*
Lag time constant	T_{fv}	0.2	*[s]*
Switch state: V/Q control	Ref_{flag}	1-0	-

Table 5.1- Parameters adopted in 'Qext control' block.

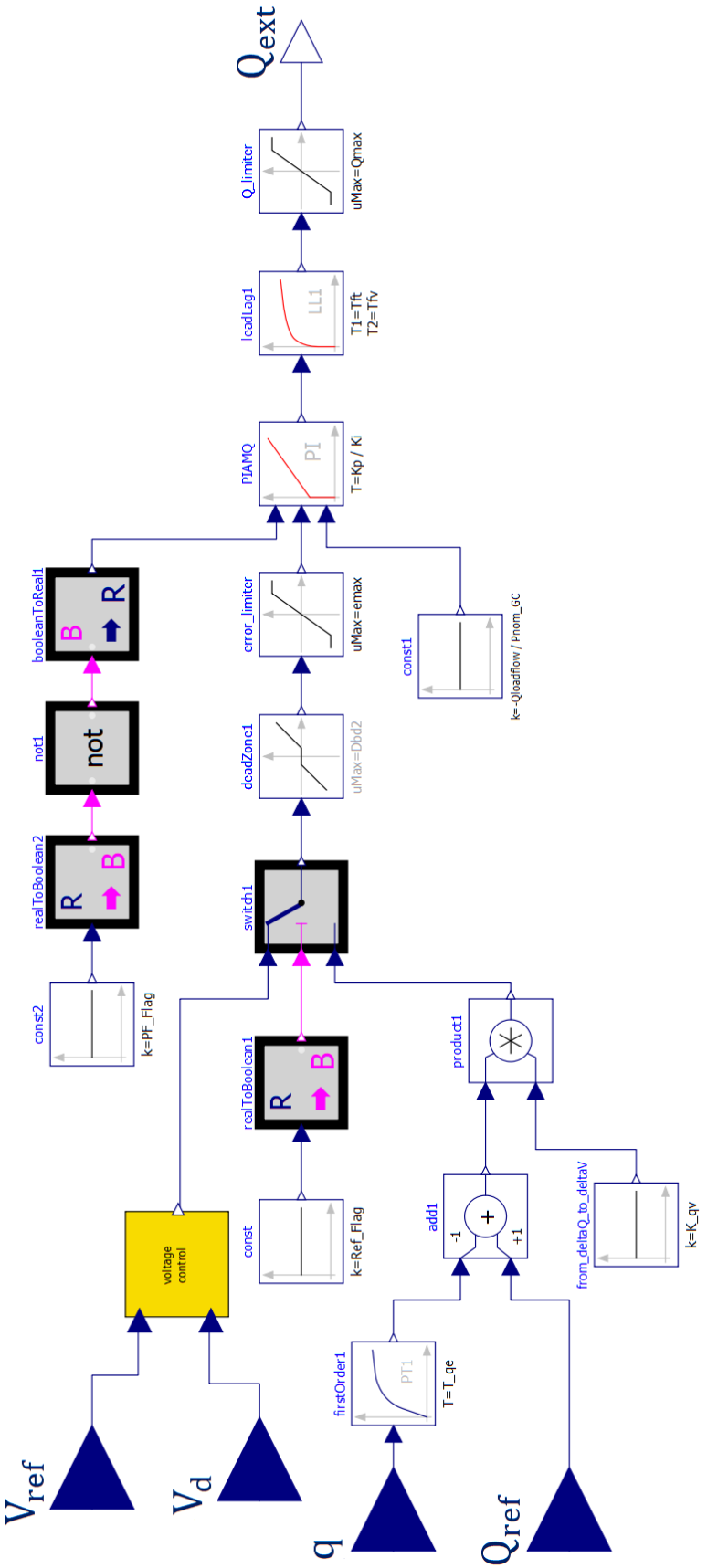

Figure 5.8- Diagram of the 'Qext control' block.

5.2.2 The Active Power Control

The 'P_{ext} control' block is intended to provide the active power (P_{ext}) as reference input in the REEC subsystem for the computation of the real current component I_{pcmd}, whose injection into the grid will make the generated power p compliant with the reference quantity P_{ref}, thus satisfying the network demand. As for the reactive power q, even the measured quantity p is given by an estimation, according to the equation (5.4). The complete diagram is shown in Figure 5.11. It includes a logic switch $Freqref_{flag}$ that users should set to make the following choice:

- $Freqref_{flag} = 1 \rightarrow$ The real power flow is regulated through the use of a PI controller. This mode also features the frequency adjustment by means of a droop control, which can be eventually disabled setting the slope to zero.
- $Freqref_{flag} = 0 \rightarrow$ The controller regulates the active power flow to follow the reference real power command P_{ref} using a feed-forward linear path (bypassing the PI controller) without the influence of frequency response.

As aforementioned, in case of $Freqref_{flag} = 1$, the module includes the possibility of handling the reference active power providing a governor response. This control has been implemented inside the 'frequency control' block, depicted in orange in Figure 5.11 and explained below.

The Frequency Response Control

Incorporated in the 'P_{ext} control block', the frequency regulation model consists of a droop control, whose diagram is illustrated in Figure 5.9. The error between reference frequency and measured frequency provides the input $deltaF$. If a frequency excursion occurs, this module computes a real power quantity ($deltaP$), which boosts the original active power reference P_{ref} in order to respond to the frequency change. The operation is graphically illustrated in Figure 5.10. In this case, the measured power quantity p should meet the new reference value:

$$P_{refNew} = P_{ref} + deltaP \tag{5.7}$$

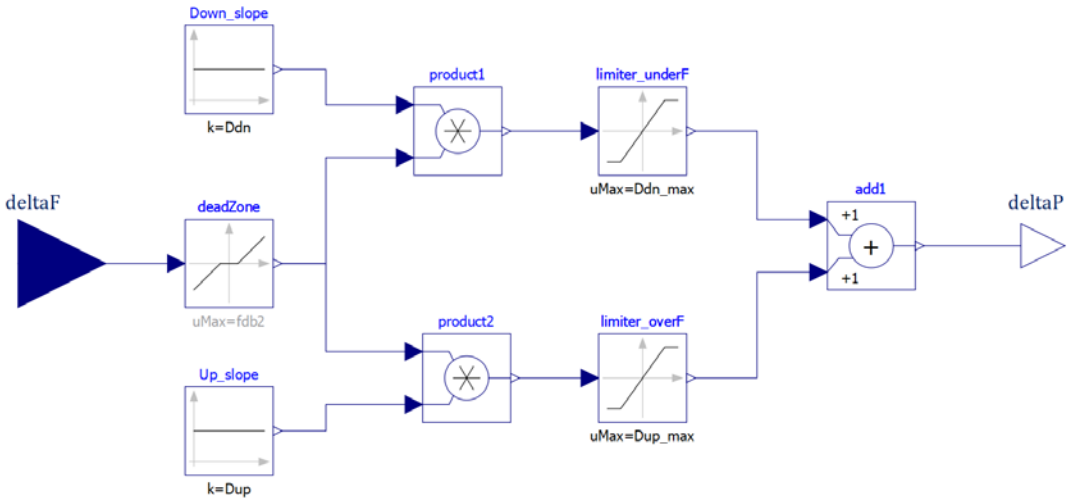

Figure 5.9- Droop control diagram for frequency response.

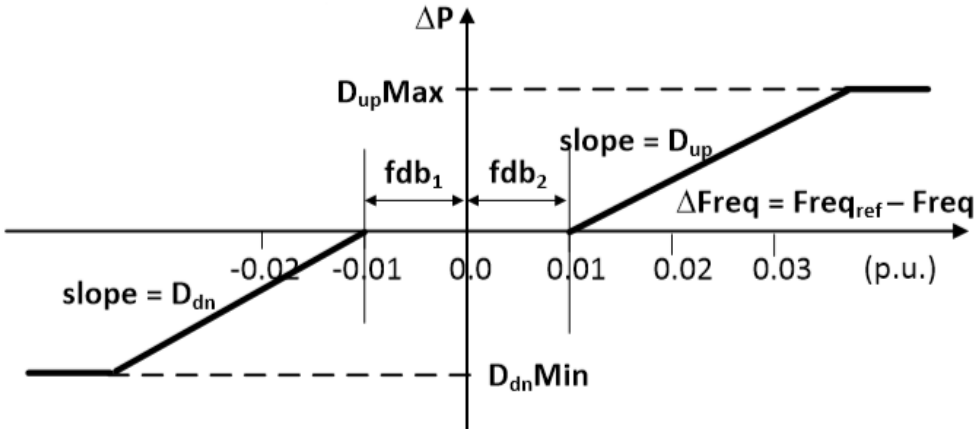

Figure 5.10- Graphical illustration of real power regulation during a frequency excursion.

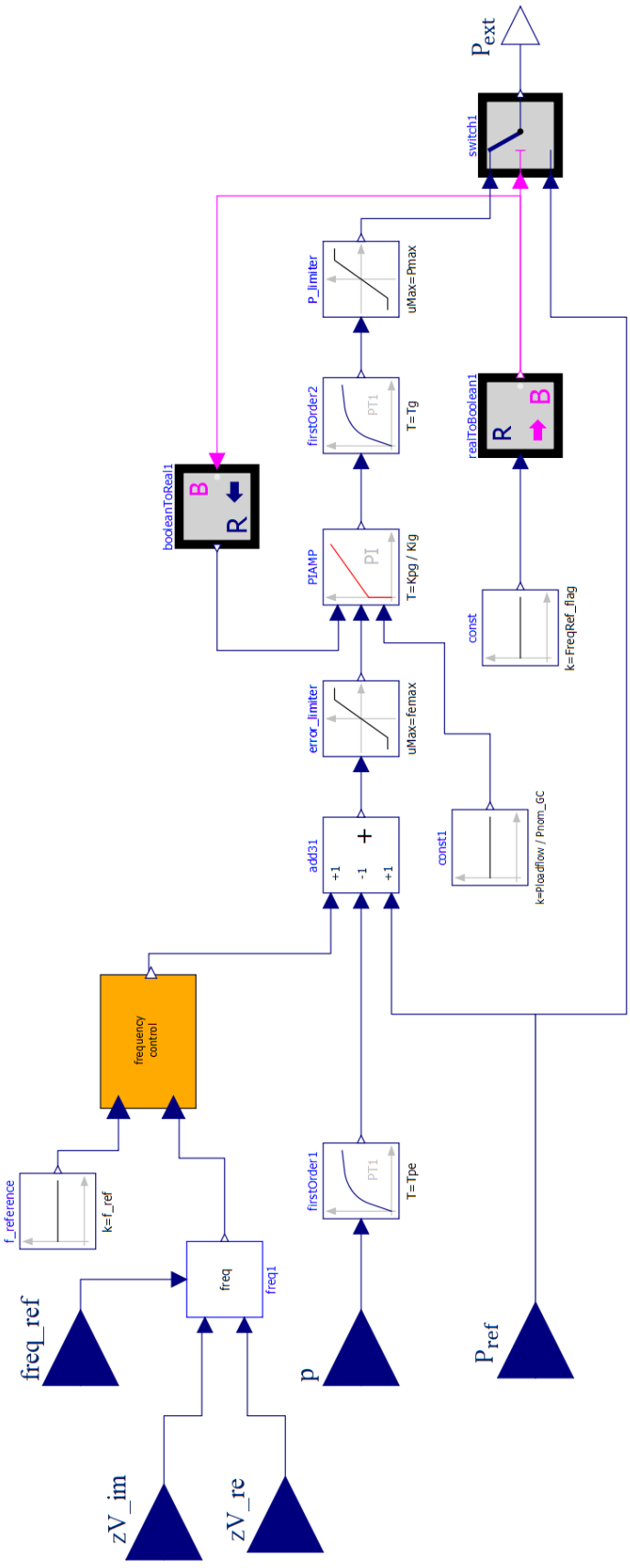

Figure 5.11- Diagram of the 'Pext control' block.

Table 5.2 shows the P_{ext} control parameters adopted in the simulations.

Name	***Symbol***	***Value***	***Unit of measurement***
Real power measurement filter gain	K_{pe}	1	*[p.u.]*
Real power measurement filter time constant	T_{pe}	0.02	*[s]*
Max active power limit	P_{max}	1.2	*[p.u.]*
Min active power limit	P_{min}	0	*[p.u.]*
Max power error	fe_{max}	1	*[p.u.]*
Min power error	fe_{min}	-1	*[p.u.]*
Switch state	$Freq_{flag}$	0-1	-
PI proportional gain for power control	K_{pg}	1	*[p.u.]*
PI integral gain for power control	K_{ig}	8	*[p.u.]*
Power controller filter gain	$K_{\_pg}$	1	*[p.u.]*
Power controller filter lag time constant	T_g	0.1	*[s]*
Dead-band lower threshold	*fdb1*	0	*[p.u.]*
Dead-band upper threshold	*fdb2*	0	*[p.u.]*
Droop for under-frequency conditions	D_{dn}	20	*[p.u.]*
Droop for over-frequency conditions	D_{up}	20	*[p.u.]*
Under frequency regulation max limit	D_{dn_max}	0	*[p.u.]*
Under frequency regulation min limit	D_{dn_min}	-999	*[p.u.]*
Over frequency regulation max limit	D_{up_max}	999	*[p.u.]*
Over frequency regulation min limit	D_{up_min}	0	*[p.u.]*

Table 5.2- Parameters adopted in the 'Pext control' block.

The active power (P_{ext}) and reactive power (Q_{ext}) results, output of the REPC block, are the reference inputs of the next implemented module, called REEC.

5.3 The Electrical Control Model: REEC

In order to provide good integration into the network, the PV controller has to guarantee fault ride-through capability, current limit protection, instantaneous and independent control of real and reactive power, and ancillary services to the grid. The REEC represents the electrical control of the inverter and is designed to manage the real and the reactive power both under normal and transient conditions. It gives the references for the REGC block, providing appropriate current set points (I_{qcmd}, I_{pcmd}) through the use of PI regulators. Thanks to the introduction of *dq* axes and PLL, active and reactive current control has been achieved separately through two independent systems:

- The Reactive Current Control: 'I_{qcmd} control' block.
- The Active Current Control: 'I_{pcmd} control' block.

Additional blocks for current limits control and fault detection are part of the REEC module, and therefore described in this section.

5.3.1 The Reactive Current Control

This module has the function to produce the set point of the reactive current value I_{qcmd}, which will be the input reference of the next block REGC. The system presents several possible routes, selectable by switches, which involve various control combinations aimed at achieving this goal:

- Reactive power control through constant power factor.
- Reactive power regulation by a linear control.
- Reactive power control via a cascaded set of PI regulators.
- Voltage control through a PI regulator.

Depending on the setting of the switches, these modes can be coupled together (e.g. linear control with reactive power input in constant power factor mode). Therefore, in order to provide a clearer explanation of the complex control, the following description is carried out considering one stage at a time, defining each sub-system incorporated in the 'I_{qcmd} control' block, illustrated in Figure 5.12.

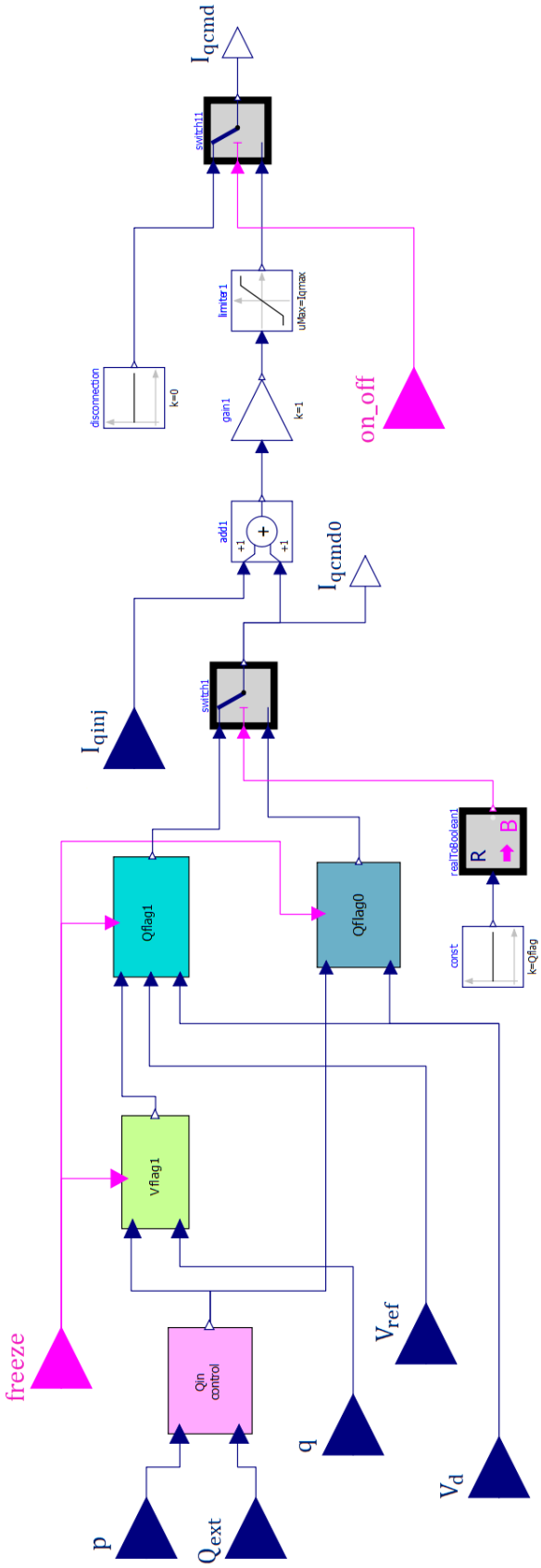

Figure 5.12- Complete reactive current control scheme.

The Reactive Power Reference Control

The first block encountered is the 'Q_{in} control' block, directly interfaced with the previous REPC module and depicted in pink in Figure 5.12. Its task is to provide a reactive power reference (Q_{in}) in case of the I_{qcmd} generation is based on a reactive power control mode (which can be linear or use PI regulators). Two options are available depending on the position of the switch PF_{flag}:

- $PF_{flag} = 1 \rightarrow Q_{in}$ is computed based on a constant power factor ($power_{factor}$) and therefore proportional to the measured real power p:

$$Q_{in} = p * \text{tg}\,(arcos(power_{factor})) \tag{5.8}$$

- $PF_{flag} = 0 \rightarrow Q_{in}$ matches the external reactive power command Q_{ext}, driven by the supervisory control REPC.

The scheme implemented to achieve this objective is illustrated in Figure 5.13, while the adopted parameters for the conducted simulations are reported in Table 5.3.

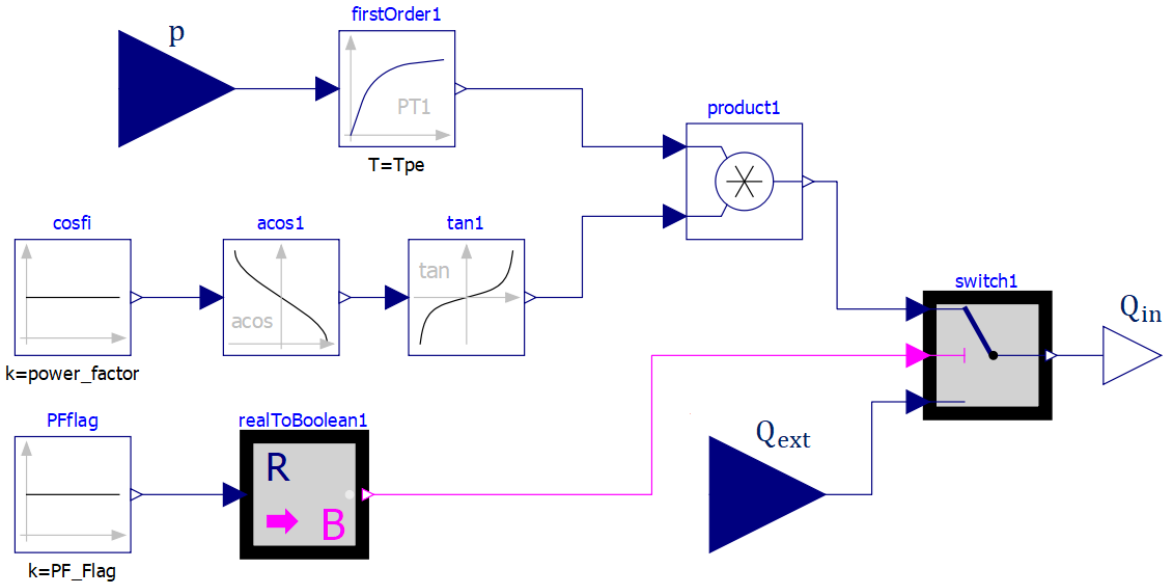

Figure 5.13- Scheme of the 'Qin control' block.

Name	*Symbol*	*Value*	*Unit of measurement*
Active power filter gain	K_{pe}	1	*[p.u.]*
Active power filter time constant	T_{pe}	0.02	*[s]*
Power factor	$power_{factor}$	0.9	-
PF switch state	PF_{flag}	0-1	-

Table 5.3- Control parameters for 'Qin control' block.

The Linear Reactive Power Control

This modality, chosen by setting the switch $Q_{flag} = 0$, involves the reactive current generation I_{qcmd} through a linear reactive power control and it is implemented in the 'Q_{flag0} control' block, depicted in Figure 5.12. It consists on a feed-forward linear loop, without the PI regulator, which provides the reactive set point current value according to the ratio between the reactive power input (Q_{in}), given by the 'Q_{in} control' block, and the measured voltage V_d. The configuration is illustrated in Figure 5.14.

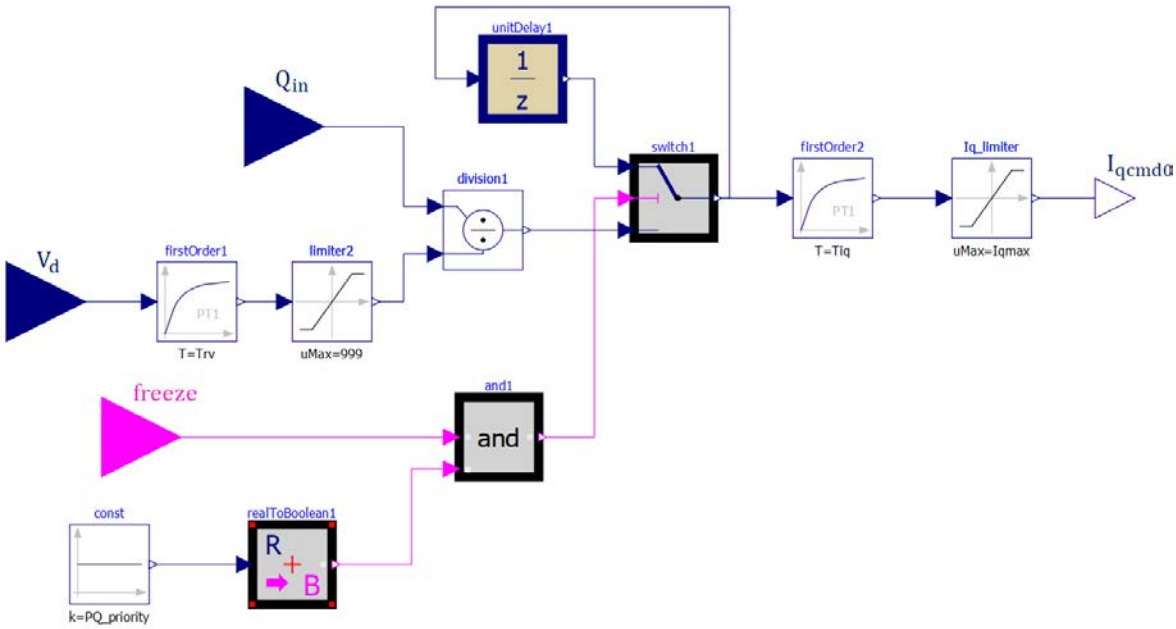

Figure 5.14- Reactive power control through a linear path.

The diagram also shows further elements adopted in the logic for the freeze control, explained later. Table 5.4 contains the values of the parameters used in the simulations.

Name	*Symbol*	*Value*	*Unit of measurement*
Voltage filter gain	K_{rv}	1	*[p.u.]*
Voltage filter time constant	T_{rv}	0.02	*[s]*
Filter gain in Qflag0 control	K_{iq}	1	*[p.u.]*
Filter time constant in Qflag0 control	T_{iq}	0.02	*[s]*
Max reactive current limit	I_{qmax}	1	*[p.u.]*
Min reactive current limit	I_{qmin}	-1	*[p.u.]*
Sampling time for unit delay	T_{sample}	0.1	*[s]*
PQ priority switch state	$PQ_{priority}$	0-1	-

Table 5.4- Qflag0 block parameters.

The Voltage Control through a PI

This mode of operation, implemented in the 'Q_{flag1} control' block, depicted in Figure 5.12, is intended to produce a reactive current set point I_{qcmd} aimed at controlling the voltage measured at the POI (V_d). It is achieved by setting the switches $Q_{flag} = 1$ and $V_{flag} = 0$, which cause the by-pass of all the other sub-systems displayed in Figure 5.12. The illustrated diagram is shown in Figure 5.15 and the relative parameters are written in Table 5.5. Its functioning involves the use of a PI regulator, which outputs a reactive current command I_{qcmd}, based on the comparison between the desired reference voltage V_{ref}, given by the steady-state computation, and the measured voltage quantity V_d.

Name	*Symbol*	*Value*	*Unit of measurement*
Voltage filter gain	K_{rv}	1	*[p.u.]*
Voltage filter time constant	T_{rv}	0.02	*[s]*
Max voltage limit	V_{max}	1.15	*[p.u.]*
Min voltage limit	V_{min}	0.85	*[p.u.]*
Switch state V_{flag}	V_{flag}	1-0	-
Sampling time for unit delay	T_{sample}	0.1	*[s]*
PQ priority switch state	$PQ_{priority}$	0-1	-
Voltage regulator proportional gain	K_{vp}	0.85	*[p.u.]*
Voltage regulator integral gain	K_{vi}	8.5	*[p.u.]*

Table 5.5- Parameters adopted in the 'Qflag1 control' block.

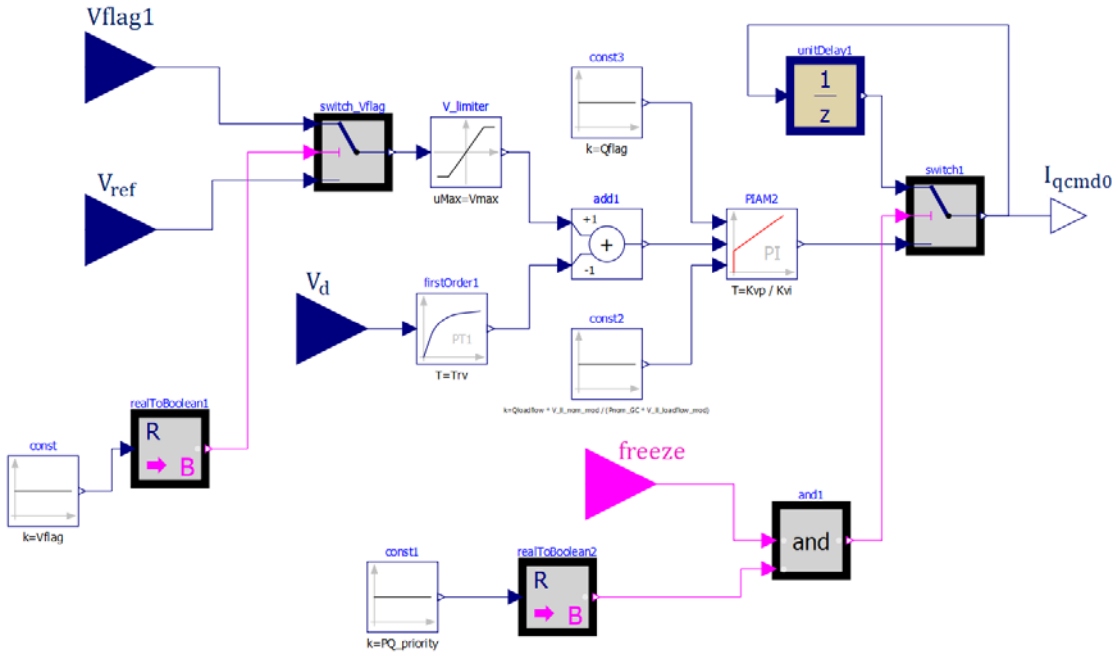

Figure 5.15- Scheme of the 'Qflag1 control' block.

The Reactive Power Control via a cascaded set of PIs

This mode of functioning has the purpose of achieving the reactive current command I_{qcmd} through a reactive power control, based on a double stage of regulation. This option is possible by selecting $V_{flag} = 1$ and $Q_{flag} = 1$. The first phase of operation is carried out in the 'V_{flag1} control' block, depicted in green in Figure 5.12 and schematized in Figure 5.16. By comparing the reference reactive power (Q_{in}), given by the 'Q_{in} control' block, with the actual measure q, it provides, through a PI, a suitable voltage value (*Vflag1*). This quantity represents the desired potential the system should achieve at the POI in order to inject into the grid the reactive power Q_{in}. The parameters used are shown in Table 5.6. In addition, the configuration presents a freeze state and a unit delay block, whose behaviour are explained below. The regulatory procedure continues with the entry of *Vflag1* in the subsequent stage of control, conducted by the previously defined 'Q_{flag1} control' block (Figure 5.15). Here, a second PI generates the reactive current set point I_{qcmd}, whose injection into the network should cause the measured voltage (V_d) to match the *Vflag1* value, with a resultant production of reactive power Q_{in}.

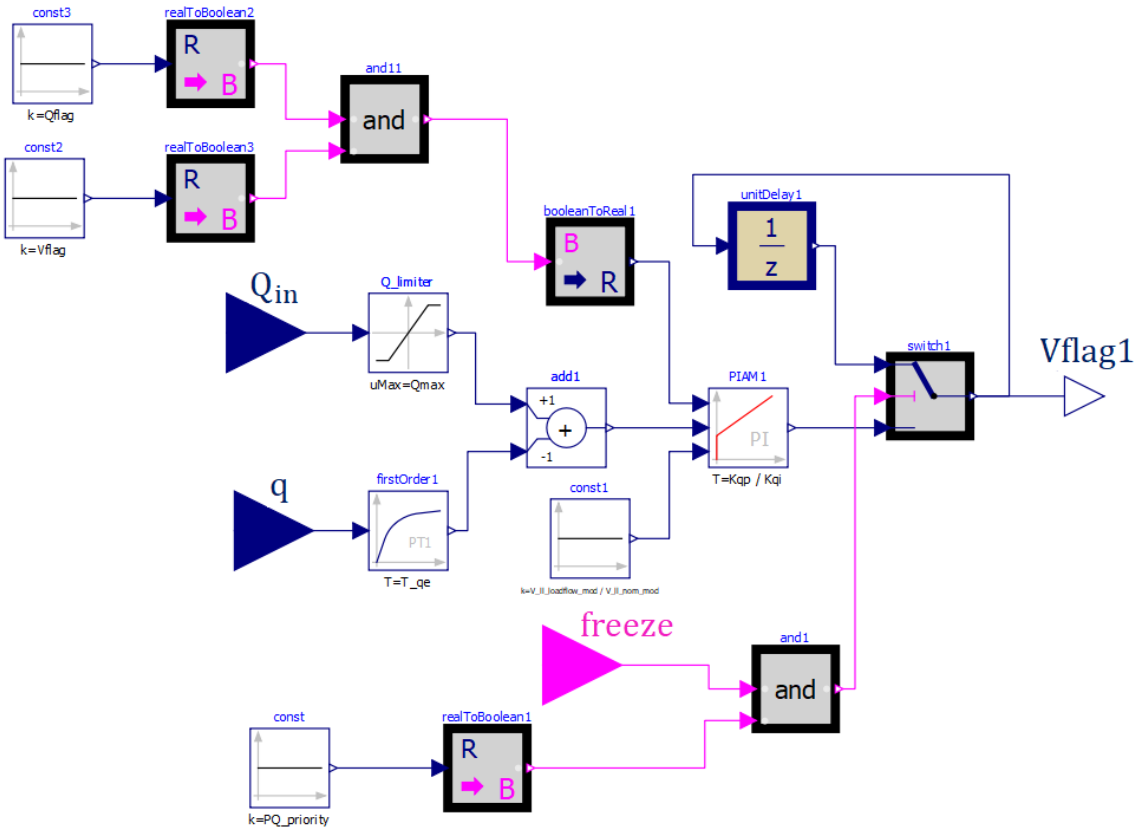

Figure 5.16- Reactive power control scheme with one PI regulator**.**

Name	***Symbol***	***Value***	***Unit of measurement***
Reactive Power filter gain	$K_{\_qe}$	1	*[p.u.]*
Reactive Power filter time constant	$T_{\_qe}$	0.02	*[s]*
PI proportional coefficient	K_{qp}	0.8	*[p.u.]*
PI integral coefficient	K_{qi}	6	*[p.u.]*
Maximum reactive power limit	Q_{max}	1	*[p.u.]*
Minimum reactive power limit	Q_{min}	-1	*[p.u.]*
Sampling time for unit delay	T_{sample}	0.1	*[s]*
PQ priority switch state	$PQ_{priority}$	0-1	-
Max voltage anti-windup	ve_{max}	1.15	*[p.u.]*
Min voltage anti-windup	ve_{min}	0.85	*[p.u.]*

Table 5.6- Parameters adopted in the 'Vflag1 control' block.

Referring to Figure 5.12, the control also provides an additional reactive current injection (I_{qinj}) in case of over or under-voltage conditions, and a function of disconnection for permanent failure situations, whose behaviours are explained in the next paragraphs.

5.3.2 The Real Current Control

This module is responsible for generating the set point of the active current value I_{pcmd}, which will be the input reference of the next block REGC. This quantity is computed by the following calculation, based on the equation (5.4):

$$I_{pcmd} = \frac{P_{ext}}{V_d} \tag{5.9}$$

The diagram of the control implemented is shown in Figure 5.17. It is directly connected with the REPC module, which provides to this system the active power reference value P_{ext}, desirable at the grid interface. The parameters used in the simulations are reported in Table 5.7.

Name	***Symbol***	***Value***	***Unit of measurement***
Voltage filter gain	K_{rv}	1	*[p.u.]*
Voltage filter time constant	T_{rv}	0.02	*[s]*
Max active current limit	I_{pmax}	1.2	*[p.u.]*
Min active current limit	I_{pmin}	-1.2	*[p.u.]*
Derivative time constant for slew rate	T_{-dP}	0.001	*[s]*
Sampling time for unit delay	T_{sample}	0.1	*[s]*
PQ priority switch state	$PQ_{priority}$	0-1	-
Maximum rising slew rate	$dPmax$	500	*[p.u./s]*
Maximum falling slew rate	$dPmin$	-500	*[p.u./s]*
Power filter gain	K_{pord}	1	*[p.u.]*
Power filter time constant	T_{pord}	0.02	*[s]*
Max power limit	P_{max}	1.2	*[p.u.]*
Min power limit	P_{min}	0	*[p.u.]*

Table 5.7- Parameters adopted in the 'Ipcmd control' block.

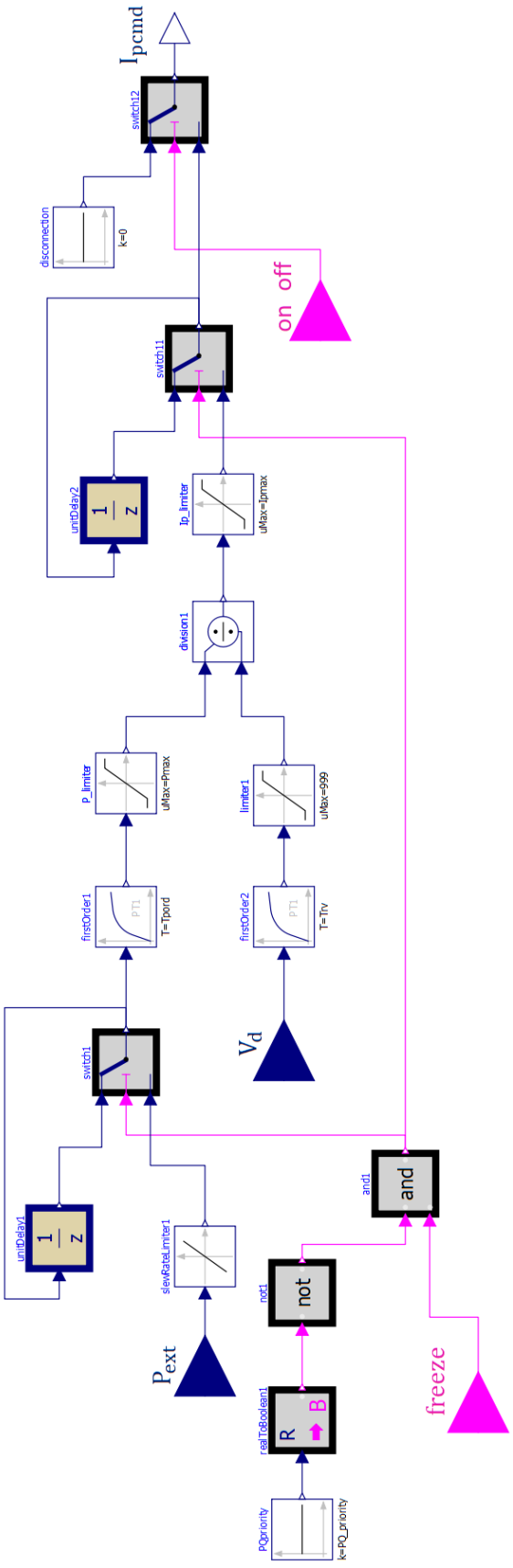

Figure 5.17- Diagram of the active current regulation.

5.3.3 The Maximum Current Limiter

This control block has been implemented with the purpose of preventing high currents injection, dangerous for the power switches (IGBTs and diodes) damage. To ensure over-current protection, the sum of active and reactive current contributions must not exceed the maximum current-carrying capability. The system, then, provides the choice to prioritize either the real or the quadrature component through the selection of the $PQ_{priority}$ switch. Figure 5.18 illustrates the current limiter diagram, Table 5.8 shows the parameters.

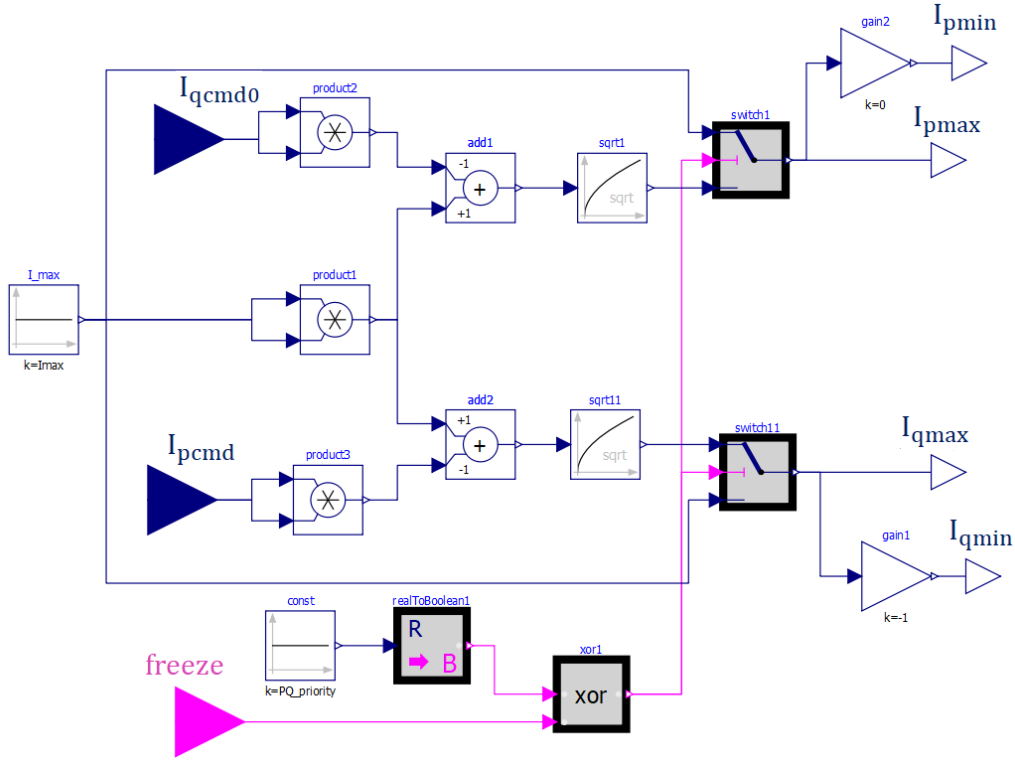

Figure 5.18- Current limiter control diagram.

Name	***Symbol***	***Value***	***Unit of measurement***
Maximum current limit	I_{max}	1.2	*[p.u.]*
PQ priority switch state	$PQ_{priority}$	0-1	-

Table 5.8- Current limiter block parameter.

- $PQ_{priority} = 1 \rightarrow$ P priority is selected: the controller's priority is to maximize the range of the real current component I_{pcmd} and use the remaining current capability for the reactive current component, I_{qcmd}. It is governed by the following equations:

$$I_{pmax} = I_{max} \tag{5.10}$$

$$I_{pmin} = 0 \tag{5.11}$$

$$I_{qmax} = \sqrt{{I_{max}}^2 - {I_{pcmd}}^2} \tag{5.12}$$

$$I_{qmin} = -I_{qmax} \tag{5.13}$$

- $PQ_{priority} = 0 \rightarrow$ Q priority is chosen: : the controller's priority is to maximize the range of the reactive current component I_{qcmd} and use the remaining current capability for the active current component, I_{pcmd}. It is managed by the following equations:

$$I_{qmax} = I_{max} \tag{5.14}$$

$$I_{qmin} = -I_{qmax} \tag{5.15}$$

$$I_{pmax} = \sqrt{{I_{max}}^2 - {I_{qcmd}}^2} \tag{5.16}$$

$$I_{pmin} = 0 \tag{5.17}$$

During normal operation the P-Priority is usually set, in order to maximize the energy production of the photovoltaic plant. In case of voltage dip, instead, the Q-Priority is generally preferred, since it allows a faster restore of the voltage magnitude within its acceptable range. However, the user can select the operation that best suits his needs.

5.3.4 The Fault Control

This subsystem, schematized in Figure 5.19, is responsible for detecting voltage drops or voltage rises beyond the permitted limits and it provides the safety measures to overcome the failure.

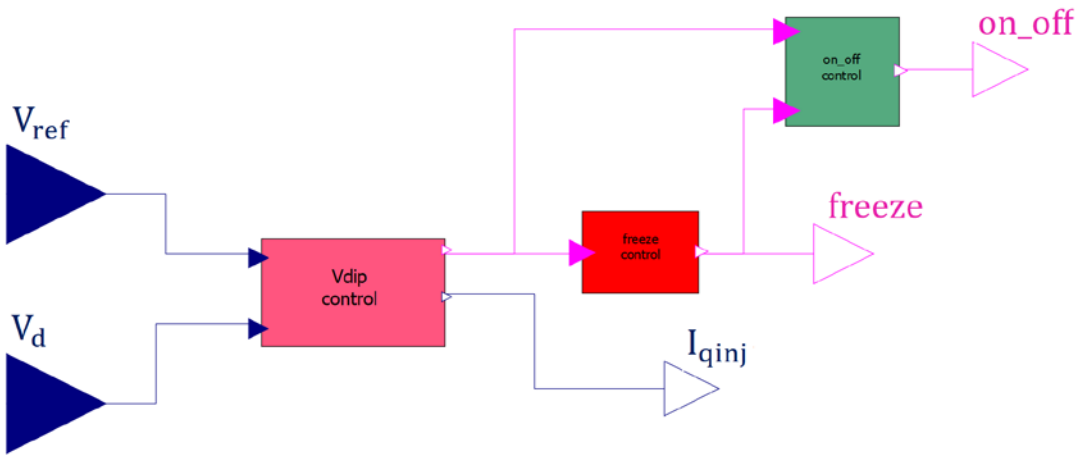

Figure 5.19- Fault control diagram.

It consists of:

- Abnormal voltage identification: 'V_{dip} control' block.
- Freezing of pre-failure states: 'Freeze control' block.
- Disconnection of the plant in extreme situation: 'On-Off control' block.

The Abnormal Voltage Detection

Represented by the 'V_{dip} control' block, it has been implemented with the aim of identifying over- and under- voltage situations at the terminals of the power converter. It is defined by a logic of comparison between the measured voltage (V_d) and its acceptable limits (V_{dip}, V_{up}), as shown in Figure 5.20. When the exceeding of one of these thresholds occurs, the switch is activated, and it provides an additional reactive current injection, proportional to the difference between the reference (V_{ref}) and the measured voltage (V_d), in order to restore the nominal condition. This operation follows the linear model of Figure 5.21, which involves a capacitive reactive current injection in case of voltage drop and an inductive injection in case of voltage excess. The values applied in this control are represented in Table 5.9.

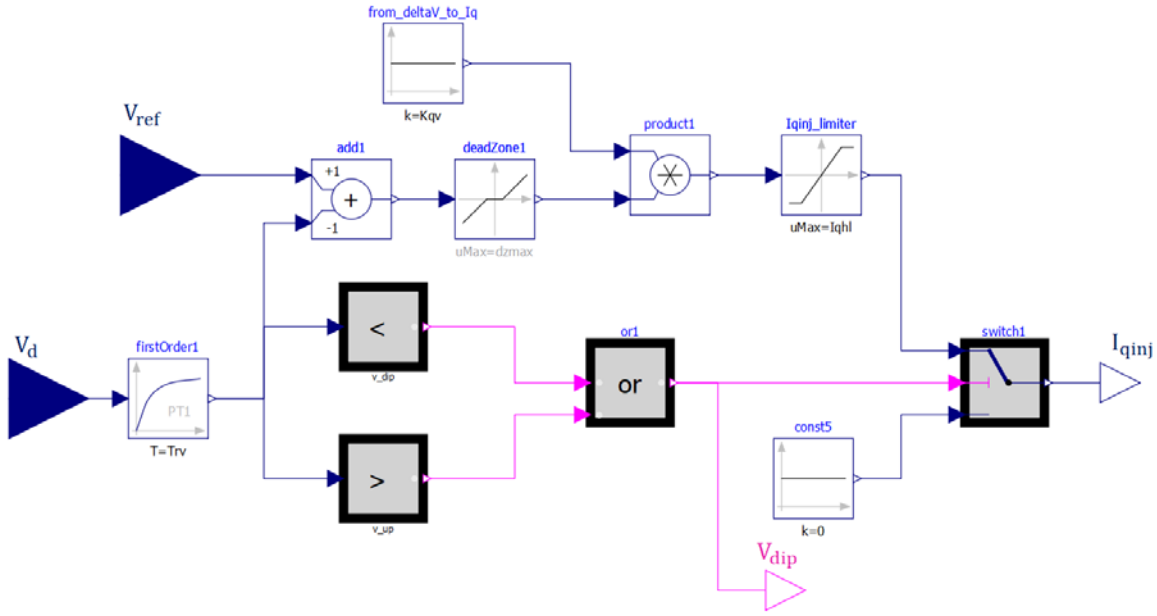

Figure 5.20- Abnormal voltage detection and additional reactive current injection diagram.

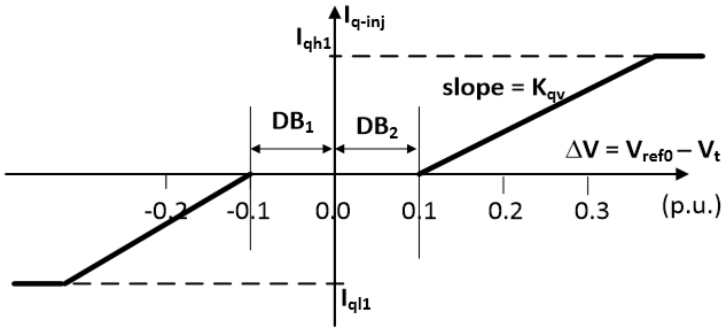

Figure 5.21- Diagram illustrating an additional reactive current injection during an abnormal voltage event.

Name	***Symbol***	***Value***	***Unit of measurement***
Voltage filter gain	K_{rv}	1	*[p.u.]*
Voltage filter time constant	T_{rv}	0.02	*[s]*
Higher voltage threshold	V_{up}	1.15	*[p.u.]*
Lower voltage threshold	V_{dip}	0.85	*[p.u.]*
Max dead zone limit	*dzmax*	0	*[p.u.]*
Min dead zone limit	*dzmin*	0	*[p.u.]*
Reactive current injection gain	K_{qv}	5	*[p.u.]*
Max current injected limit	I_{qhl}	1	*[p.u.]*
Min current injected limit	I_{qll}	-1	*[p.u.]*

Table 5.9- Parameters adopted in the 'Vdip control' block.

The Freeze Control

The impact of short disturbances may exaggerate the transient situation, causing instability in the power system when they are removed from the grid. Therefore, the 'freeze control' block has been implemented in order to freeze the output current value to the pre-failure state until the fault is cleared or, alternatively, the time available for recovery ends. Figure 5.22 illustrates the logic applied, while Table 5.10 reports the parameter used in the simulations. When abnormal voltage condition occurs, detected by the 'V_{dip} control' block, the Boolean variable V_{dip} assumes the state of 1 and activates the freeze.

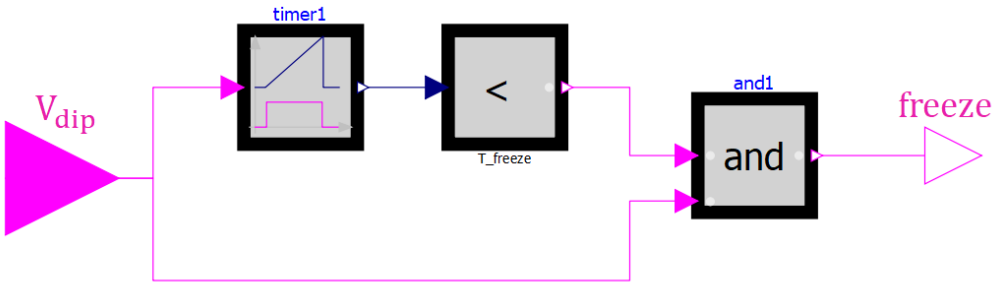

Figure 5.22- Freeze control diagram.

Name	*Symbol*	*Value*	*Unit of measurement*
Freeze time constant	T_{freeze}	1	*[s]*

Table 5.10- Freeze control parameters.

To obtain frozen current variables, the 'I_{qcmd} control' and 'I_{pcmd} control' blocks have been provided, as mentioned before, of a unit delay element, which samples the current signals and outputs their previous sampled values, belonging to the pre-fault conditions. Two cases of functioning have been distinguished:

a) The fault occurs in P-Priority operation.

If P-Priority option is selected, when a disturbance in the transmission line occurs, the controller prioritizes the active current component injection to satisfy the active power demand. According to (5.4), it may happen, in voltage drop situation, that the active current required to keep an unaltered active power is higher than the maximum allowable limit, due to the low value of V_d. In this condition, the current limiter involves a significant decrease in the reactive component, which should give extra-headroom to the active one. It

is therefore appropriate to freeze the I_{qcmd0} state and invert the logic of the current limiter, computing the upper real current values as:

$$I_{pmax} = \sqrt{{I_{max}}^2 - {I_{qcmd0}}^2} \tag{5.18}$$

$$I_{qmax} = I_{max} \tag{5.19}$$

Therefore in this case, the real current component I_{pcmd} has still the possibility to increase, trying to maintain the desired active power, without causing the total cancelling of the reactive current value I_{qcmd0}, which is frozen and consequently it will never reach the limit I_{max}.

b) The fault occurs in Q-Priority operation

Similar to the P-Priority functioning, if a transient failure occurs during the Q-Priority operation the controller prioritize the reactive current component. Therefore, I_{pcmd} is maintained at its original value through the freeze activity and the maximum reactive current limit is calculated as:

$$I_{qmax} = \sqrt{{I_{max}}^2 - {I_{pcmd}}^2} \tag{5.20}$$

The Plant Disconnection

If the fault is not cleared within the set time limit, decided through the time constant T_{freeze} (Figure 5.22), the immediate disconnection of the system is commanded. The logic used to achieve this goal is shown in the scheme of Figure 5.23.

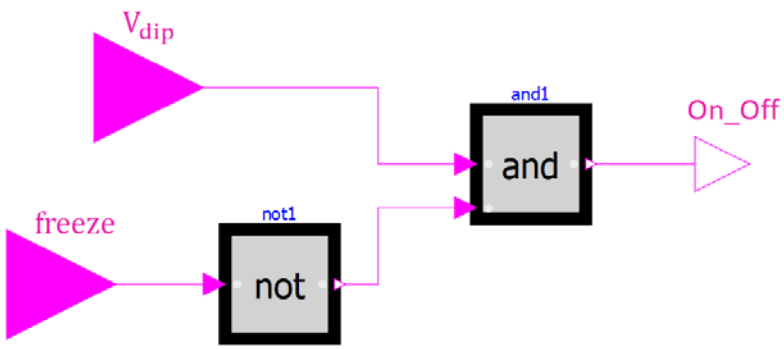

Figure 5.23- On-Off block scheme.

5.4 The Generator Model: REGC

The REGC is the interface block with the network, represented by the third module among the series of blocks of Figure 5.2, and it is intended to ensure that the power converter has ride-through capability when exposed to local disturbances or transmission line faults. It is responsible for the injection of the active and reactive current components (I_{pord}, I_{qord}) into the grid, based on the set point values (I_{pcmd}, I_{qcmd}) received as input by the REEC module, and readjusted in case of high or low voltage events. This operation is carried out through the following dedicated subsystems:

- HVRCM: high voltage reactive current management.
- LVACM: low voltage active current management.

5.4.1 The High Voltage Reactive Current Management

The HVRCM functions to alter the control behaviour of the reactive power during high-voltage operation, by acting on the reactive current injection (I_{qord}). The term reactive current describes both inductive and capacitive behaviour, which respectively cause reactive power absorption and production by the inverter. The goal of this block is to provide, during high voltage event, an inductive behaviour, in order to achieve a potential reduction at the POI. The mechanism of control implemented in the HVRCM block is illustrated by the diagram of Figure 5.25. The output I_{qord} is computed according to:

$$I_{qord} = \frac{I_{qcmd} * V_d - \Delta Q_{cmd}}{V_d} \tag{5.21}$$

where ΔQ_{cmd} represents the additional inductive power required by the system to counteract the voltage rise. Therefore, under normal circumstances ($\Delta Q_{cmd} = 0$), the injected current I_{qord} coincides with the set point value I_{qcmd}, belonged to the 'I_{qcmd} control' block of the REEC module. On the other hand, when the voltage V_d exceeds the threshold value (V_{0lim}), the switch of Figure 5.25 is activated and an additional inductive current injection is provided, governed by the following equations:

$$\Delta V = V_d - V_{0lim} \tag{5.22}$$

$$\Delta Q_{cmd} = K_{hv} \Delta V \tag{5.23}$$

The reactive power change due to the voltage variation is shown in Figure 5.24. The slope of the line is specified as the constant K_{hv} and it is determined according to the voltage range variation of the local network.

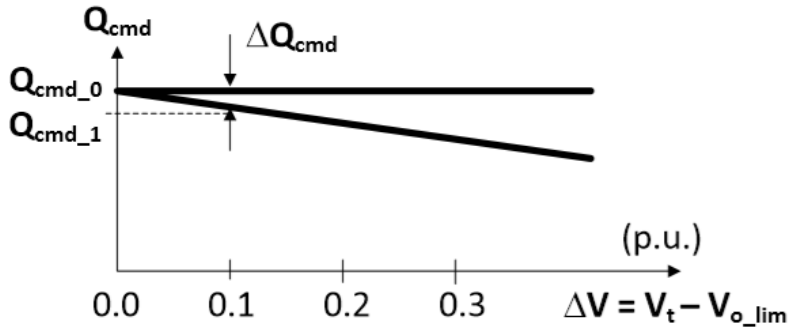

Figure 5.24- Scheme illustrating the link between voltage and reactive power variations.

The HVRCM also provides a current limiter to ensure that I_{qmax} and I_{qmin}, computed in the REEC block, are not exceeded. Table 5.11 indicates the values of the adopted parameters.

Name	***Symbol***	***Value***	***Unit of measurement***
Voltage filter gain	K_{rv}	1	*[p.u.]*
Voltage filter time constant	T_{rv}	0.02	*[s]*
Reactive current filter gain	$K_{\_Iq}$	1	*[p.u.]*
Reactive current filter time constant	$T_{\_Iq}$	0.02	*[s]*
Maximum rising slew rate	I_{qrmax}	100	*[p.u./s]*
Maximum falling slew rate	I_{qrmin}	-100	*[p.u./s]*
Derivative time constant for slew rate	$Td_{\_Iq}$	0.001	*[s]*
Voltage limit	V_{0lim}	1.15	*[p.u.]*
Conversion coefficient from ΔV to ΔQ	K_{hv}	0.7	*[p.u.]*
Maximum ΔQ	$deltaQ_{max}$	1	*[p.u.]*
Minimum ΔQ	$deltaQ_{min}$	-1	*[p.u.]*

Table 5.11- HVRCM parameters.

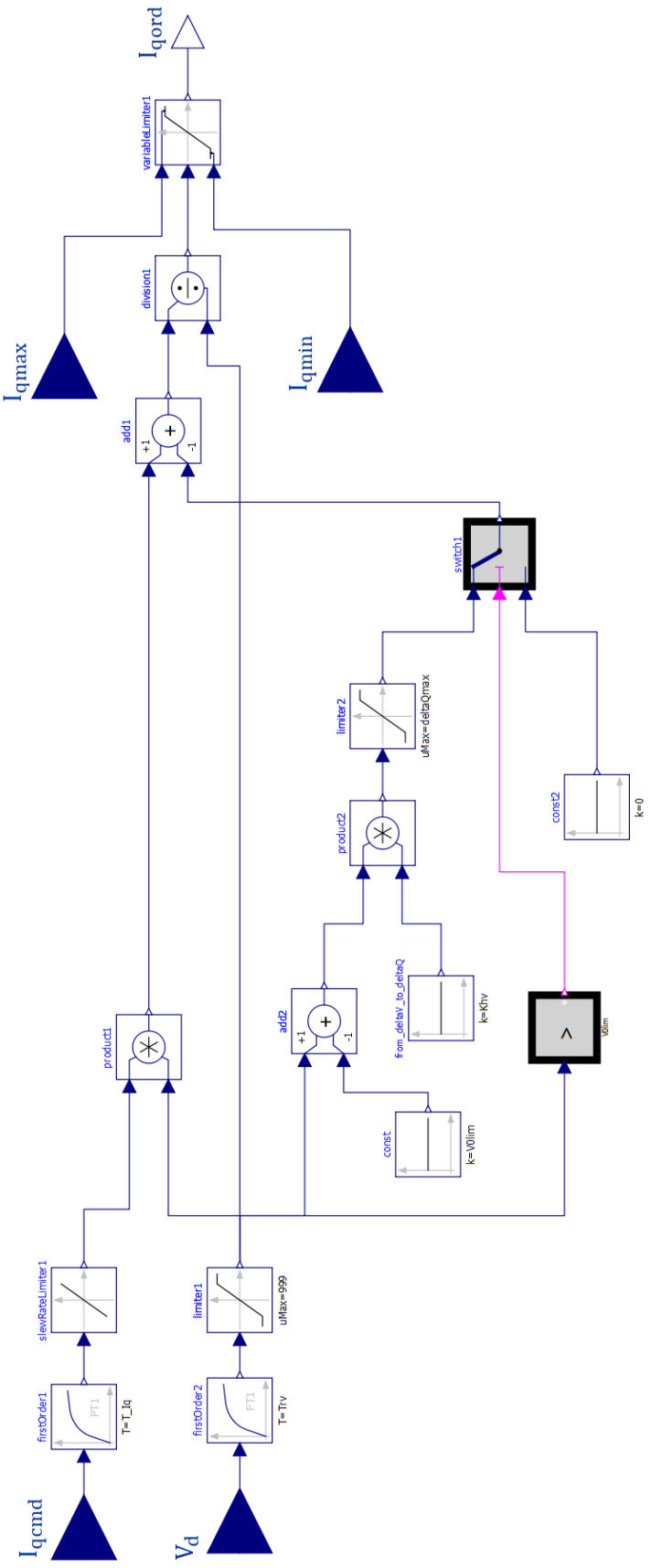

Figure 5.25- Block diagram illustrating the HVRCM controller.

The Low Voltage Active Current Management: LVACM

The LVACM functions to alter the control behaviour of the active power during low-voltage operation. As previously stated, when a voltage drop at the POI occurs, the generator should provide capacitive reactive current to help it rise again within acceptable limits. In this situation, in order to accommodate both the current-carrying capability of the power switches (IGBT and diodes) and the capacitive current increment, it is advisable to limit the real current component I_{pord} giving extra headroom to the I_{qord} behaviour. This process is carried out in the LVACM block by the computation of two quantities:

- The scaled voltage Vt_{scaled}.
- The upper limit current I_{pmax} through LVPL logic.

whose modalities of calculation, obtained through the look-up tables shown in Figure 5.26, are explained later. The implemented mechanism of control is depicted in Figure 5.26. During normal conditions, the output real current coincides with the set point value calculated in the 'I_{pcmd} control' block of the REEC module, and it is computed as:

$$I_{pord} = \frac{P_{ord}}{V_d} = \frac{V_d * I_{pcmd}}{V_d} \tag{5.24}$$

On the other hand, when the measured voltage at the POI (V_d) drops under the tolerable limit (V_{dip}), the output current is obtained according to:

$$I_{pord} = \frac{P_{ord}}{V_d} = \frac{Vt_{scaled} * I_{pcmd}}{V_d} \tag{5.25}$$

where P_{ord}, and consequently I_{pord}, have now achieved a lower value compared to the ones assumed in the normal situation (5.24).

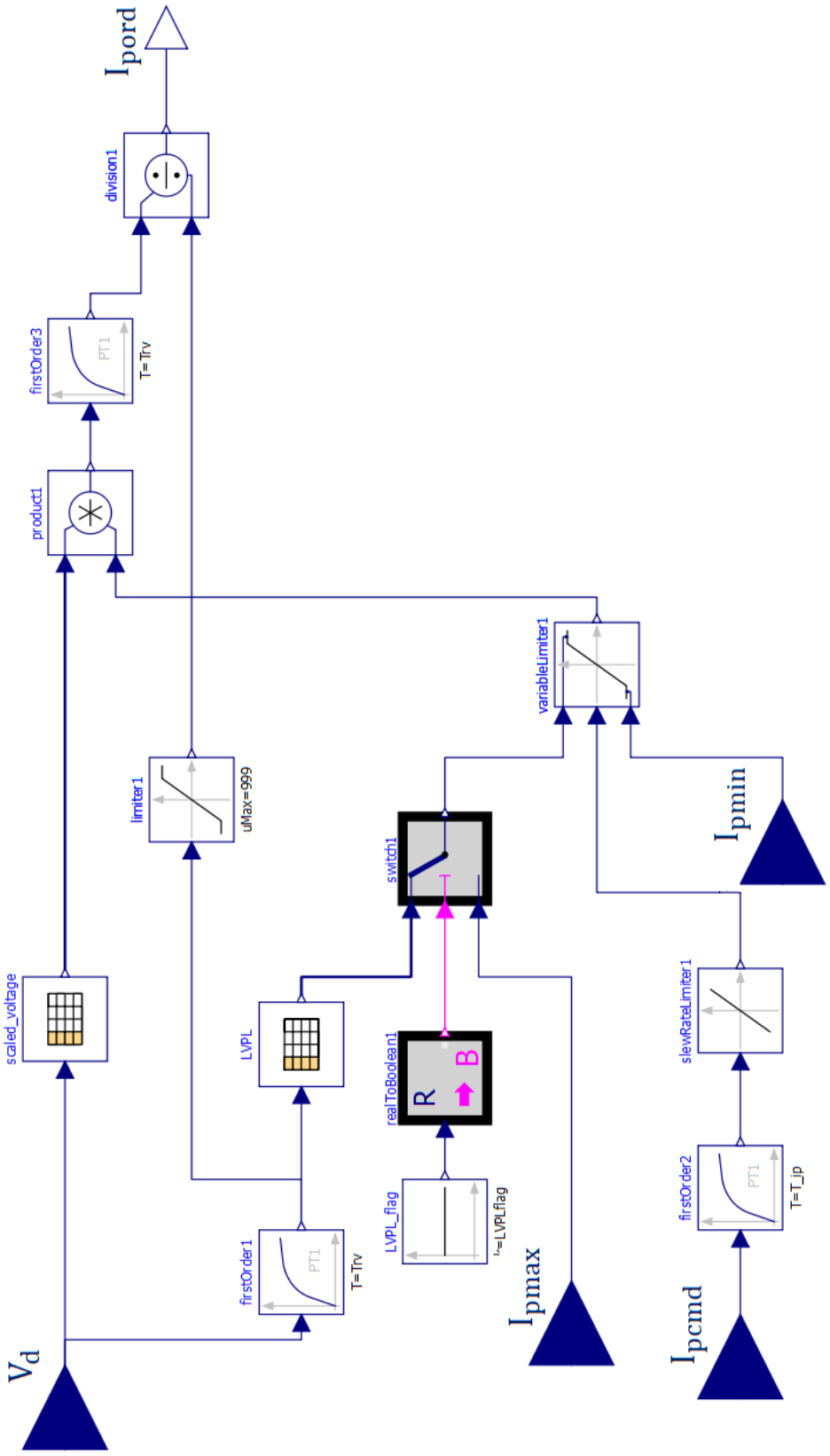

Figure 5.26- Scheme of the LVACM controller.

Computation of Vt_{scaled}

As aforementioned, during low-voltage event it is convenient to limit the active current output to boost the voltage within its acceptable range again. To achieve this goal, LVACM calculates a scaled voltage value, which results in a reduced active power command (P_{ord}) and in a consequent lower real current production I_{pord}. Vt_{scaled} is computed by the look-up table 'scaled_voltage', depicted in Figure 5.26. It is based on a pre-programmed map, as the one shown in Figure 5.27, and readjusted to meet our needs.

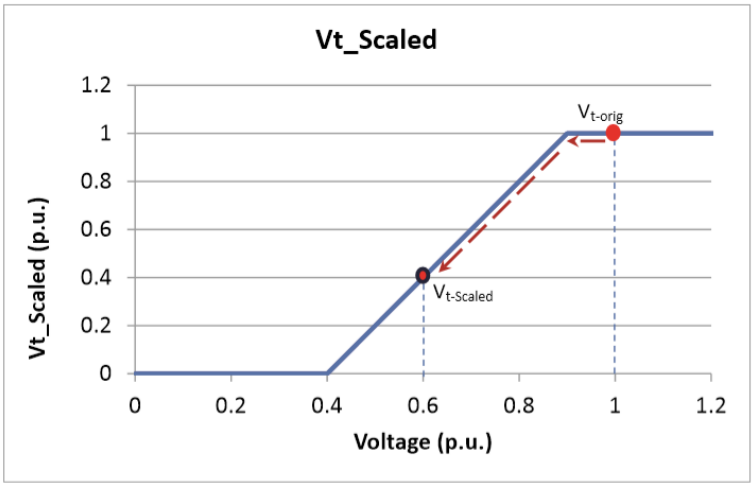

Figure 5.27- Scaled voltage to adjust the Pord during a low-voltage event.

The 'scaled_voltage' look-up table of Figure 5.26, whose parameters are reported in Table 5.12, receives as input the measured voltage (V_d), represented by the x-axis in Figure 5.27, and results in output the scaled voltage value (Vt_{scaled}).

V_d [p.u.]	Vt_{scaled} [p.u.]
0	0
0.4	0
0.5	0.2
0.6	0.4
0.7	0.6
0.8	0.8
0.85	0.85
1	1

Table 5.12- Look-up table indicating the Vtscaled map.

Therefore, in normal situations, the output Vt_{scaled} coincides with the original value V_d, and the active current I_{pord} is obtained according to (5.24). During low-voltage event, instead, the resulting Vt_{scaled} assumes a lower value with respect to the input V_d, and the real current is obtained following (5.25).

Computing I_{pmax}

In order to decrease the output active current I_{pord}, an additional strategy can be applied, aimed at lowering the maximum active current limit I_{pmax}, with consequent possible reduction of the variable I_{pcmd}. Depending on the position of the switch $LVPL_{flag}$ (Figure 5.26), two operations are available to calculate the upper active current limit I_{pmax}:

- $LVPL_{flag} = 0 \rightarrow I_{pmax}$ corresponds to the value computed in the REEC block. In this case, no further reduction are involved for I_{pcmd}.
- $LVPL_{flag} = 1 \rightarrow I_{pmax}$ is reduced through the use of the look-up table 'LVPL' (Figure 5.26), whose value are reported in Table 5.13. This element, based on the voltage measurement (V_d) received as input, provides, in case of low-voltage event, a correspondent value of I_{pmax}, reduced with respect to the original one.

$\boldsymbol{V_d}$ $[\boldsymbol{p.u.}]$	$\boldsymbol{LVPL - I_{pmax}}$ $[\boldsymbol{p.u.}]$
0	0
0.4	0
0.5	0.25
0.6	0.48
0.7	0.65
0.8	0.83
0.85	1.2
1.2	1.2

Table 5.13- Look-up table indicating the LVPL values.

The parameters of Table 5.13 have been set following a pre-programmed map, as the one shown in Figure 5.28, and readjusted to meet our needs.

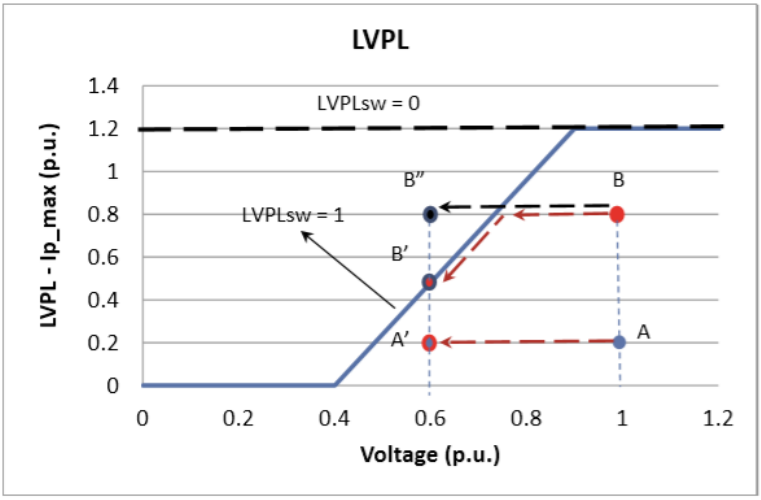

Figure 5.28- LVPL calculation to set the upper limit of Ipcmd during low-voltage event.

The parameters adopted in the LVACM block are reported in Table 5.14.

Name	***Symbol***	***Value***	***Unit of measurement***
Voltage filter gain	K_{rv}	1	*[p.u.]*
Voltage filter time constant	T_{rv}	0.02	*[s]*
Active current filter gain	$K_{\_Ip}$	1	*[p.u.]*
Active current filter time constant	$T_{\_Ip}$	0.02	*[s]*
Maximum rising slew rate	$Rrpwr_{\_max}$	100	*[p.u./s]*
Maximum falling slew rate	$Rrpwr_{\_min}$	-100	*[p.u./s]*
Derivative time constant for slew rate	$Td_{\_Ip}$	0.001	*[s]*
LVPL switch state	$LVPL_{flag}$	0-1	-

Table 5.14- LVACM parameters.

6. The Model Validation

The validation procedure of the model is important in order to ensure a proper representation of PV generation power plants in bulk power system studies. In fact, a model is valid if its dynamic behaviour, consistent with the implemented structure and the hypotheses made, influences the network of interest in a way close enough to reality. To achieve this goal, two categories of tests have been performed:

- Individual subsystems tested in OpenModelica.
- Dynamic simulation of the entire PV plant connected to the test network in Dyana/TESEO environment.

In both cases, the analysis of the model has been carried out by creating representative situations, sometimes extreme, and verifying through the relative graphs, the correspondence between the trends of the system variables and the expected results.

6.1 Test in OpenModelica

The tests conducted in OpenModelica environment have the only purpose of verifying the correct functioning of the components adopted and the logic implemented in the control system. In fact, in this validation stage, the feedback provided by the system is not included, as the model is not yet connected to the network. Consequently, the responses of the PI regulators must be considered approximate and not conclusive, since their tuning operations are carried out in the next step. In order to achieve the aforementioned goals, the main blocks of the model have been tested individually applying input signals provided by the “Source” package of the OpenModelica library. The following sections show some of the simulations carried out.

6.1.1 HVRCM Test

HVRCM acts providing additional inductive current in case of high voltage event, while does not involve current changes under normal situations.

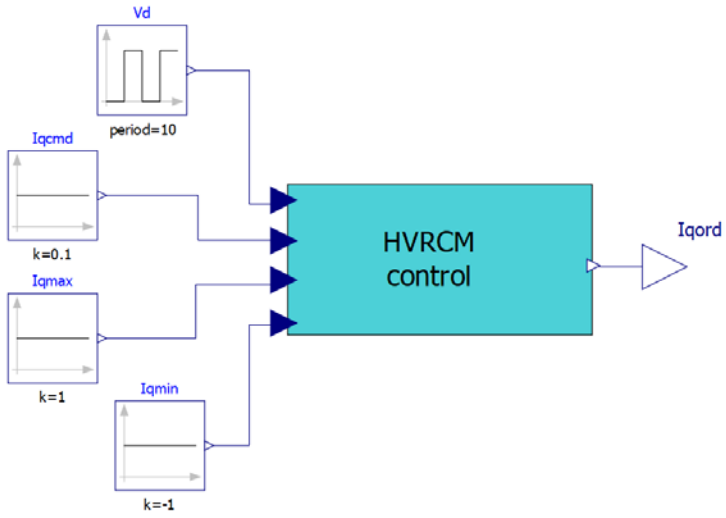

Figure 6.1- HVRCM block.

In the test, a normal operating condition at $1\ p.u.$ voltage was supposed for the first 5 seconds followed by a sudden increase to $1.2\ p.u.$ (Figure 6.1). It has been also assumed that the system has the capability of returning the voltage to its nominal value within one second, thus avoiding the disconnection of the entire plant from the grid.

Input	***Value***
V_d	$1\ p.u\ for\ t < 5\ s\ and\ t \geq 6\ s;\ 1.2\ p.u.\ for\ 5\ s \leq t < 6\ s$
I_{qcmd}	$0.1\ p.u.$
I_{qmax}	$1\ p.u.$
I_{qmin}	$-1\ p.u$

Table 6.1- Input values for HVRCM testing.

Since the system considered involves an open loop, the voltage variation has been simulated through a square wave input; the reactive current values in entrance to the block have instead been set at constant per unit values, readable in Table 6.1. The purpose of the test is to verify that the trend of I_{qord} coincides with the commanded current signal (I_{qcmd}) in normal operation, while showing an additional inductive injection during high-voltage

conditions, in accordance to the equations (5.22) and (5.23). Figure 6.2 illustrates the results of the simulation.

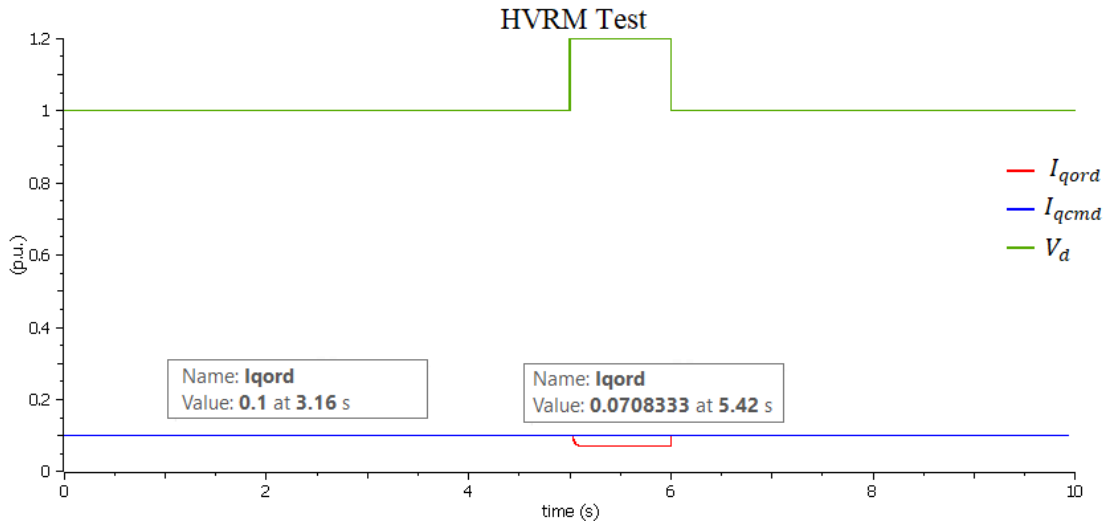

Figure 6.2- Simulation results showing the output current (in red), the commanded current provided by REEC block (in blue) and the voltage at the POI (in green).

Since the starting reactive current (I_{qcmd}) has been set to a positive value, the injection of reactive current (I_{qord}) into the grid, during the voltage raising, is reduced by the additional inductive contribution.

6.1.2 The LVACM Test

To verify the correct operation of LVACM, it is appropriate to test the block under both $LVPL = 1$ and $LVPL = 0$ conditions. The two experiments have been carried out considering a voltage transition from $1\ p.u.$ to $0.7\ p.u$, for the duration of 1 second, applying a pulse source (Figure 6.3).

Input	***Value***
V_d	$1\ p.u\ for\ t < 5\ s\ and\ t \geq 6\ s;\ 0.7\ p.u.\ for\ 5\ s \leq t < 6\ s$
I_{pcmd}	$0.8\ p.u.$
I_{pmax}	$1\ p.u.$
I_{pmin}	$-1\ p.u$

Table 6.2- Input values for LVACM testing.

The remaining input variables are represented by constants, whose values are shown in Table 6.2.

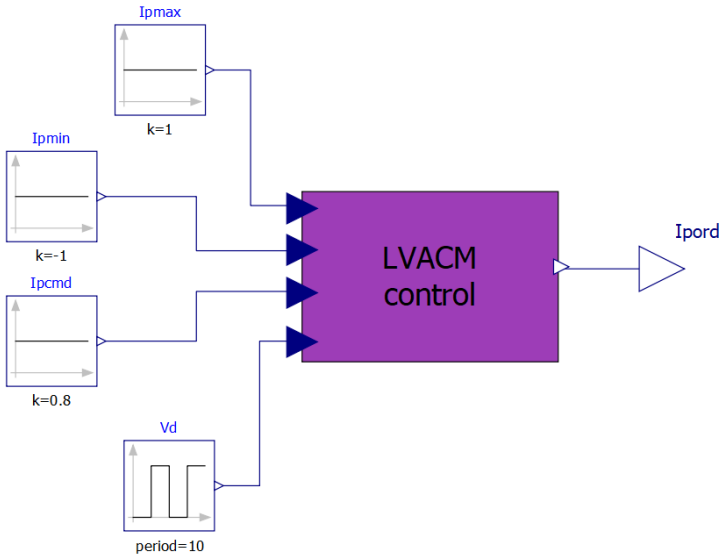

Figure 6.3- LVACM block.

Inducing a voltage drop to 0.7 p.u. the LAVCM has to decrease the injected active current into the grid in order to provide extra headroom for the reactive component. For LVPL=1, the reduction is affected both by the scaled voltage and by the limitation on the upper current value. The results are shown in Figure 6.4.

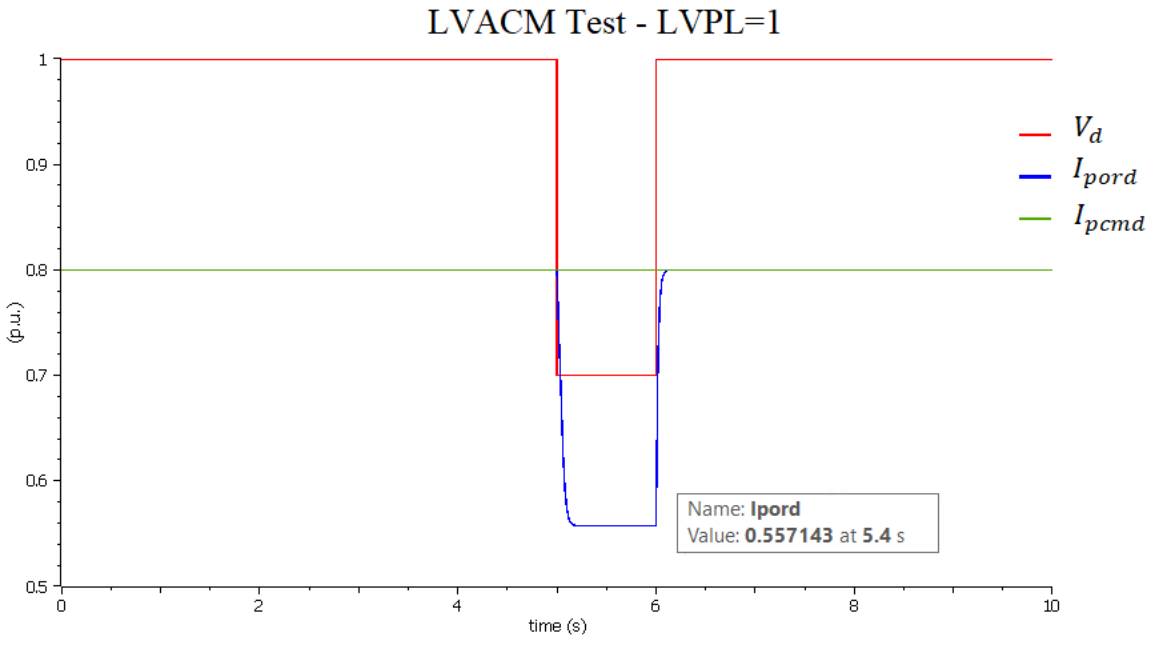

Figure 6.4- Simulation results showing the output current (in blue), the commanded current provided by REEC block (in green) and the voltage at the POI (in red) in LVPL=1 condition.

On the other hand, when the switch is deactivated (LVPL=0), only the reduced potential influences the output current (Figure 6.5). A lower I_{pord} value is therefore expected in the case of LVPL=1.

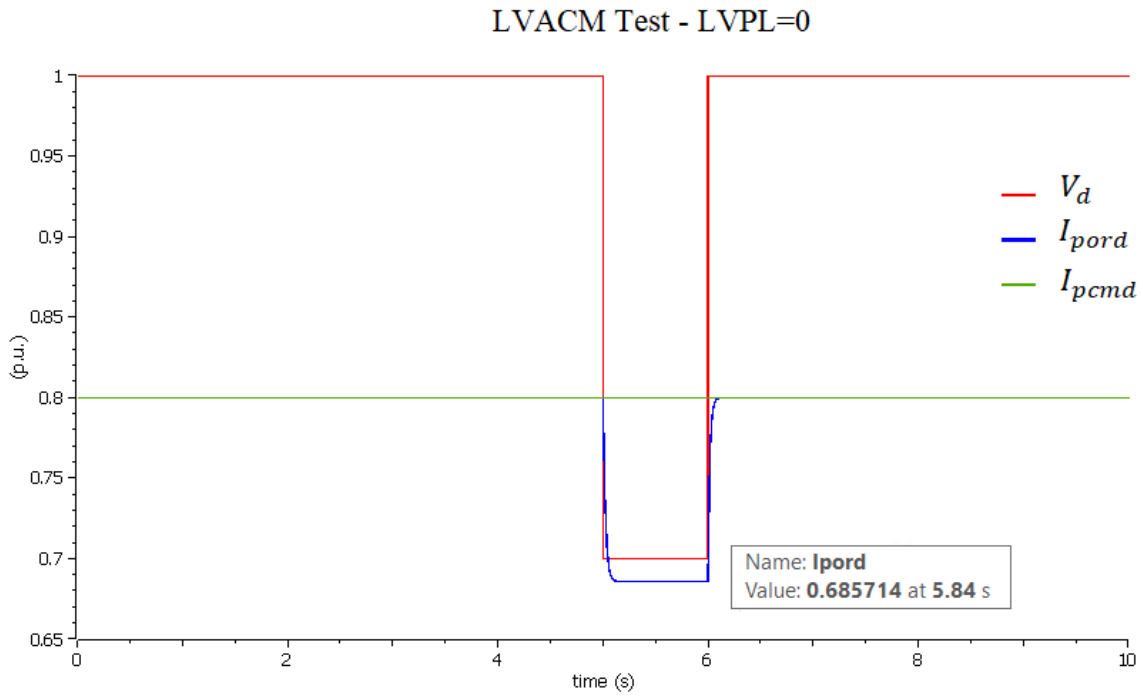

Figure 6.5- Simulation results showing the output current (in blue), the commanded current provided by REEC block (in green) and the terminal voltage (in red) in LVPL=0 condition.

6.1.3 Reactive Current Regulation Test

The main purpose of these tests is to verify the correct operation of the 'I_{qcmd} control' block under multiple selectable paths. Two examples are considered in the following, where the entry "N/A" specifies that the state of the switch does not affect the indicated control mode.

a) $PF_{flag} = 0$; $V_{flag} = N/A$; $Q_{flag} = 0$: Linear Q control path.

A step function has been used to simulate the sudden change of the reference Q_{ext}, while the voltage was represented by a constant at $1\,p.u$ value. As the linear control has been selected, the output current, delayed by the filter action, linearly follows the change in reactive power. The results are shown in Figure 6.6; the test parameters are reported in Table 6.3.

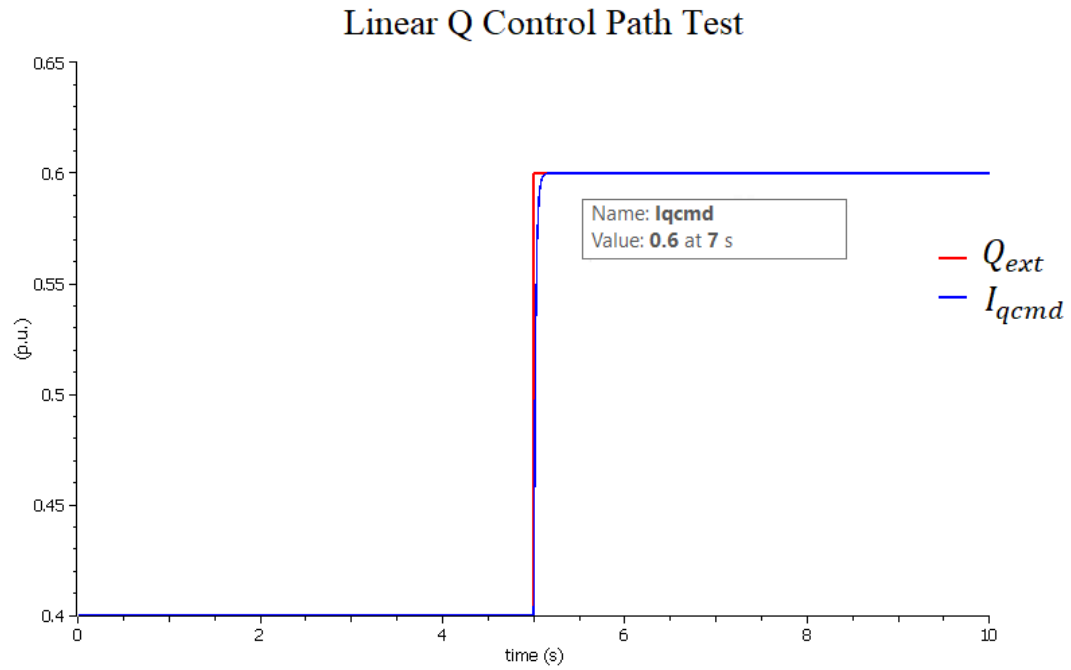

Figure 6.6- Simulation results showing the commanded reactive output current (in blue) and the reference reactive power provided by REPC block (in red).

Input	***Value***
Q_{ext}	$0.4\ p.u\ for\ t < 5\ s\ ;\ 0.6\ p.u.\ for\ t \geq 5\ s$
V_{ref}	$1\ p.u.$
V_d	$1\ p.u.$
I_{inj}	$0\ p.u$
p	$0.8\ p.u$
q	$0.4\ p.u$
freeze	*false*
On_off	*false*

Table 6.3- Parameters for linear Q control path.

b) $PF_{flag} = N/A\ ;\ V_{flag} = 0\ ;\ Q_{flag} = 1$: Voltage control.

For the reactive current regulation analysis, a change in the reference voltage from $0.9\ p.u.$ to $1\ p.u.$ at $t = 3\ s$ has been set via a step function. To emulate a closed loop, the measured voltage V_d has been represented by a ramp signal, which starts from $0.85\ p.u.$ and reaches 1 p.u. at $t = 4\ s$ (Figure 6.7).

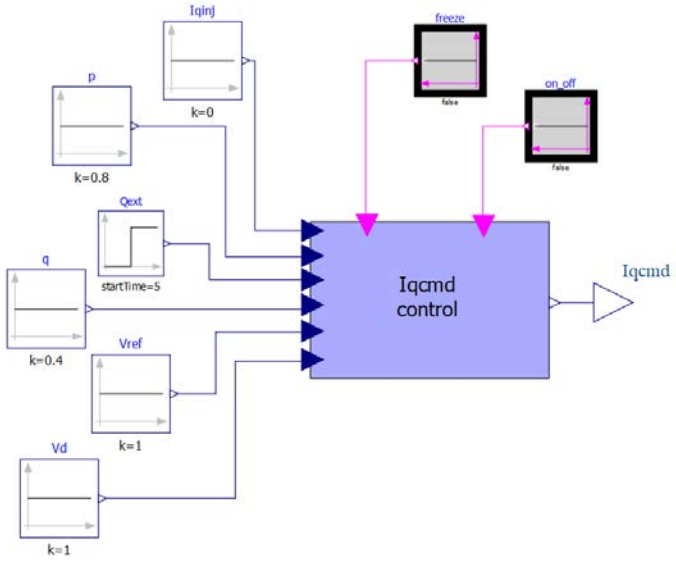

Figure 6.7- Iqcmd control block.

The results of Figure 6.8 verifies the approximate correct performance of the PI regulator, which induces the positive reactive current injection into the grid to rise in the positive error region ($V_{ref} > V_d$) and to decrease in case of negative error ($V_{ref} < V_d$).

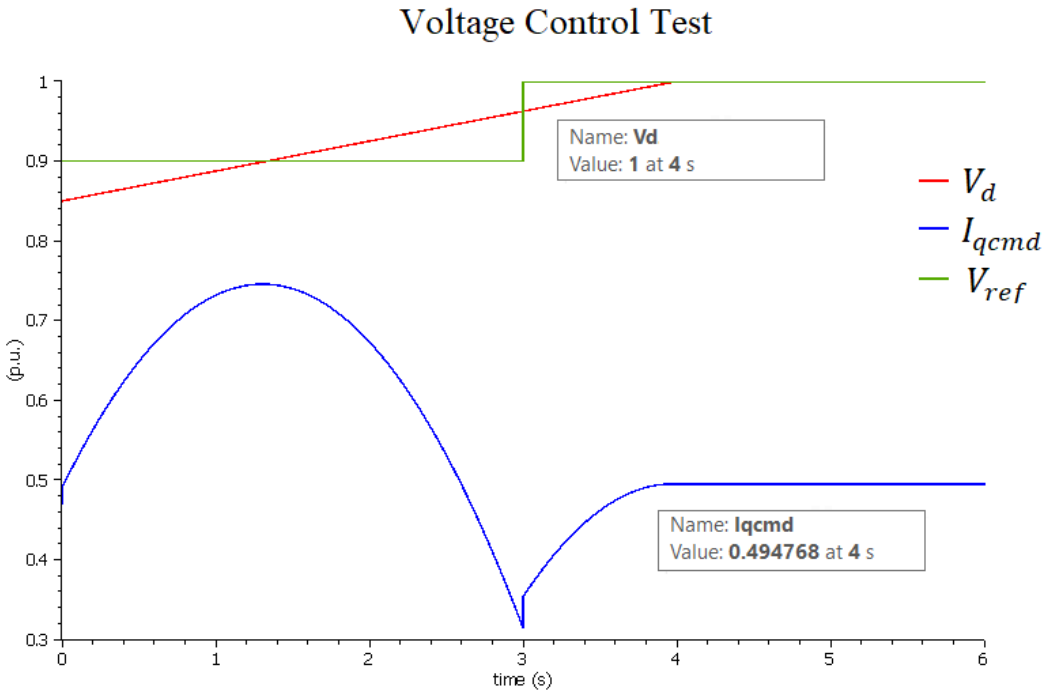

Figure 6.8- Simulation results showing the commanded reactive output current (in blue), the reference voltage (in green) and the measured voltage (in red).

Input	***Value***
Q_{ext}	$0.4\ p.u.$
V_{ref}	$0.9\ p.u\ for\ t < 3\ s\ ;\ 1\ p.u.\ for\ t\ \geq 3\ s$
V_d	$0.85\ p.u\ at\ t = 0\ s\ ;\ 1\ p.u.\ for\ t \geq 4\ s$
I_{inj}	$0\ p.u.$
p	$0.8\ p.u.$
q	$0.4\ p.u.$
freeze	*false*
On_off	*false*

Table 6.4- Voltage control parameters.

6.1.4 Real Current Regulation Test

The test was conducted to verify the operation of the 'I_{pcmd} control' block, aimed at providing the appropriate active current component. Being a linear feed-forward control, the output must be able to follow the variation of the real power reference P_{ext}. The analysis was conducted through a pulse input source to simulate the power reference, while the voltage at the inverter terminals was assumed to be constant at its nominal value of $1\ p.u.$ (Figure 6.9).

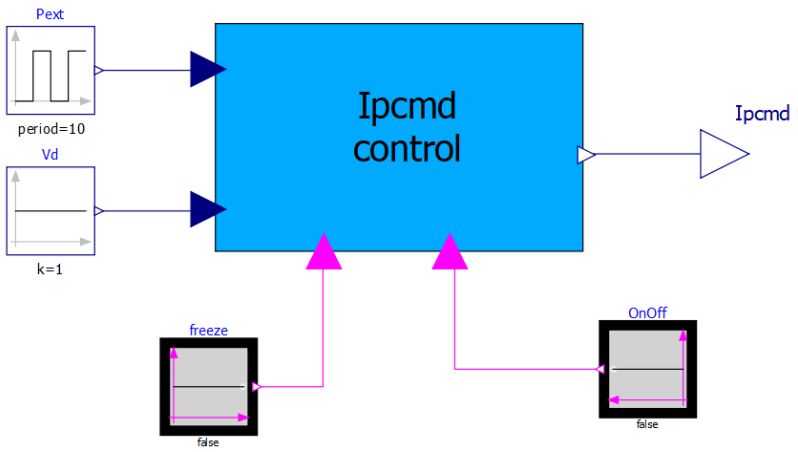

Figure 6.9- Block testing the active current control.

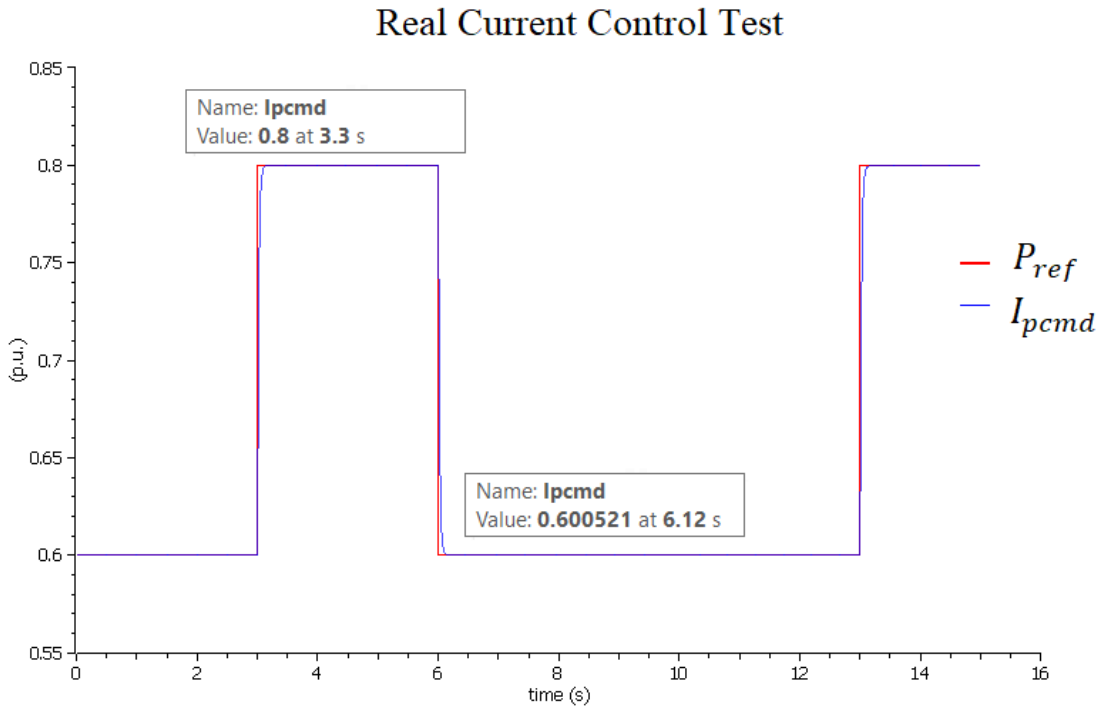

Figure 6.10- Simulation results showing the commanded active output current (in blue) and the reference active power (in red).

The simulation results of Figure 6.10 verify the linear behaviour of the output current, delayed only by the filter effect. The adopted input variables are reported in Table 6.5.

Input	***Value***
P_{ext}	$0.6\ p.u\ for\ t < 3\ s\ and\ for\ 6\ s \leq\ t < 13\ s$; $0.8\ p.u.\ for\ \ 3\ s \leq\ t < 6\ s\ and\ \ t\ \geq 13\ s$
V_d	*1 p.u.*
freeze	*false*
On_off	*false*

Table 6.5- Active current regulation test parameters.

6.1.5 Reactive Power Control in REPC block

This test involves the adoption of the 'Q_{ext} control' block in reactive power control mode ($Ref_{flag} = 0$).

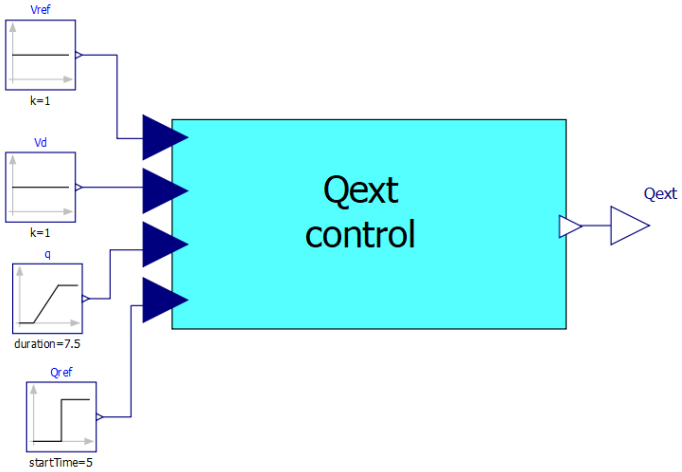

Figure 6.11- Reactive power control test for REPC block.

The aim is to obtain an output response according to the variable difference between reference (Q_{ref}) and measured (q) reactive power, provided as input. The first one has been represented by a step function that rises from $0.2\ p.u.$ to $0.4\ p.u.$ 5 seconds after the start of the simulation. The measured reactive value has been emulated through the use of a ramp signal instead (Figure 6.11). The values of the input parameters are listed in Table 6.6; the simulation results are displayed in Figure 6.12.

Input	***Value***
Q_{ext}	$0.2\ p.u\ for\ t < 5\ s\ \ ;\ 0.4\ p.u.\ for\ \ t \geq 5\ s$
q	$0.2\ p.u\ for\ t < 1.5\ s\ \ ;\ 0.4\ p.u.\ for\ \ t \geq 9\ s$
V_{ref}	*1 p.u.*
V_d	*1 p.u.*
Ref_{flag}	*0*

Table 6.6- Input parameters for reactive power control test in REPC block.

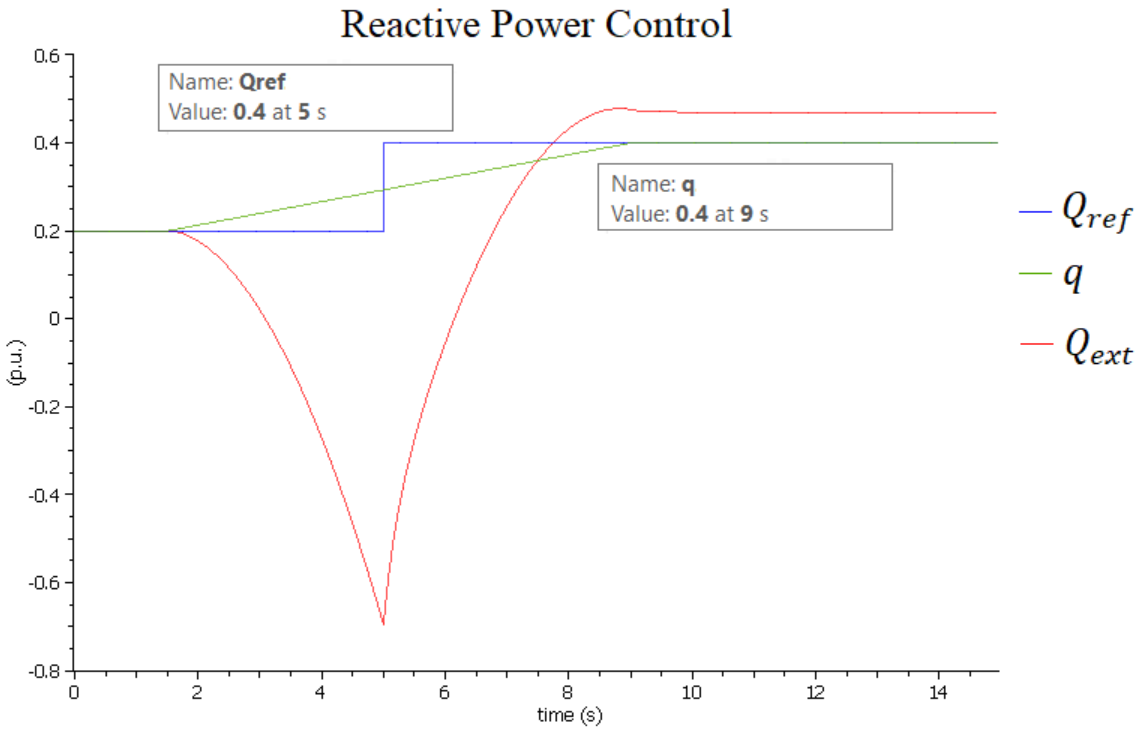

Figure 6.12- Simulation results of the reactive power control in REPC showing: the reference reactive power (in blue), the measured reactive power (in green) and the output reactive power (in red).

6.1.6 Active Power Control in REPC block

This test involves the adoption of the 'P_{ext} control' block including the governor response mode ($Freq_{flag} = 1$). In the first simulation (Figure 6.14) a normal operation has been evaluated, aimed at showing the PI regulator's behaviour.

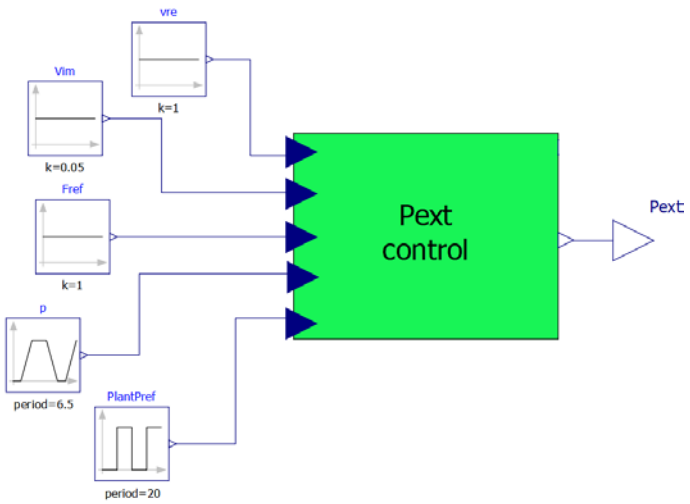

Figure 6.13- Active power control test for REPC block.

An increase in reference active power ($Plant_{Pref}$) was considered through a pulse wave, while a trapezoidal signal representing the measured power (p) was used to emulate the closed loop (Figure 6.13). The graph of Figure 6.14 shows how the controller response follows the error variation between the two variables.

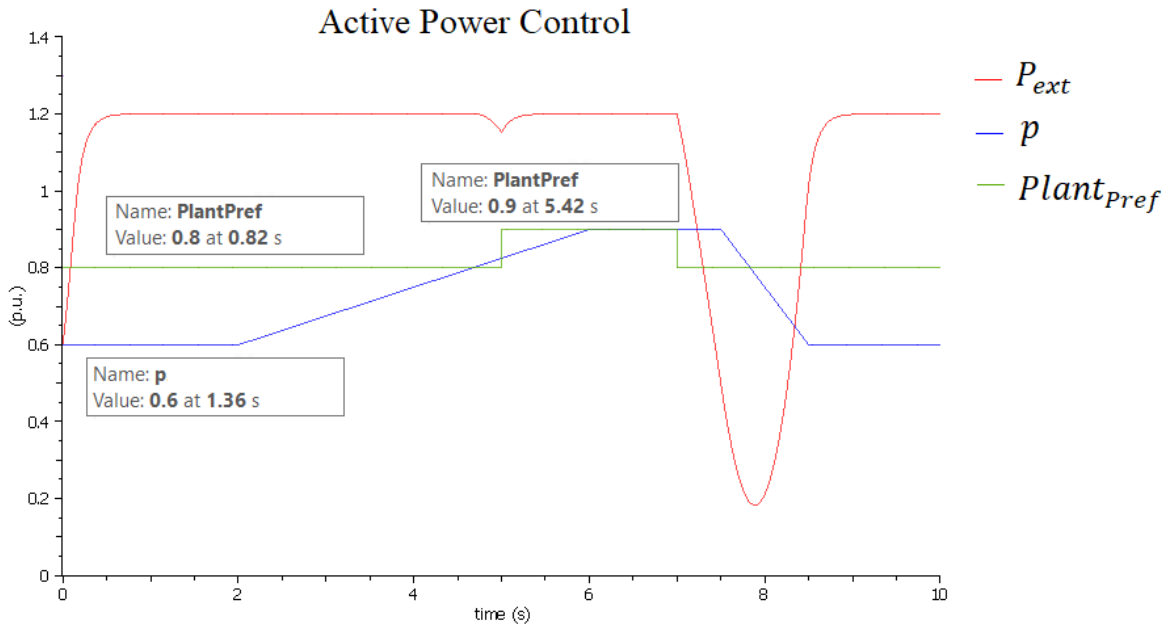

Figure 6.14- Simulation results of active power control in normal condition showing: the commanded reference active power (in red), the measured real power value (in blue) and the active power reference of the plant (in green).

The adopted values for input parameters are written in Table 6.7, where the real and imaginary parts of the measured voltage have been appropriately set in order to not involve an incident frequency variation.

Input	***Value***
$Plant_{Pref}$	$0.8\ p.u\ for\ t < 5\ s\ and\ \ t \geq 7\ s\ ;\ 0.9\ p.u.\ for\ 5\ s < t \leq 7\ s$
p	$0.6\ p.u\ for\ t < 2\ s\ and\ \ t \geq 8.5\ s\ ;\ 0.9\ p.u.\ for\ 6\ s < t \leq 7.5\ s$
V_{re}	*1 p.u.*
V_{im}	*0.05 p.u.*
F_{ref}	*1 p.u.*
$Freq_{flag}$	*1*

Table 6.7- Input parameters for the active power control test.

A further simulation (Figure 6.16) was carried out to observe the system's response to frequency variations. For this purpose, a voltage drop was simulated by appropriately altering the real voltage input through a ramp signal, resulting in a frequency change from 1 $p.u.$ to 0.988 $p.u$, illustrated in Figure 6.15.

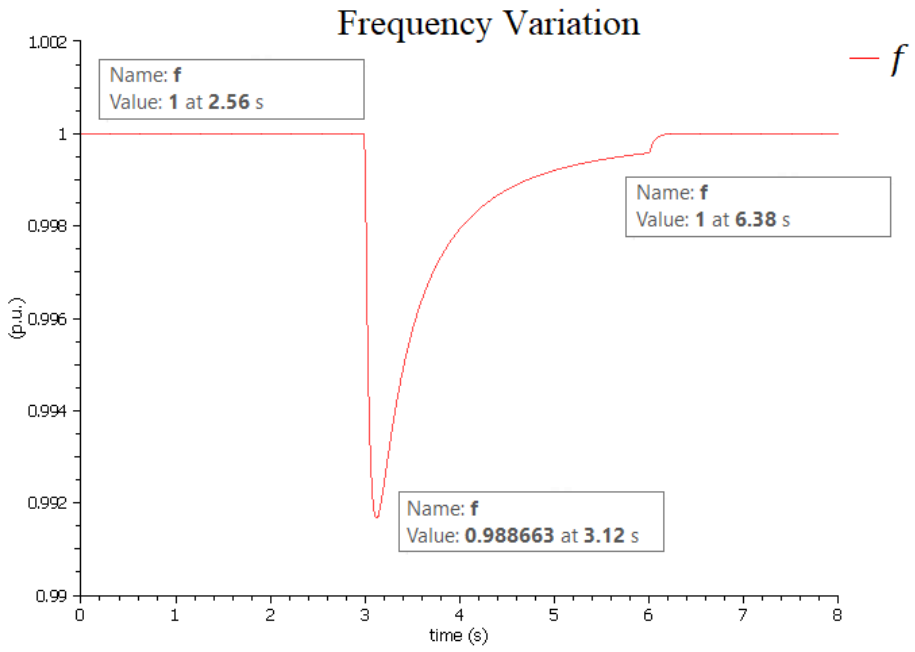

Figure 6.15- Simulation result showing the frequency variation due to the voltage drop at the inverter terminal.

As displayed in Figure 6.16, the droop controller reacts to the under-frequency event by generating an active power signal ($deltaP$) in order to boost the total active power reference (P_{refNew}) and consequently cause an additional active current injection I_{pcmd} by the REEC block. In Table 6.8 the parameter adopted for this simulation are shown.

Input	***Value***
$Plant_{Pref}$	*0.8 p.u.*
p	$0.8\ p.u\ for\ t < 3\ s\ and\ \ t \geq 5.2\ s\ ;\ 0.9\ p.u.\ for\ 4\ s \leq t < 4.2\ s$
V_{re}	$1\ p.u\ for\ t < 3\ \ ;\ 5.3\ p.u.\ for\ t \geq 6\ s$
V_{im}	*0.05 p.u.*
F_{ref}	*1 p.u.*
$Freq_{flag}$	*1*

Table 6.8- Input parameters for the active power control test during under-frequency event.

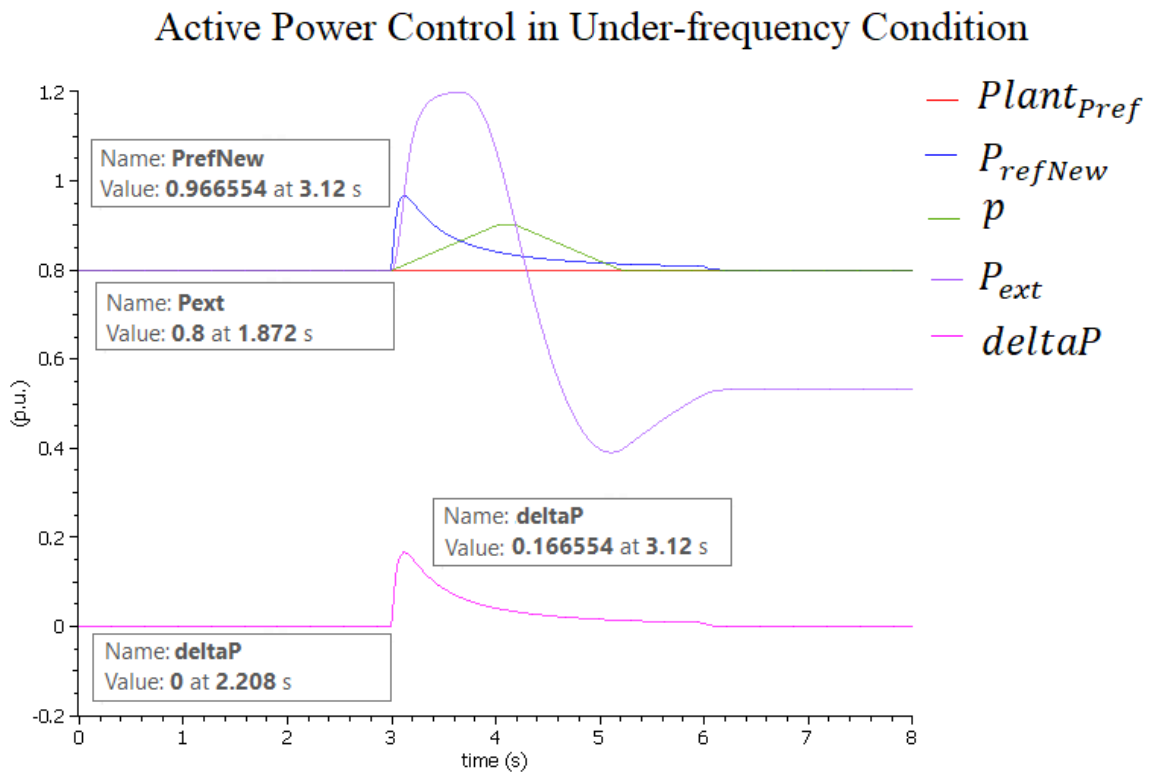

Figure 6.16- Simulation results of active power control in under-frequency condition showing: the active power reference of the plant (in red), the reference active power under abnormal condition (in blue), the measured real power value (in green), the commanded reference active power (in violet) and the active power additional quantity (in pink).

6.2 Test in Dyana/TESEO

As detailed in chapter 4, through the generation of the FMU it was possible to transfer the model information to Dyana/TESEO simulation environment, allowing the connection of the implemented PV generator to a sample grid provided by CESI, shown in Figure 6.17. This phase of work has therefore enabled the tuning of the PI controllers, finding the appropriate values of the proportional and integration constant. A first power flow calculation has been performed to assign the initialization values to the system variables. Through appropriate commands it was also possible to modify the model reference inputs, to emulate load variations, and create fault situations on specific nodes and network lines, in order to observe the PV generator behaviour. Below are some of the tests carried out for dynamic validation.

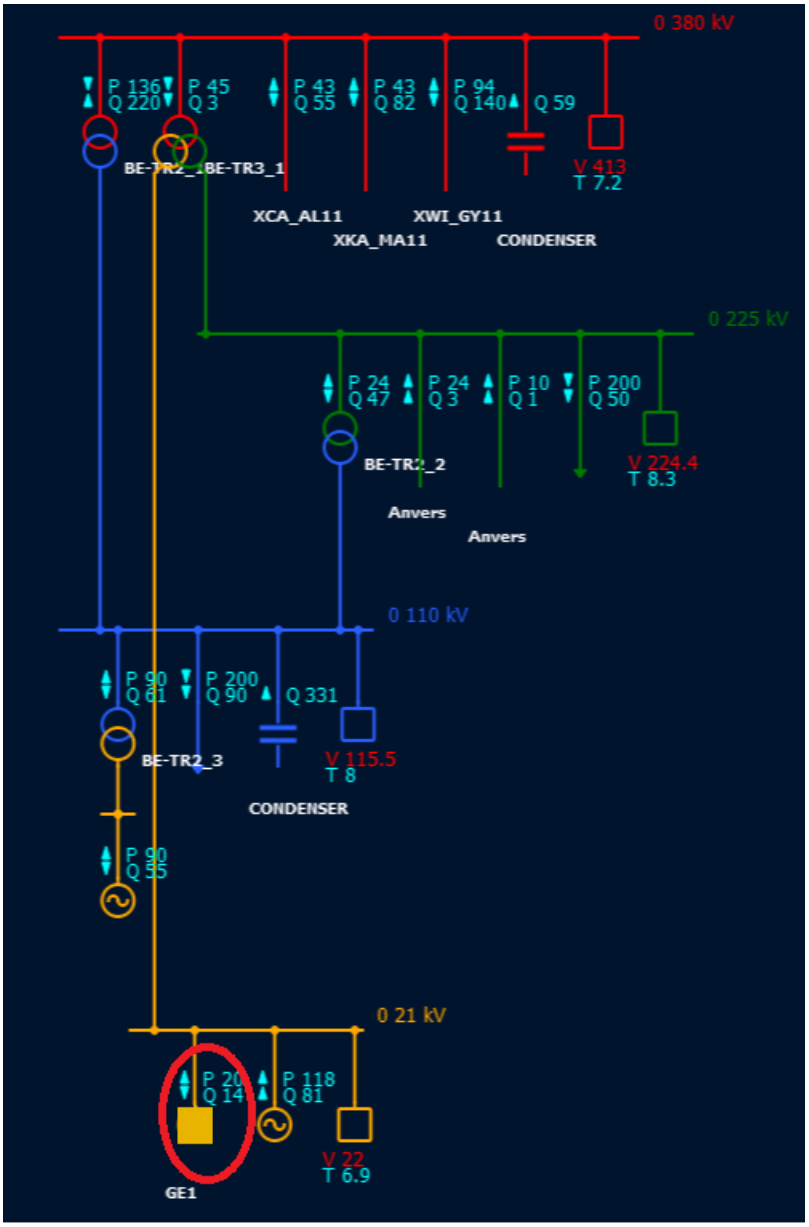

Figure 6.17- Illustration of the micro test network. The photovoltaic generator is highlighted by the circle in red.

6.2.1 Simulation in Linear Q Control Mode

The selected mode provides the reactive current regulation through linear reactive power control. Both tests for normal and fault conditions have been executed in this paragraph. The switch setting values for these simulations are listed in Table 6.9.

SWITCH	VALUE
Ref_{flag}	0
$Freq_{flag}$	1
$PQ_{priority}$	1-0
Q_{flag}	0
PF_{flag}	0
V_{flag}	0
$LVPL_{flag}$	0

Table 6.9- Switches parameters.

Normal Condition

A load variation, emulated by a step signal as a reference input both for active and reactive power, was taken into account. In particular, an increase in active power from $20\,MW$ to $25\,MW$ and a change in reactive power from $-14\,Mvar$ to $-10\,Mvar$ have been assumed. Tests conducted in this situation have allowed the tuning of the PI regulators involved, belonging to the REPC block. The power transients, illustrated in Figure 6.18 and in Figure 6.19 show the proper functioning of the PV generator, able to follow the load variation. Furthermore, the correct parameterization of the PI controllers is proved by the trend of the measured power quantities P_e and Q_e, characterized by a fast-transient response without excessive over-shootings and oscillations.

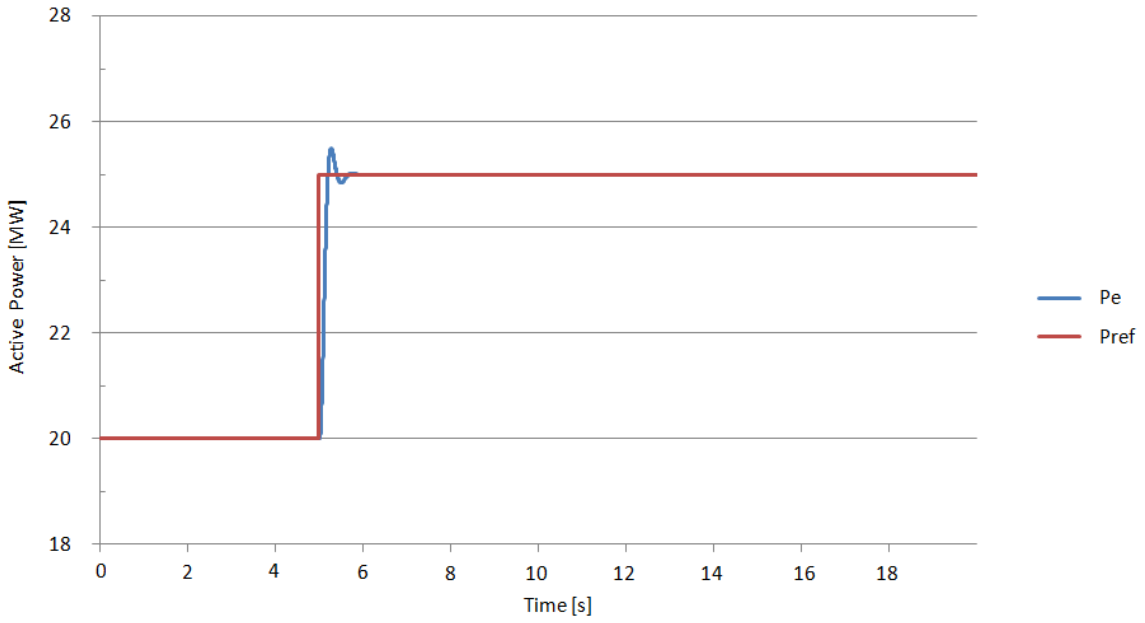

Figure 6.18- Active power output behaviour in linear Q control mode.

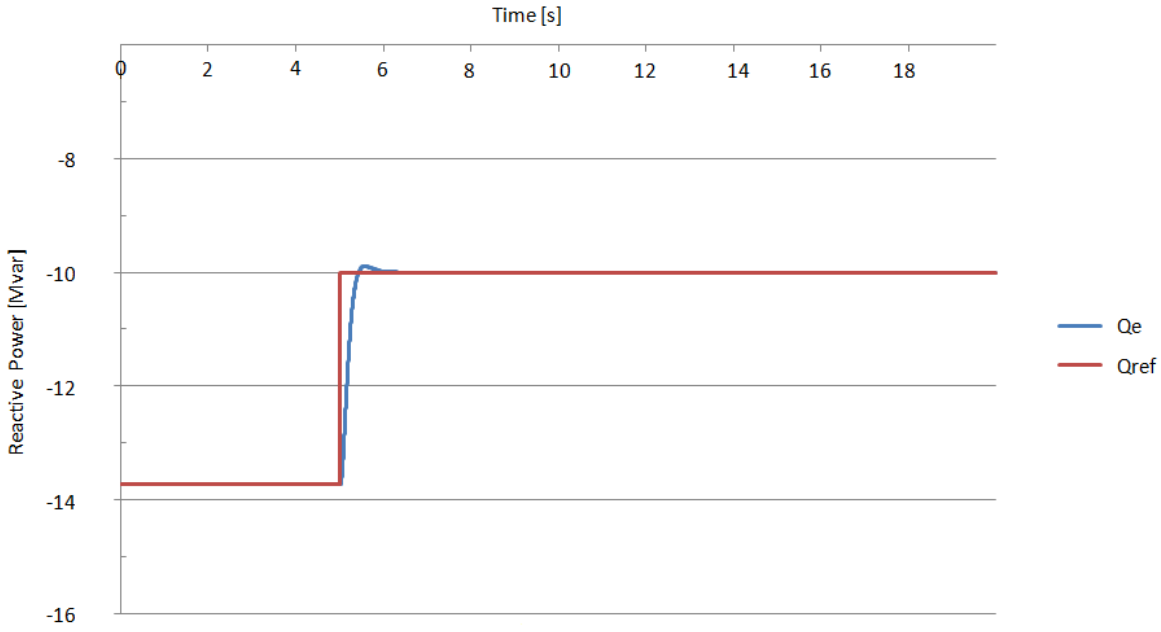

Figure 6.19- Reactive power output behaviour in linear Q control mode.

A zoom of the active and reactive power transients has been provided in Figure 6.20 and Figure 6.21 respectively. From these graphs, it emerges that the new power references (P_{ref}, Q_{ref}) are reached, in both cases, within one second after the load variation.

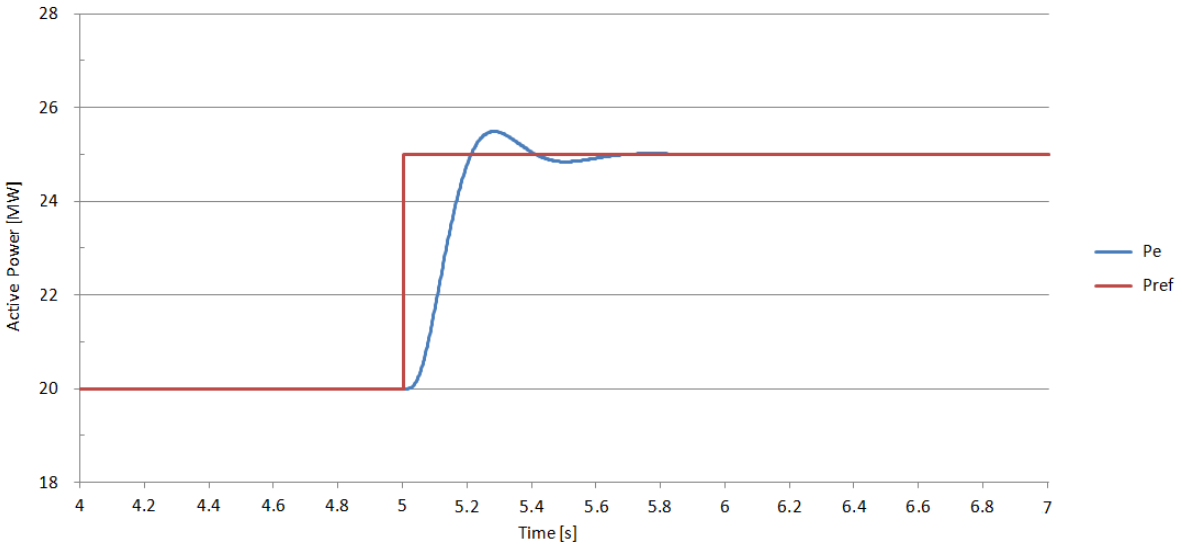

Figure 6.20- Zoom of the active power output trend.

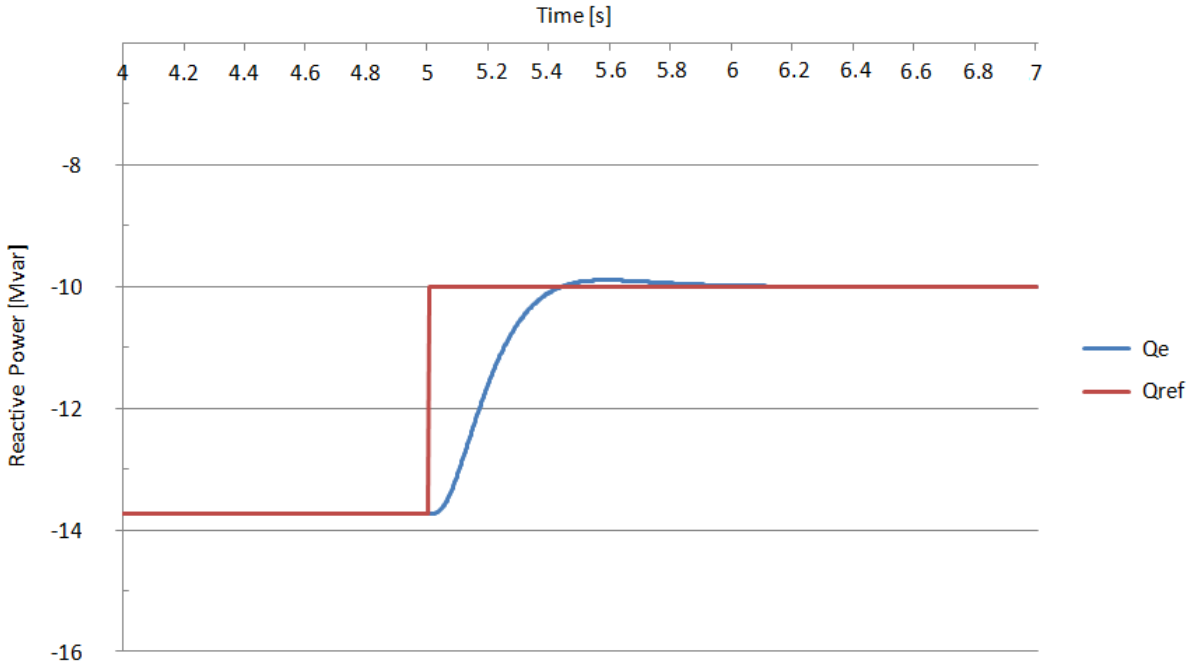

Figure 6.21- Zoom of the reactive power output trend.

The curves of the active and reactive currents, shown in Figure 6.22 and in Figure 6.23 respectively, follow linearly the evolution of the correspondent powers.

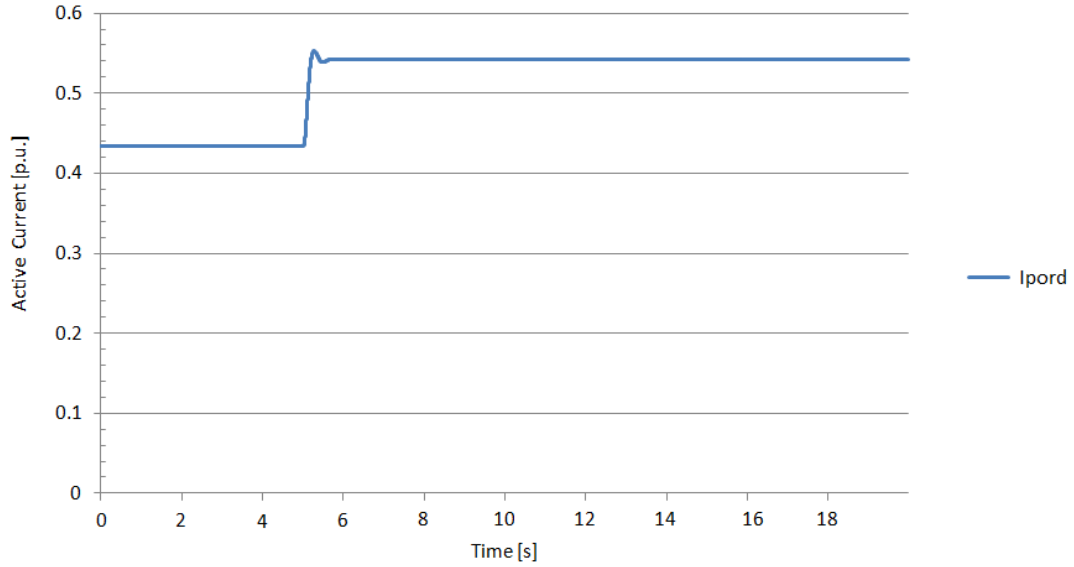

Figure 6.22- Output active current behaviour.

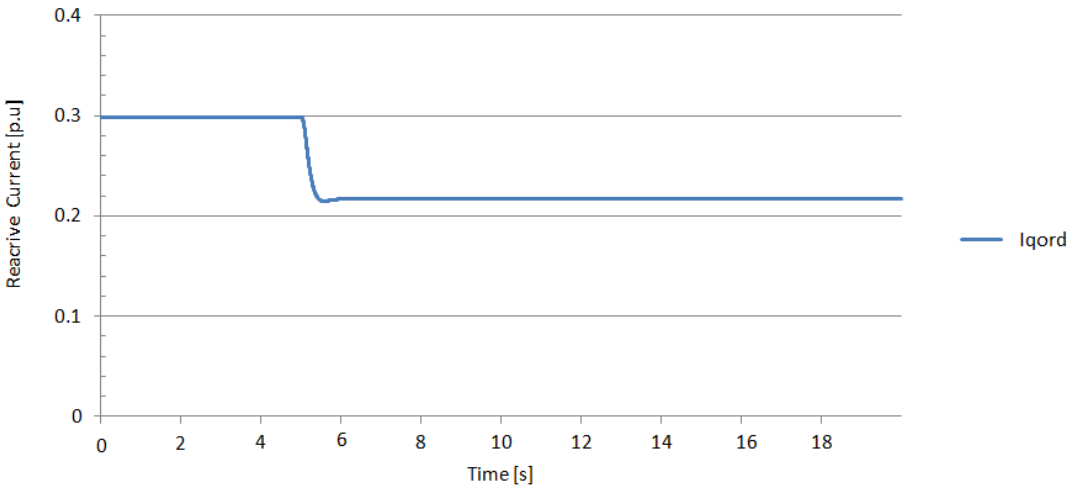

Figure 6.23- Output reactive current behaviour.

Figure 6.24 shows the voltage behaviour (V_d), measured at the point of interconnection with the grid. During normal situations, this quantity respects the allowable range defined by the limits of v_{dip} and v_{up}, set, according to the grid code, at 0.85 and $1.15\,p.u.$ respectively.

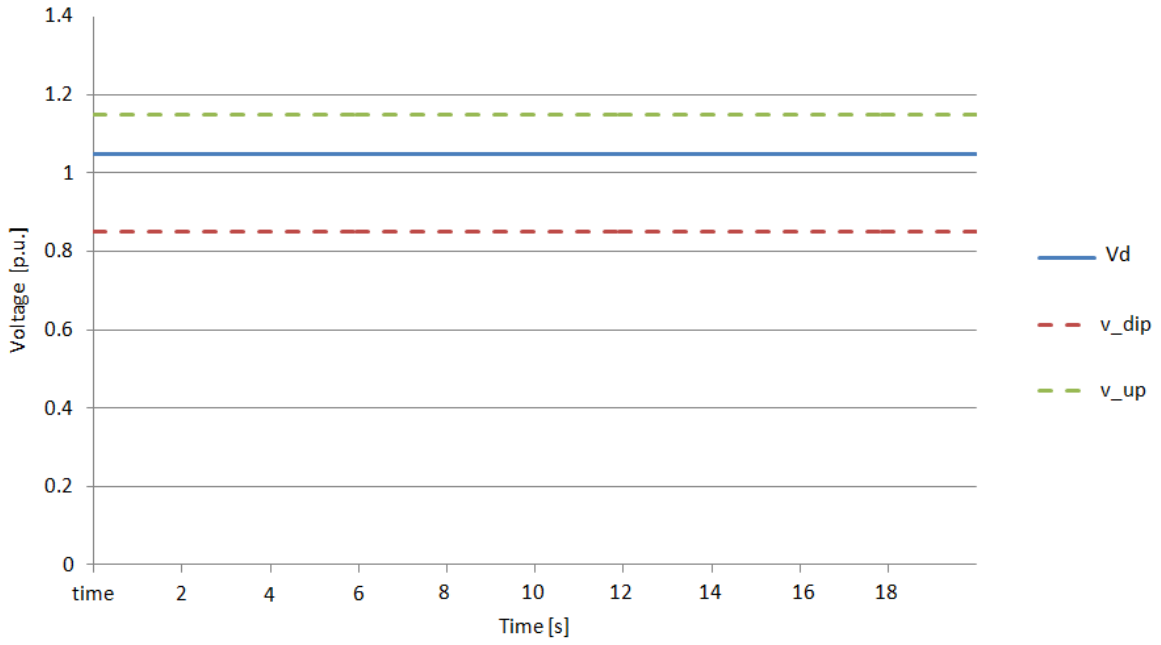

Figure 6.24- Voltage behaviour during normal situation. The green and red lines represent the upper and lower allowable voltage limits respectively.

High Load Variation

In the condition described above, the generator can fully satisfy the grid demand in terms of both active and reactive power. However, it can happen that the load variations are too high for the generator to completely comply with them. In these extreme cases, the user must choose to prioritize the active or reactive power demand. The next test has been conducted to highlight the priority option, available through the $PQ_{priority}$ switch. A large load change, from $20\,MW$ to $44\,MW$ and from $-14\,Mvar$ to $-30\,Mvar$, in P-Priority operation, has been assumed. Figure 6.25 and Figure 6.26 show the active and reactive power output behaviour respectively. Due to the high grid demand for active and reactive power, the controller cannot meet both requirements. Therefore, only the generated real power (P_e) can reach the reference (P_{ref}), since the P-priority mode has been selected.

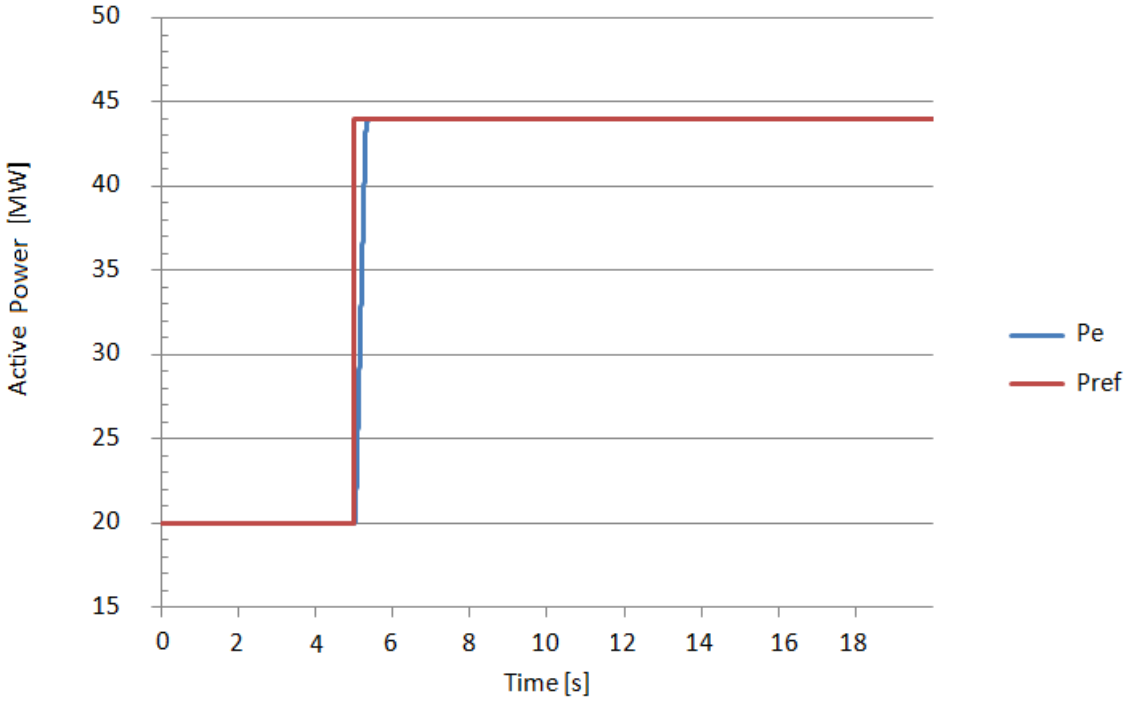

Figure 6.25- Active power output behaviour.

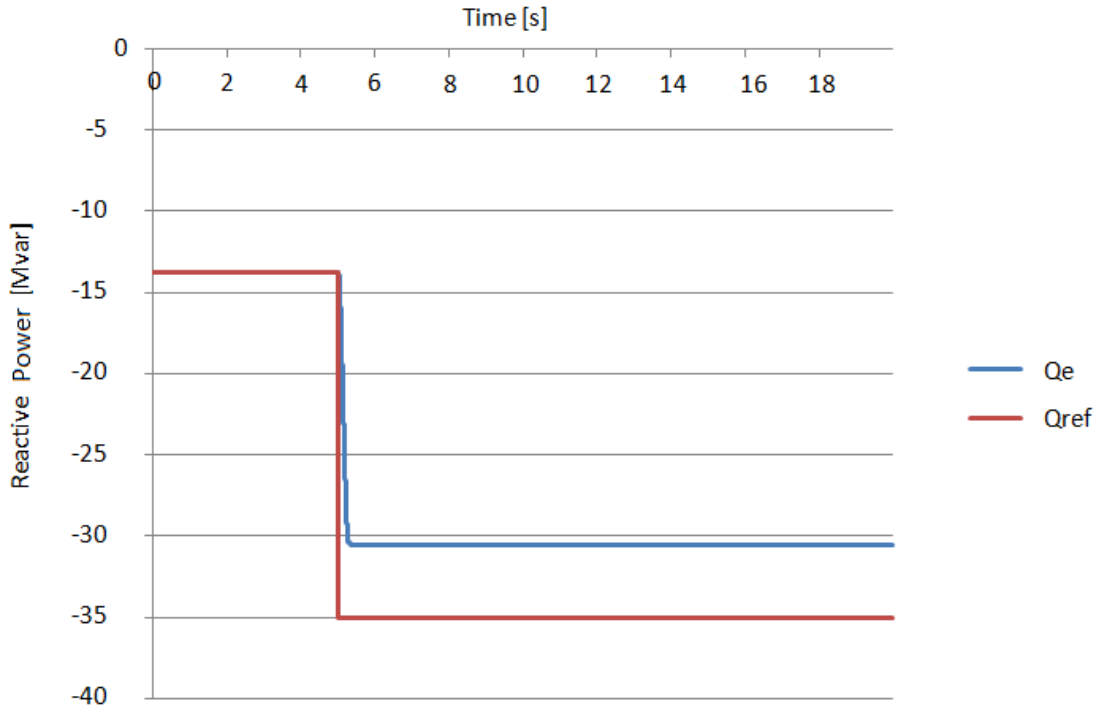

Figure 6.26- Reactive power output behaviour.

In fact, in order to satisfy both power requirements, the system should generate a current above the acceptable limit, as shown in Figure 6.27, causing possible damaging of the converter power switches (IGBTs and diodes).

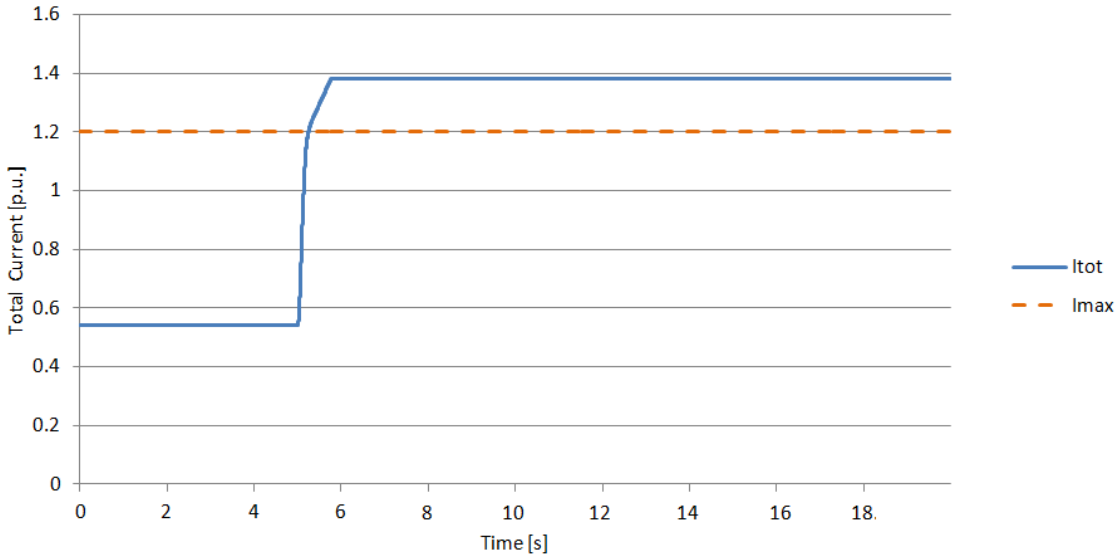

Figure 6.27- Total current behaviour without 'current limiter control' block. The orange line represents the maximum allowable current limit.

This problem is avoided by the 'current limiter control' block (5.3.3), which limits the output current within the acceptable range, by lowering the reactive current component from I_{qcmd} to I_{qord}, as shown in Figure 6.28.

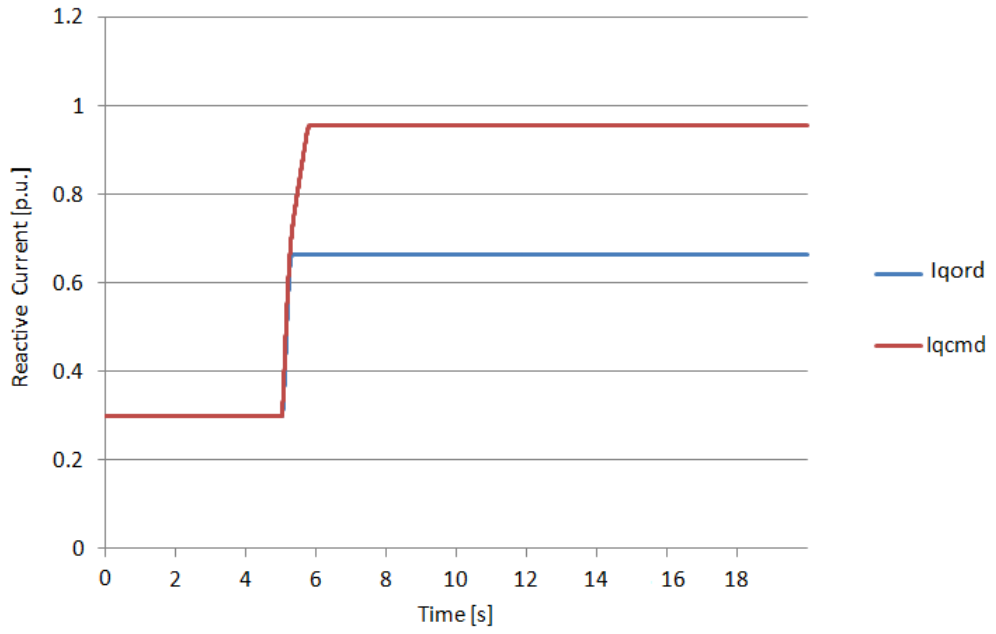

Figure 6.28- Reactive current behaviour in P-priority.

Fault Condition

The generator operation during fault situations has been tested by simulating a short circuit in the second line for Anvers (depicted in green in Figure 6.17), resulting in approximately 50 ms of PV terminal voltage drop under the tolerable limits. The Q-Priority mode has been selected for this simulation. The per unit voltage trend of the photovoltaic system is displayed in Figure 6.29, while its zoom during the failure is depicted in Figure 6.30.

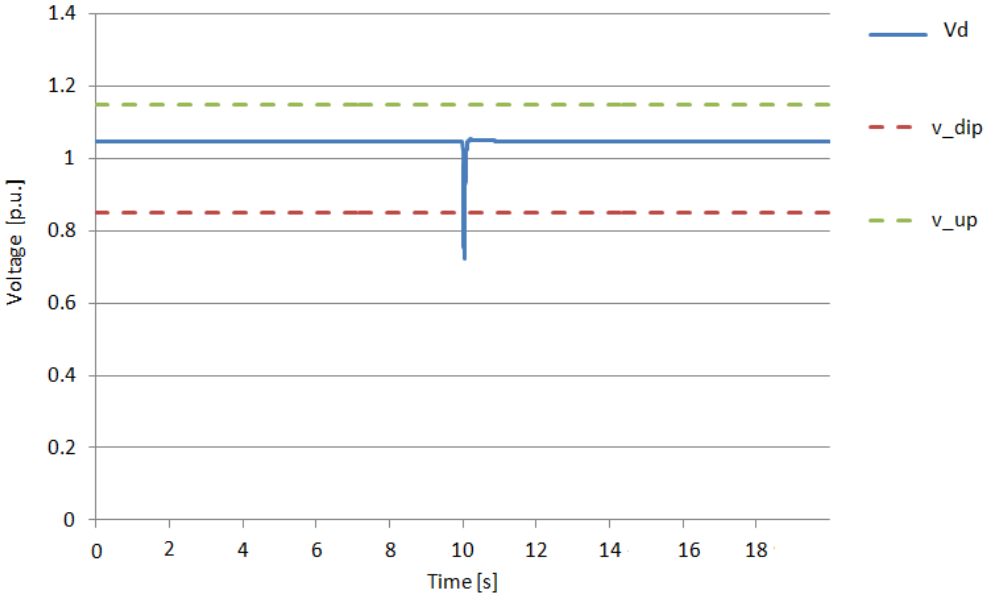

Figure 6.29- Voltage behaviour during a fault situation. The green and red lines represent the upper and lower allowable voltage limits respectively.

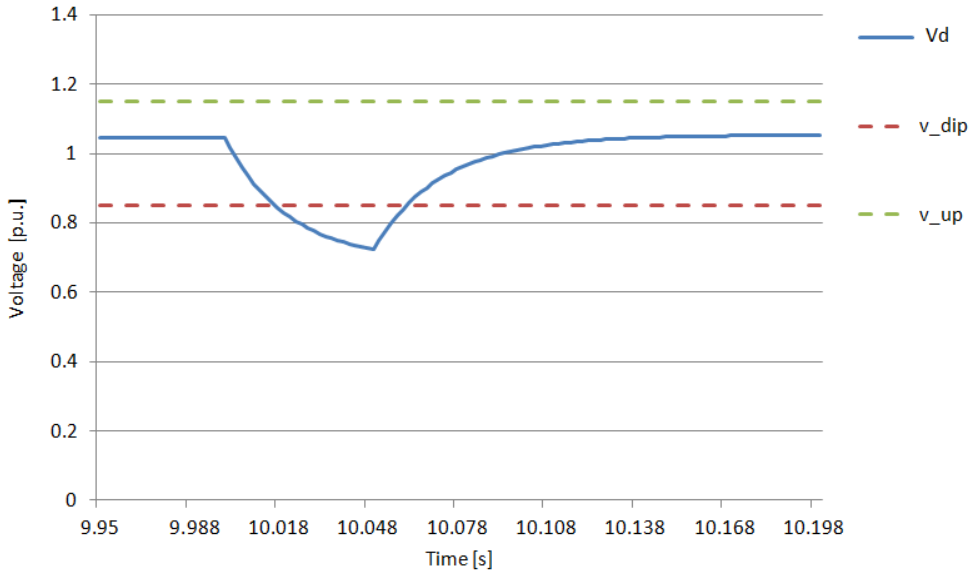

Figure 6.30- Zoom of the voltage behaviour during a fault situation.

In the pre-fault situation, being the reactive power reference (Q_{ref}) required by the grid negative, the generator behaviour was inductive, resulting in a positive reactive current injection (I_{qord}) from the generator to the network (5.5). During the fault event, instead, in order to restore the normal condition, the generator should behave as a capacitor, to help the increment of the voltage value, providing additional negative current injection towards the grid, as shown in Figure 6.31. This mechanism is promptly activated when the potential exceeds its lower limit (v_{dip}), while it is disabled under acceptable conditions.

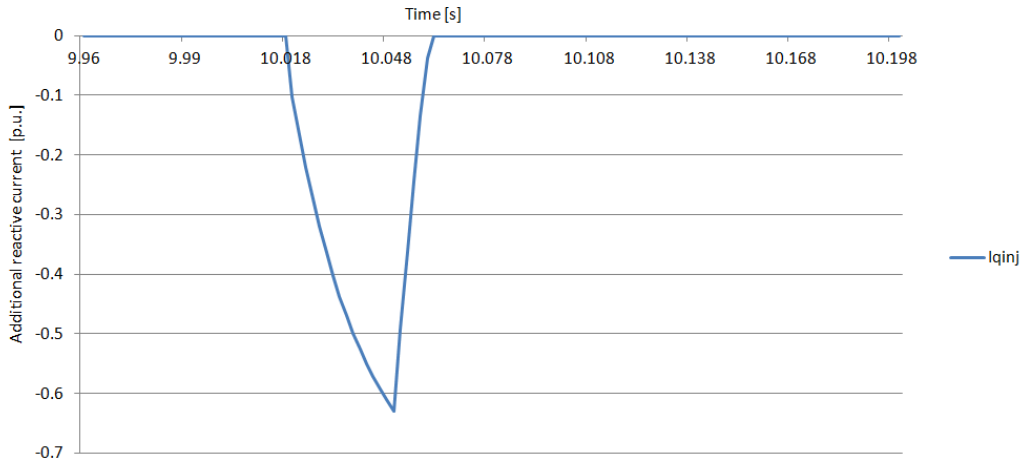

Figure 6.31- Zoom of the additional reactive current injection during voltage drop.

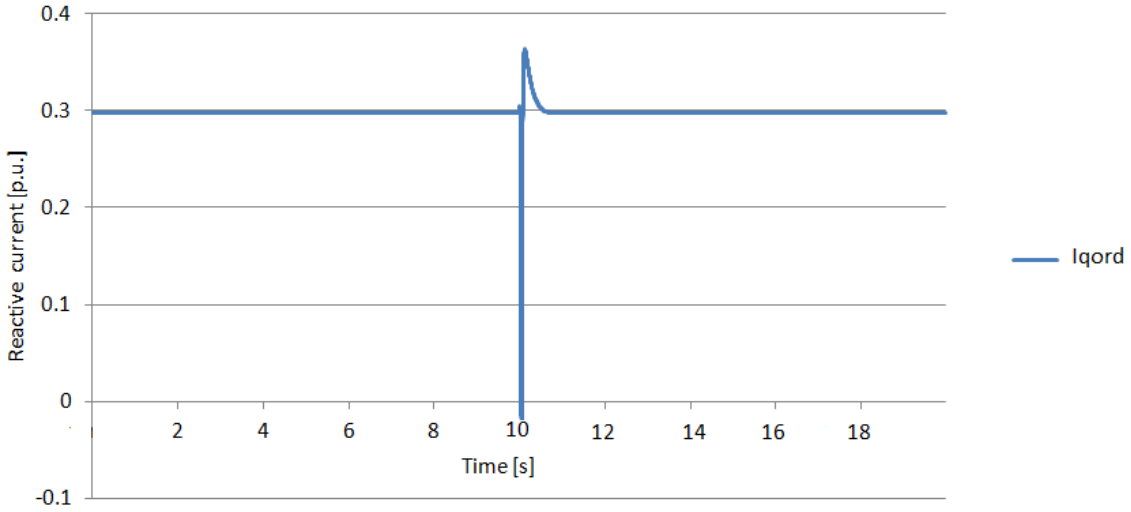

Figure 6.32- Reactive current output behaviour during voltage drop.

Figure 6.32 illustrates the resultant reactive current (I_{qord}) injected by the generator towards the network, obtained, during the failure, by the summation between the previous value of the pre-fault situation and the additional capacitive term (I_{qinj}). A zoom of the output reactive current behaviour during the fault is provided in Figure 6.33.

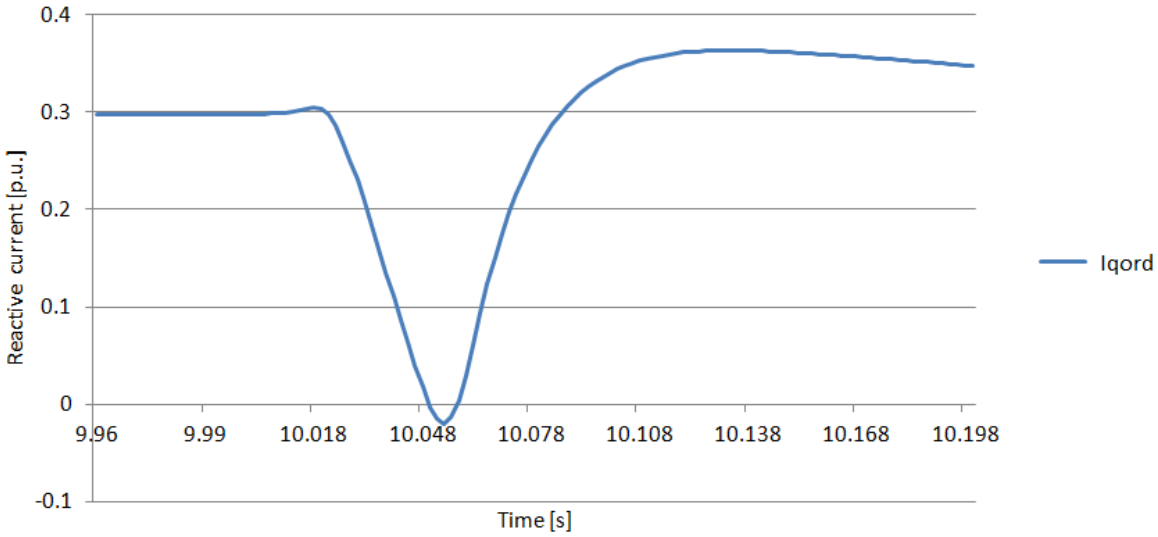

Figure 6.33- Zoom of the reactive current output behaviour during voltage drop.

Moreover, during under-voltage limit operation, the freeze control functioning is turned on.

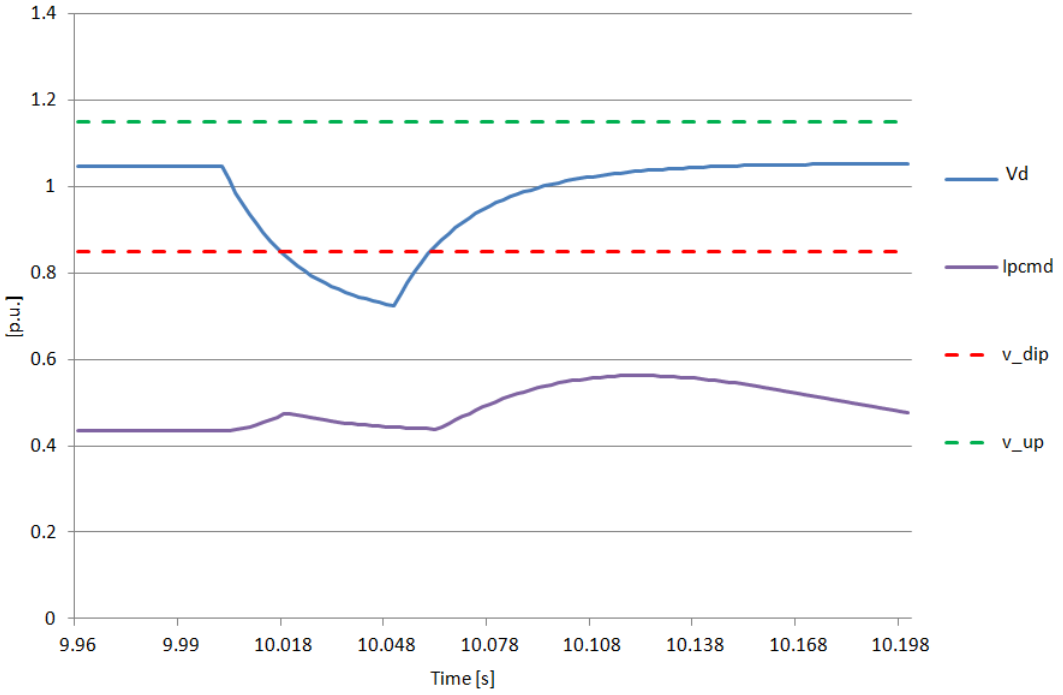

Figure 6.34- The graph shows the measured voltage Vd (in blue), the set point active current (in violet) and the voltage limits.

In this case, since the controller has been set in Q-Priority, the active current command (I_{pcmd}) has been frozen. Its behaviour during the failure is illustrated in Figure 6.34, where the set point active current (I_{pcmd}) results almost constant when the voltage drops under v_{dip} limit.

6.2.2 Simulation in Constant Power Factor Control Mode

This modality involves a reactive current regulation through the reactive power reference, which is dependent on the active power response (p) and the set power factor value, according to:

$$Q_{ref} = p * \text{tg}\,(arcos(power_{factor}))$$

The switch setting values for this test are listed in Table 6.10.

SWITCH	VALUE
Ref_{flag}	0
$Freq_{flag}$	1
$PQ_{priority}$	1
Q_{flag}	0
PF_{flag}	1
V_{flag}	0
$LVPL_{flag}$	1

Table 6.10- Switches parameters.

For the simulation a load variation has been taken into account, obtained by a change in the active power reference from 20 MW to 30 MW, shown in Figure 6.35, whose behaviour during the change is illustrated in detail in Figure 6.36.

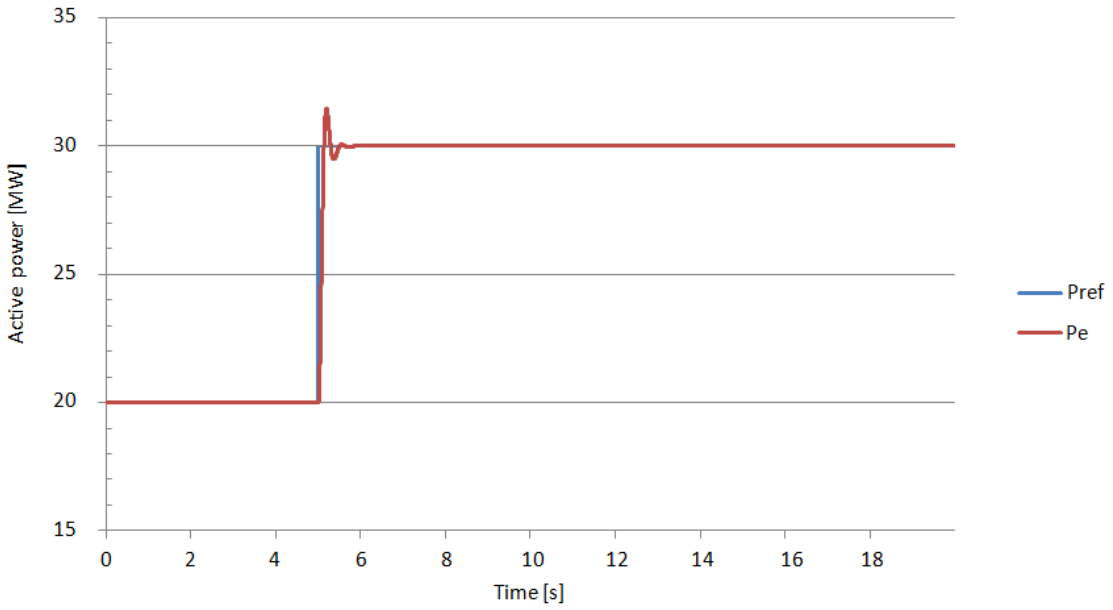

Figure 6.35- Active power output behaviour in constant power factor control mode.

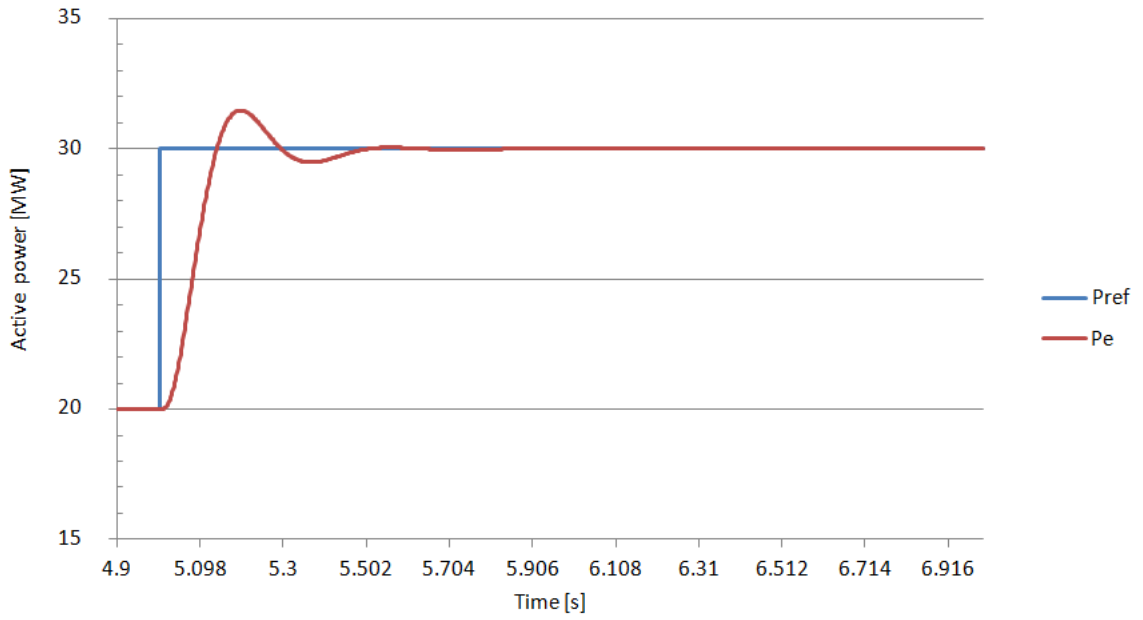

Figure 6.36- Zoom of the active power output behaviour in constant power factor control mode.

A power factor of 0.9 rad has been chosen for this test, resulting in the reference reactive power trend depicted in Figure 6.37 and detailed in Figure 6.38.

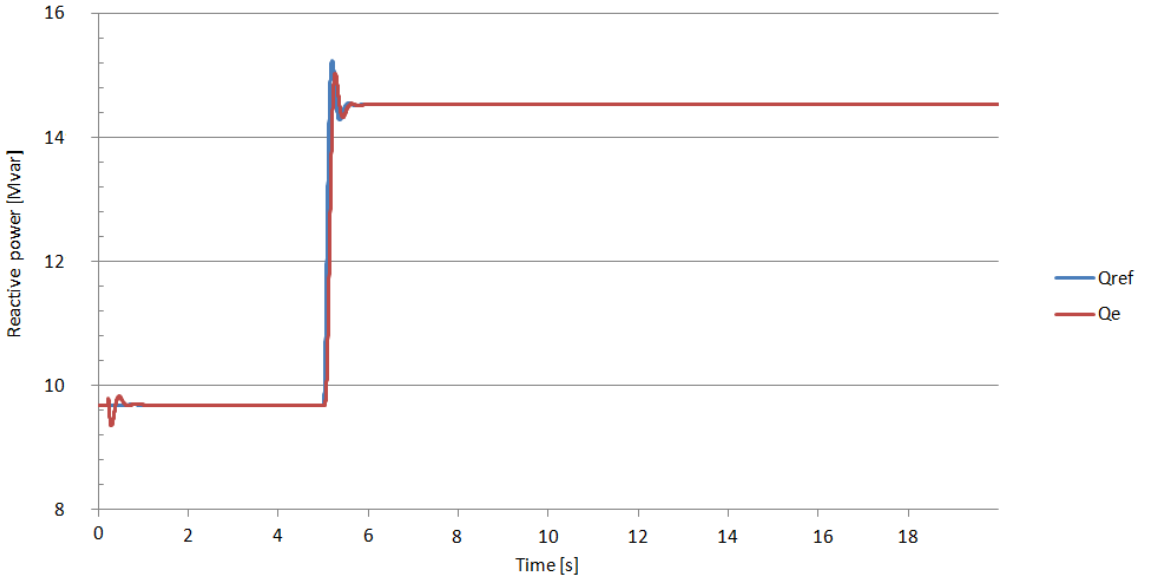

Figure 6.37- Reactive power output behaviour in constant power factor control mode.

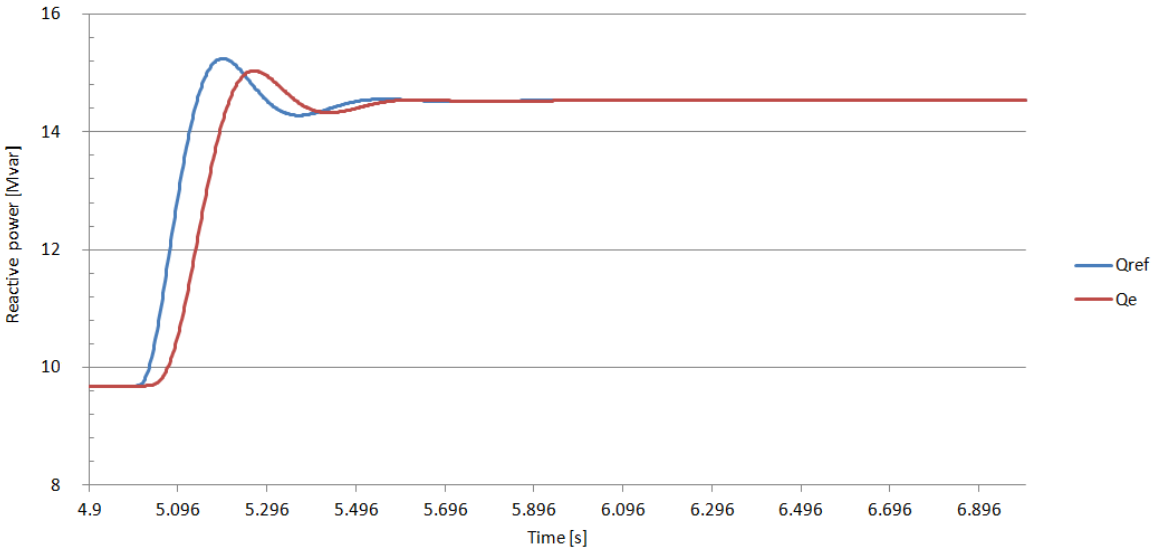

Figure 6.38- Zoom of the reactive power output behaviour in constant power factor control mode.

Both in graph of Figure 6.35 and Figure 6.37 the correct performance of the PV model is ensured by the curves of the measured power quantities, which follow their own reference values. In addition, the active and reactive current components, generated by the PV plant, are depicted in Figure 6.39 and in Figure 6.40 respectively, whose behaviours correspond to the active and reactive power rising.

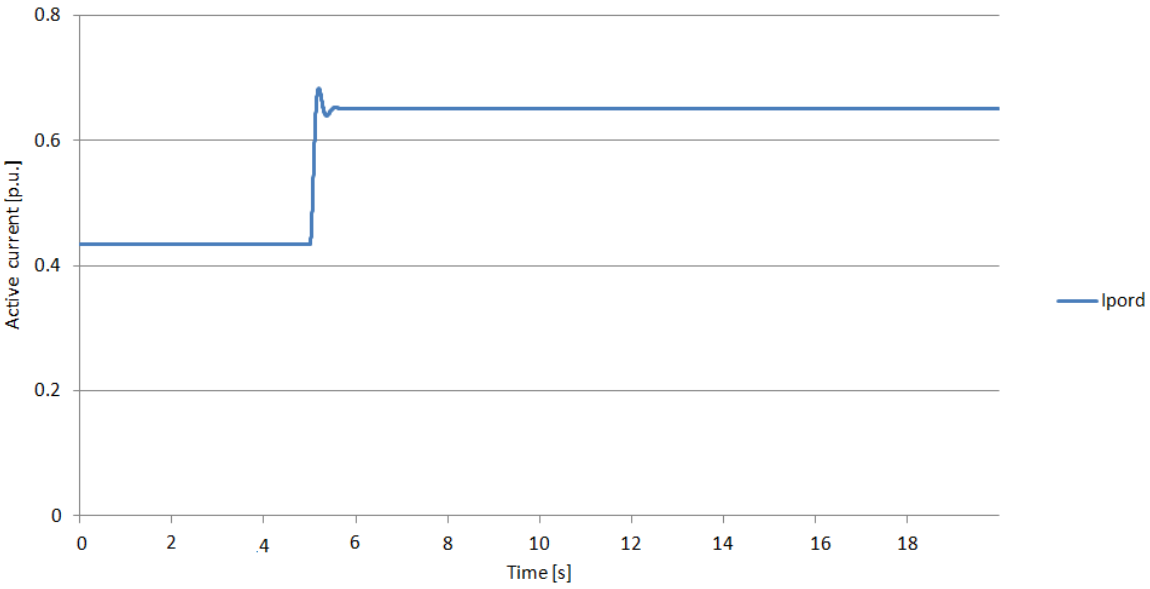

Figure 6.39- Output active current behaviour.

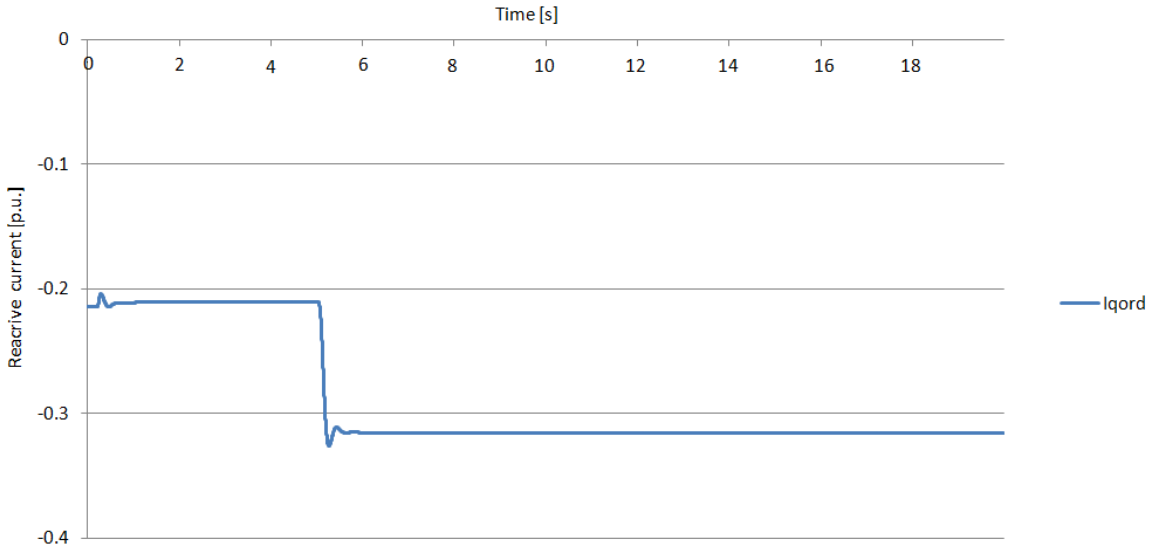

Figure 6.40- Output reactive current behaviour.

Conclusions

This thesis work was born as an activity proposed by CESI S.p.A, aimed at developing a dynamic model of large-scale photovoltaic system, to be included in its network simulator tool TESEO, developed for the Italian TSO Terna S.p.A, for voltage transients and grid stability studies. The project is part of an international energy transition, in which the use of solar photovoltaic in distribution and transmission network plays an increasingly important role. For this reason, the implementation of an appropriate PV model, able to give realistic and correct results when used for bulk power system performance studies becomes necessary. According to the CGMES standard, aimed at sharing common models among various TSOs, the OpenModelica® tool was selected for this activity. The solar plant model presented in this thesis is based on the presently available standard provided by the WECC-REMTF and it follows the paperwork realized by the National Renewable Energy Laboratory. The developed activity can be summarized in three main phases of operation:

1. Bibliographic survey and study of the selected model.
2. Implementation and individual sub-system tests in OpenModelica® environment.
3. Final tests validation in Dyana/TESEO simulation tool, with the connection of the PV generator to a sample test grid provided by CESI.

From the answers obtained in the simulation tests, the implemented model results in accordance with the expected behaviour of the assumed photovoltaic plant. However, it is worth mentioning that the evaluations were carried out on a limited test network, made up of 18 nodes. Additional detailed analysis will have to be carried out to ensure its complete performance even in more complex and wide grid configurations. In order to support and optimize future works in OpenModelica® and Dyana/TESEO platforms, a personal feedback, on positive and negative aspect encountered, is released below:

- The use of the OMEdit interface proved to be an appropriate choice as it is characterized by an intuitive implementation language and a rich library of elementary blocks, which simplified the realization of the photovoltaic generator.
- The possibility of splitting the model into blocks and the aggregation of these parts into more complex systems, allowed a clean and easy reading of the final work. In

addition, the creation of separated modules let their individual testing directly in OpenModelica® and implies also their possible reuse in other future models.

- During the modelling phase, errors, not always easy to detect, led to the unavoidable elongation of the correction time. Among the most frequent ones, it is worth mentioning that the removal of a block from the diagram does not always imply its deletion from the code.
- OpenModelica® is constantly updated, making continuous software improvement available. However, by providing different versions, care must be taken when choosing the most appropriate one, as it has been verified that modules implemented in new versions are not fully read by the older ones. Moreover, it is not always convenient to use the most updated edition. For example, during the thesis work, incompatibility problems occurred between the PV system, initially written in the newest version 13, and Dyana environment, based on the previous version 12. It was therefore necessary to rewrite the generator model in the oldest version to match the dynamic simulation platform characteristic.

Being the PV plant dynamic modelling still an area of active research, the implementation of solar photovoltaic system will continue to evolve as equipment improves and interconnection requirements change. Future developments to increase the accuracy of the model could include:

- The solar radiation variability.
- The DC/DC converter side, involving the MPPT algorithm.
- The internal system failures consideration.
- Additional compensation devices and external protections.
- The employment of storage systems.

Bibliography

[1] Modelica Association, "*OpenModelica User's guide*", 1998-2013.

[2] C. Bovo, Notes of the course *"Impianti di Produzione dell'Energia Elettrica",* Politecnico di Milano, 2018.

[3] M. Brenna, Notes of the course "*Electric Power System II*", Politecnico di Milano, 2019.

[4] Modelica Association , "*Modelica® - A Unified Object-Oriented Language for Physical Systems Modeling*", 2013.

[5] C. Belli, Notes of the course "*Conversione dell'energia*", Università degli studi di Pavia, 2010.

[6] S. Pasquini, F. Parma, A. Gobessi, M. Ciccotelli, F. Pretolani, E. Soda and C. Candia, "*Analisi dell'adozione del linguaggio Modelica per la descrizione dei modelli*. *Rapporto B6006762*", CESI S.p.A, 2016.

[7] OSMC - Open Source Modelica Consortium. [Online]. Available: https://www.openmodelica.org/.

[8] C. Bruno, R. Zacheo, M. Ciccotelli and C. Candia, "*Specifica funzionale dell'architettura di Teseo. Archirettura softwre. Rapporto B4018346*", CESI S.p.A, 2014.

[9] F. Parma and M. Ciccotelli, "*Dyana: Sviluppo e implementazione modulo import dati dinamici. Rapporto B7003947*", CESI S.p.A, 2017.

[10] S. Pasquini, F. Parma, M. Ciccotelli, F. Pretolani and E. Soda, "*NTCD - Specifica funzionale dell'architettura di Dyana: architettura software. Rapporto B6026373*", CESI S.p.A, 2016.

[11] S. Pasquini, M. Ciccotelli, F. Parma and A. Gobessi, "*Documento di analisi dei requisiti software e dei casi d'uso*" CESI S.p.A, 2015.

[12] Y. Yang, K. A. Kim, F. Blaabjerg, A. Sangwongwanich, "*Advances in Grid-Connected Photovoltaic Power Conversion Systems"*, Woodhead, 2019.

[13] João Paulo N. Torres, Carlos Alberto Fernandes, João C. Leite, "*Photovoltaic Cell String Layout*." Sustainable Energy, vol. 5, no. 1 (2017): 16-25. doi: 10.12691/rse-5-1-3.

[14] T. Orłowska-Kowalska, F. Blaabjerg, J. Rodríguez, " *Advanced and Intelligent Control in Power Electronics and Drives*", Springer International Publishing, 2014.

[15] N. Mohan, T. M. Undeland, W. P. Robbins, "*Power Electronics: Converters, Applications, and Design*", John Wiley & Sons, 2003.

[16] R. Teodorescu, M. Liserre, P. Rodríguez, "*Grid Converters for Photovoltaic and Wind Power Systems*", John Wiley & Sons, 2011.

[17]Western Electricity Coordinating Council Modeling and Validation Work group, " WECC *Solar Plant Dynamic Modeling Guidelines*", WECC Renewable Energy Modeling Task Force, April 2014.

[18] E. Muljadi, M. Singh, and V. Gevorgian, "*User Guide for PV Dynamic Model Simulation Written on PSCAD Platform*", National Renewable Energy Laboratory, November 2014, NREL/TP-5D00-62053.

[19] NERC Special Report, "*Standard Models for Variable Generation*", 2010.

[20] NERC Reliability Guideline*,* "*Distributed Energy Resource Modeling*", September 2017.

[21] K. Clark, N. W. Miller, R. Walling, "*Modeling of GE Solar Photovoltaic Plants for Grid Studies*"*,* General Electrical international, Inc. (GEII), September 2009.

[22] CEI 82-25 -*Guida alla realizzazione di sistemi di generazione fotovoltaica collegati alle reti elettriche di Media e Bassa Tensione*, 2008-12.

[23] S. Pasquini, "*Sviluppo di un Modello di Impianto Fotovoltaico e implementazione nei simulatori di rete CRESO e SICRE. Rapporto B2023597*", CESI S.p.A, 2012.

[24] S. Pasquini, "*Sviluppo e implementazione in SICRE di un modello semplificato di impianto fotovoltaico. Rapporto B3013883*", CESI S.p.A, 2013.

[25] Mario Lullo Master's Thesis - *Dimensionamento e Simulazione di un Inverter Fotovoltaico a tre livelli*- Università degli studi di Padova, 2010.

[26] Francesco Groppi, Speciale tecnico, "*Inverter e connessione alla rete elettrica*", QualEnergia, 2012.

[27] Toshiba Electronic Devices & Storage Corporation, "*DC-AC Inverter Circuit",* 2018.

[28] International Renewable energy Agency (IRENA), "*Scaling up variable renewable power: the role of grid codes*", 2016.

[29] Nica Conenna - *ENTSO-E: il network dei TSO europei* - 2019. [Online]. Available: https://energycue.it/entso-e-il-network-dei-tso-europei/12544/

[30] Terna S.p.A. - *Codice di rete italiano* - 2019. [Online]. Available: https://www.terna.it/it/sistema-elettrico/codici-rete/codice-rete-italiano

[31] Terna S.p.A. - *Codice di Rete- Allegato A.68*, Dicembre 2019.

[32] A. Hoke and D. Maksimović, "Active power control of photovoltaic power systems," *2013 1st IEEE Conference on Technologies for Sustainability (SusTech)*, Portland, OR, 2013, pp. 70-77.

[33] Jäger-Waldau, A., PV Status Report 2018, EUR 29463 EN, Publications Office of the European Union, Luxembourg, 2018, ISBN 978-92-79-97465-6, doi:10.2760/826496, JRC113626.

[34] A. Agrillo, V. Surace, P. Liberatore, L. Benedetti, "*Rapporto statistico solare fotovoltaico*", Gestore dei Servizi Energetici S.p.A. (GSE), Giugno 2019.

[35] Eurostat -*Renewable Energy Statistics- 2020.* [Online]. Available: https://ec.europa.eu/eurostat/statistics-explained/index.php/Renewable_energy_statistics

[36] S. Prakesh, S. Sherine, "*Forecasting methodologies of solar resource and PV power smart grid energy management*", International Journal of Pure and Applied Mathematics, Volume 116 No. 18 2017, 313-318.

[37] T. Soga, "*Nanostructured Materials for Solar Energy Conversion*", Elsevier, 2006.

[38] C. Mustansar Hussain, "*Handbook of Nanomaterials for Industrial Appli*cations", Elsevier, 2018.

[39] Muhammad H. Rashid,"*Power Electronics Handbook*" 2nd edition, Elsevier, 2007.

[40] A. Ellis, M. Behnke, R. Elliott, "*Generic Solar Photovoltaic System Dynamic Simulation Model Specification*", Sandia National Laboratories, 2013, SAND2013-8876.

[41] WECC approved dynamic model library, May 2018. [Online]. Available: https://www.wecc.org/Administrative/10%20Approved%20Dynamic%20Models-%20Torgesen.pdf

[42] Australia's guide to environmentally sustainable homes- Photovoltaic Systems. [Online]. Available: https://www.yourhome.gov.au/energy/photovoltaic-systems

[43] Photovoltaic Cells- Generating Electricity. [Online]. Available: https://www.imagesco.com/articles/photovoltaic/photovoltaic-pg4.html

[44] PN Junction: Formation and structure- [Online]. Available: https://electricalacademia.com/electronics/pn-junction-formation-structure/